ASSESSING HISTORIC CHANGE IN SUBALPINE FOREST: A CASE STUDY IN THE WEST CASTLE WATERSHED

DAVID R. MCCAFFREY
Bachelor of Science, University of Lethbridge, 2010

A Thesis
Submitted to the School of Graduate Studies
of the University of Lethbridge
in Partial Fulfilment of the
Requirements for the Degree

MASTER OF SCIENCE

Department of Geography
University of Lethbridge
LETHBRIDGE, ALBERTA, CANADA

ASSESSING HISTORIC CHANGE IN SUBALPINE FOREST: A CASE STUDY IN THE WEST CASTLE WATERSHED

DAVID R. MCCAFFREY

Date of Defence: December 08, 2017

Dr. C. Hopkinson Supervisor	Professor	Ph.D.
Dr. H. Jiskoot Thesis Examination Committee Member	Associate Professor	Ph.D.
Dr. S. Kienzle Thesis Examination Committee Member	Professor	Ph.D.
Dr. M. Letts Chair, Thesis Examination Committee	Professor	Ph.D.

DEDICATION

To my family. Especially to my grandparents, Bob and Audrey Shea, for sharing with me their love of nature and knowledge.

To my friends, for keeping me young. Or trying, at least.

To Alanna, for everything.

ABSTRACT

Alpine treeline ecotone (ATE) is a dynamic region where tree growth is limited by atmospheric temperature. Landscape scale variation in climate, topography, and disturbance regimes cause heterogeneity in the ATE by suppressing tree elevation below the absolute thermal limit to growth. In order to understand how ATE will respond to anticipated atmospheric warming, observations of historic change are required. This research introduces a novel method of canopy cover observation using oblique historic imagery. ATE change is assessed in the West Castle Watershed between 1914-2006, and found to be correlated to elevation, aspect, and fire-exposure. A random forest model was used to test a spatial extension of observed canopy cover change into areas that were not observed in the oblique imagery. This model used proxies for climate, topography, and disturbance regime as predictive variables. Collectively, this thesis research demonstrates that oblique photography can provide valuable insights into dynamic processes in the ATE.

ACKNOWLEDGEMENTS

I would like to thank my supervisor, Dr. Chris Hopkinson, and Dr. Laura Chasmer for the mentoring, guidance, and leadership they provided at many stages throughout this research. Additionally, I extend thanks to Dr. Hester Jiskoot and Dr. Stefan Kienzle for their valued contributions as committee members. This research would not have been possible without the excellent work of Dr. Eric Higgs, Dr. Mary Sanseverino, and the entire team of the Mountain Legacy Project. Dr. Claudio Bozzini provided useful feedback on the operation of the WSL monoplotting tool. Dr. Marie-Pierre Rogeau was instrumental in both accessing and interpreting the fire history data of the West Castle area. I am grateful for the teamwork and solidarity of everyone in the ARTEMIS lab. Specifically, I thank Dr. Craig Mahoney for his assistance with learning random forest modeling, Josh Montgomery for his work as second-interpreter in the oblique classification chapter, and Kelsey Cartwright for the many productive conversations about snow-depth modeling. Reed Parsons and Benjamin Mindek provided valuable field assistance. Finally, I would like to acknowledge and thank the countless people that make Lethbridge such a wonderful community in which to live and work.

TABLE OF CONTENTS

LIST OF TABLES

LIST OF FIGURES

LIST OF ABBREVIATIONS

ATE	Alpine Treeline Ecotone
BP	Before Present
CAP	Cold Air Pooling
CTI	Compound Topographic Index
DEM	Digital Elevation Model
GNP	Glacier National Park
LiDAR	Light Detection and Ranging
IDW	Inverse Distance Weighting
JJA	June, July, August
m a.s.l	Meters Above Sea Level
MDG	Mean Decrease in Gini Coefficient
MLP	Mountain Legacy Project
NSC	Non-Structural Carbohydrate
PET	Potential Evapotranspiration
SD	Standard Deviation
SPOT	French: Satellite Pour l'Observation de la Terre English: Earth Observation Satellite
WCW	West Castle Watershed
WSL	German: Eidgenössische Forschungsanstalt für Wald, Schnee und Landschaft English: Swiss Federal Institute for Forest, Snow and Landscape Research
WSL-MT	The WSL Monoplotting Tool

Chapter 1 - Introduction

1.1 Overview

The focus of this thesis is change in the alpine treeline ecotone (ATE). The research encompasses novel methods of detecting historic ATE change, an analysis of correlations between topography and ATE change, and a model which demonstrates a spatial extension of the observed change to unobserved areas.

Chapter one provides a brief overview of the history of ATE research. The phenomenon of ATE can be viewed through the lens of many distinct disciplines (e.g. botany, landscape ecology, biogeography), and in the long history of ATE research conceptual focus of research has varied dramatically. Thus, it is important to situate the topics which are addressed by the thesis in a broader context.

Chapters two, three, and four are presented as manuscripts. Chapter two introduces a method of determining canopy cover from oblique imagery and compares that method against measurements of canopy cover from airborne lidar. Chapter three uses the oblique photography analysis method to map changes in canopy cover in the ATE over a 92-year period of record, and investigates topographic correlations to ATE change over that time. Chapter four classifies historic change in the ATE with a random forest model, trained on a suite of topo-climatic variables, in an attempt to predict the historic change in areas of the watershed that were not directly observed in oblique photographs. An attempt was made to minimize redundancy between chapters, but there is a small degree of overlap when necessary for the narrative of each manuscript. An abridged version of chapter two was accepted for publication prior to the completion of the thesis (McCaffrey & Hopkinson 2017). For the purpose of submitting the thesis,

chapters three and four can be considered as complete manuscripts, but additional analysis may be added to each prior to their final publication.

Chapter five presents a conclusion of the findings and limitations of the research in the three manuscript chapters. Potential applications for the novel methods described by the thesis are reviewed, and areas of future research are suggested.

1.2 Definitions

ATE is the region between closed canopy forest and alpine tundra, where tree height, stand density, and canopy cover are gradually reduced as a function of elevation (Tranquillini 1979). An often-confusing nomenclature has developed around treelines, which is complicated by the fact that ATE occurs as a transition zone rather than a distinct line. This research adopts the recommendations of Körner (2012, p. 18), where *timberline* refers to the elevation of closed canopy forest boundary, *tree species limit* refers to the greatest elevation at which a tree species occurs, and *treeline* is the elevation roughly midway between *timberline* and *tree species limit*. Thus, ATE is considered to extend from *timberline* to the *tree species limit*.

A tree is defined as an upright woody plant with a dominant stem that reaches a height of > 2 m. This distinction is required due the prevalence of *krummholz* forms in ATE, which occur when exposure to extreme cold and wind at high elevations causes trees to grow in stunted, prostrate positions, sometimes horizontally. *Krummholz* forms most often occur near the *tree species limit*, and are often the first indications of upslope advance in the ATE (Grace et al. 2002; Grafius & Malanson 2015; Harsch et al. 2009). *Krummholz* forms also facilitate change by providing sheltered microsites for the

seedling establishment, creating a positive feedback for vegetation presence (Maher & Germino 2006). Furthermore, the growth form of a *krummholz* tree can change over its lifespan, with formerly prostrate trees displaying upright growth in response to improved climatic conditions (Kullman 1986) (see Figure 1.1 – note that upright tree forms, ~2 m tall, can be seen in the background, growing out of the prostrate *krummholz* form in the foreground). Thus, if the goal is to understand change and succession in the ATE as it relates to climate, it is preferable to make a distinction between a tree growing in an upright form versus a *krummholz* form, rather than using the presence or absence of a given species as a metric.

Figure 1.1 - Krummholz forms of subalpine fir (Abies lasiocarpa) in Waterton Lakes National Park, Alberta, Canada, elevation 2275 m a.s.l. - Photo by DRM

Lastly, a distinction must be made between *alpine treelines* and *latitudinal treelines*. One of the fundamental findings of ATE research is that, at a global scale, both alpine treelines and latitudinal treelines form in response to an absolute lower thermal limit to tree growth (Körner 1998; Körner & Paulsen 2004). But at the landscape-scale, modulating factors can suppress treelines below their absolute thermal limit. Many of these modulating factors are related to topography (Case & Duncan 2014; Weiss et al. 2015). The present research focuses on ways in which these regional variations in climate and topography affect ATE dynamics. Thus, as the high-relief topography of mountain areas is distinct from the low-relief tundra where latitudinal treelines occur, topography will have a different modulating effect between the two treeline types. Any use of the word treeline is implied to refer to alpine treeline, unless latitudinal treeline is explicitly stated.

1.3 History of ATE Research

The transition between subalpine forest and tundra, defined by the ATE, is one example of the many vegetation boundaries that occur across climatic gradients of mountain areas. These bioclimatic patterns have been a rich area of study for centuries, and were arguably the first focus of biogeographic research.

The Prussian scientist and explorer Alexander von Humboldt (1769-1859) is often credited with founding the discipline of biogeography (MacDonald 2003, pp. 142-143). During a five-year expedition of the Americas (1799-1804), von Humboldt collected meticulous records of plant elevations across South America, finding that distinct zones of vegetation structural types were associated with bands of elevation. He

contrasted these observations with similar patterns of vegetation in European mountain ranges that had been reported by the 16th-century botanist Cardinal Bembo (1470-1547) and the 17th-century botanist Joseph Pitton de Tournefort (1656-1708); Tournefort in particular noted that elevation gradients had the same effect on plant communities as latitudinal gradients, saying that, "… the elevation of the ground above the level of the sea in mountainous districts influences the distribution of plants in the same way as distance from the pole in plains" (von Humboldt 1886, p. 381).

In 1802, von Humboldt attempted to summit Mount Chimborazo (6,236 m) in what is now Ecuador. The low latitude and high elevation of Chimborazo gave von Humboldt the opportunity to catalogue plant life across several biomes during the ascent, from rain forest to tundra. Afterwards, von Humboldt began work on the *Naturgemälde* (no English translation, but roughly means 'painting of nature', but with an implied unity or wholeness) (Wulf 2015, p. 108); this figure displayed the elevation limit of hundreds of plant genera and vegetation types, from palm trees at the foot of the mountain to cold-resistant lichens below the nival level, all super-imposed on an image of Chimborazo.

Boundaries of tree growth were clearly described in the *Naturgemälde*, such as 'the superior limit of great trees', slightly below 3000 m, and 'the limit of the last arborescent plants' at 3500 m – referring to *timberline* and *tree species limit*, respectively. Later in life, Von Humboldt collected and measured vegetation in high latitude regions of Russia and Finland, confirming that the elevation at which a given vegetation zone (including ATE) occurs negatively correlates with latitude; i.e. the highest elevation treelines are found in low latitude, equatorial and sub-tropical ranges, and the lowest elevation treelines are found in high latitude ranges. Von Humboldt's

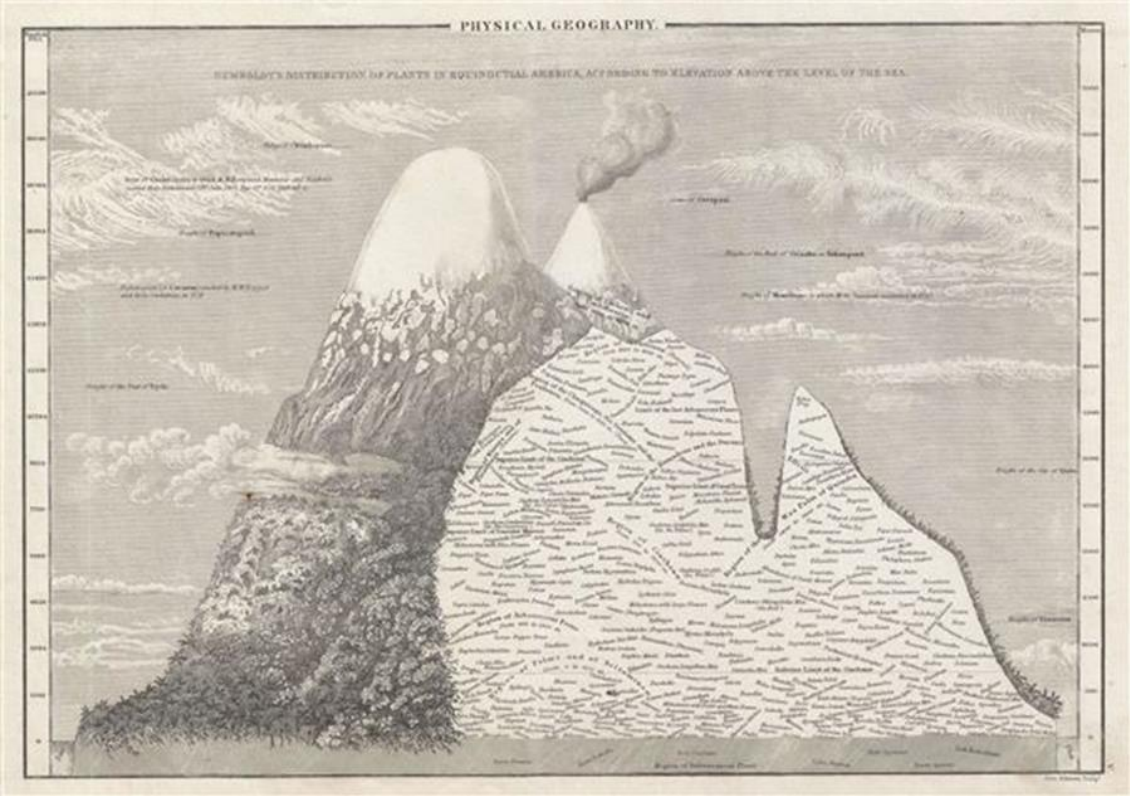

Figure 1.2 - English map of the mountains & plants of America (Black and Hall, 1840), based on the 1805 Naturgemälde published by von Humboldt.

observations demonstrated that treelines, both alpine and latitudinal, are a global bioclimatic phenomenon (Körner 2012, p. 34).

Once the bioclimatic distribution of treelines was known, attention turned to more mechanistic questions. For example, why is tree growth limited at high elevations, where other plant life persists? How do grasses, shrubs, and herbs photosynthesize and assimilate carbon in temperatures that limit tree growth? It was apparent from global observations that treeline position was correlated with low temperatures. Yet systematic, global measurements of temperature at treeline generally went unrecorded through much of the 20th-century (Körner 1998) – a notable exception is Hermes (1955), who was published only in a regional German journal. When multi-year observations were

completed at 46 globally-distributed sites (ranging between 68°N – 42°S) a surprisingly narrow range of mean annual temperature (6.7 °C , ±0.8 SD) was demonstrated (Körner & Paulsen 2004). This correlation was the strongest evidence of an absolute thermal limit to tree growth.

Alternative hypotheses were presented for processes that were both correlated to temperature lapse rates and had the potential to limit tree growth. One hypothesis was that low temperatures cause frost damage in plants (Körner 1998). Several reviews of this topic demonstrated that high elevation treelines have adaptations for minimizing frost damage, including *supercooling* and snow insulation (Neuner 2007; Neuner 2014). Temperate subalpine trees are most vulnerable to frost damage during rapid temperature changes in spring (Neuner 2014). However, frost damage is not sufficient as a global predictor of treeline, as treelines occur in equatorial regions with low temperatures but rare frosts (Körner 1998).

A separate alternative hypothesis, referred to as the *carbon balance hypothesis*, suggested that reduction in partial pressure of CO_2 at high altitudes may limit gas exchange and reduce photosynthetic capacity of trees (Körner 1998). However, a survey of non-structural carbohydrate (NSC) concentrations across four climatic regions (including alpine treeline) showed that NSCs are typically found in abundance, regardless of whether or not a plant is experiencing growth (Körner 2003b). The abundance of NSC, even at treeline, is evidence that carbon assimilation is not a limiting factor to growth at treeline (Körner 2003b). Further, the *carbon balance hypothesis* would not explain the occurrence of latitudinal treelines, as the reduction in CO_2 partial pressure is limited to high altitudes.

Körner's approach to understanding ATE position was informed by his background as a botanist, in search of the fundamental physiological mechanism which limits tree growth. The accumulated evidence confirms that this limit is thermal (Körner 2012). While Körner acknowledged that local suppression of treeline below an absolute thermal limit was not only possible, but commonplace, his stated goal was to find an explanation for treelines beyond what he called "regional peculiarities" (Körner 1998; Körner 2012, p. vii).

1.4 ATE from a Biogeographic Perspective

The questions pursued by biogeography are the very "regional peculiarities" that are dismissed by Körner. The biogeographic contribution to ATE research is an appreciation of how regional variation in climate, topography, and disturbance regimes can result in departures from the absolute thermal limit to tree growth. Collectively, these influences are referred to as *modulating factors*.

Regional modulating factors have been observed in several ATE studies (for summaries see Butler et al. (2009) and Holtmeier (2009)). A non-exhaustive list of modulating factors includes: synoptic climate (Alftine et al. 2003), wind exposure (Broll & Holtmeier 2010; Cairns 2001), snow accumulation (Walsh et al. 1994), moisture availability (Elliott & Cowell 2015; Moyes et al. 2015), positive feedback with other vegetation (Bader et al. 2008), rockslides and avalanches (Butler & Walsh 1994; Walsh et al. 1994), fires (Cansler et al. 2016; Stine & Butler 2015; Stueve et al. 2009), volcanic debris (Efford et al. 2014), geomorphic conditions (Butler et al. 2007; Leonelli et al. 2016; Macias-Fauria & Johnson 2013; Resler 2006; Walsh et al. 2003), topography

(Greenwood et al. 2014; Holtmeier & Broll 2012), the mountain mass elevation effect (Yao & Zhang 2015; Zhao et al. 2015), in additon to seasonality of temperature (Hagedorn et al. 2014; Kullman 2014). These modulating factors may interact to varying degrees, and also elicit taxa specific responses. The potential combinations of modulating factors are, in theory, as myriad as the number of locations at which treelines occur and the number of taxa that occur there.

Attempts have been made to organize these various modulating factors into a nomenclature of treeline types (Harsch & Bader 2011; Holtmeier & Broll 2005). One such organizational structure was proposed by Holtmeier and Broll (2005) who made a distinction between anthropogenic treelines (i.e. those occurring as a result of human-mediated disturbances, such as grazing and pastoralism (Colombaroli et al. 2010; Speed et al. 2014)), orographic treelines (i.e. those responding to topographic influence, such as increased disturbance in high slope regions (Fagre et al. 2007; Holtmeier & Broll 2012)), and climatic treelines (i.e. those that reach an altitudinal limit caused by climatic variables, such as the absolute thermal limit to growth (Körner & Paulsen 2004)). This organizational structure is hierarchical; orographic effects only become the primary modulating factors of treeline in the absence of human modulation, and climatic effects only become the primary modulating factors in the absence of orographic effects.

The classification structure set out by Holtmeier and Broll (2005) demonstrates the necessity of understanding the relative influence of modulating factors. This becomes particularly relevant when dynamic responses to warming in the ATE are considered. Anticipated increases in atmospheric temperatures are expected to have unique impacts on mountain systems (Pepin et al. 2015), and there has been debate as to whether ATE

will experience upslope advance in response (Grace et al. 2002; Paulsen & Körner 2014). In many temperate mountain ranges, there is evidence that historic treelines were present at higher elevations during the Holocene thermal maximum, 9000-5000 BP (Beaudoin 1986; Lloyd & Graumlich 1997; Schwörer et al. 2017; Schwörer et al. 2013), which suggests that upslope advance is a plausible outcome of warmer climate. However, the Holtmeier and Broll (2005) treeline definitions underscore the notion that not all treelines are expected to advance with atmospheric warming. Climatic treelines would potentially respond to atmospheric warming, while orographic and anthropogenic treelines would remain subject to modulating factors, which would not be expected to change in a warming climate. Thus, the ability to differentiate between treelines which are influenced by absolute thermal limits and those which are influenced by modulating factors is critical for anticipating how ATE will respond to atmospheric warming.

There is increasing recognition that the influence of modulating factors on ATE varies with spatial scales (Case & Duncan 2014; Holtmeier & Broll 2017; Weiss et al. 2015), e.g. climatic factors like temperature and precipitation can be the primary determiners of ATE position at continental scales, while topographic effects like slope and curvature can influence ATE position at landscape and microsite scales (Weiss et al. 2015). This concept is articulated in a theoretical model put forward by Case and Duncan (2014) (Figure 1.3) – if the absolute thermal limit to growth is curve A, then the given modulating factor may reduce the elevation of ATE to curve B (the model uses the term *stress* in place of *modulating factor*). The multiscale approach suggests that the distance between curve A and B (i.e. capacity of a modulating factor to reduce ATE elevation below the absolute thermal limit) can vary as a function of spatial scale. For example, at a

microsite scale, thermal effects from aspect or curvature could dramatically suppress treeline from what would otherwise be the absolute thermal limit to growth (large gap between B and A), but at a continental scale, aspect and curvature would have little effect on position (small gap between B and A). Multi-scale studies have provided valuable insight into the role of modulating factors, but to date there are no known studies that have used multi-scale analysis to understand change dynamics in the ATE.

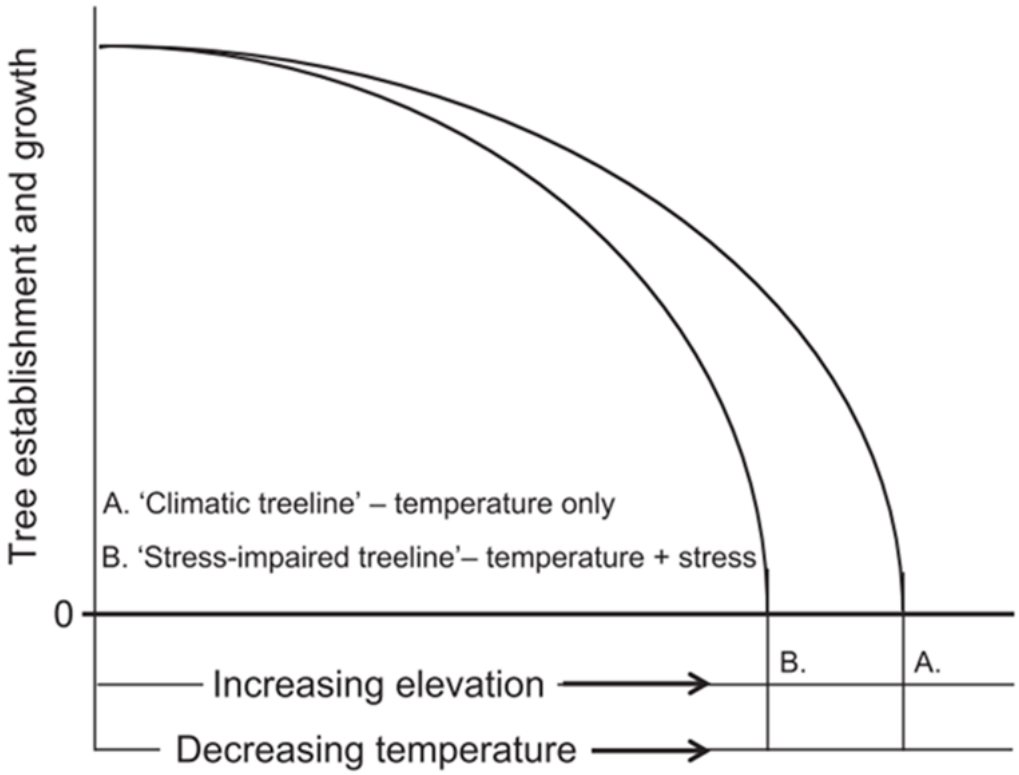

Figure 1.3 - Theory diagram of relative influences of absolute thermal limit (A) and modulating factors limit (B). Source: Case and Duncan (2014)

1.5 Research Goals

The overarching goal of the thesis is to better understand how modulating factors affect ATE dynamics, using novel techniques to increase the temporal extent and spatial resolution of ATE observations. The specific utility of improving ATE observations is addressed in each of the three research chapters. Broadly, the goals were as follows:

1) to develop a method of assessing canopy cover from oblique photography, using monoplotting software and high-resolution elevation models from airborne lidar;
2) to use that canopy cover analysis method to compare repeat photographs of a watershed, identifying correlations between historic canopy cover change, terrain variables, and disturbances (anthropogenic and wildfire);
3) to apply machine learning algorithms to predict historic canopy cover change in areas of the watershed that were unobserved by repeat photography.

The ability to extract quantitative canopy cover information from historic photography, to correlate canopy change with environmental factors, and to predict change in unobserved areas is intended to serve as a basis for developing new hypotheses and experimental tests for understanding the relationship between modulating factors and ATE position. Additionally, the conclusion of the thesis reviews the possibility of applying multi-scale analysis to these datasets, and the potential use of these historic land cover parameters in hydrologic modeling.

Chapter 2 - Oblique Photography and Canopy Cover Classification

2.1 Introduction

This chapter introduces a methodology which increases both the spatial and temporal scale of ATE observation through historical analysis of oblique repeat photography. A variety of observation methods have been applied to monitor change in the ATE, including repeated plot measurements (Weiss et al. 2015), dendrochronology (Liang et al. 2014), remote sensing (Coops et al. 2013), and historical records (e.g. oblique photography) (Hagedorn et al. 2014). While each method has advantages, observation methods are ultimately limited in the temporal and spatial extents at which they can resolve change (Danby 2011). For example, forest structure parameters that characterize ATE, such as fractional cover, can be observed at a high spatial resolution (< 1 m) using airborne lidar, but few extended lidar records presently exist for periods longer than 20 years. Conversely, oblique photograph records of ATE exist for periods exceeding 100 years (Trant et al. 2015), but quantitative analysis of century-scale land cover change using oblique photographs has been restricted to low spatial resolutions (~100 m) (Stockdale et al. 2015).

In the Canadian Rockies, where advance of ATE species such as subalpine fir (*Abies lasiocarpa*) has been observed at a rate of 0.28-0.62 m yr^{-1} (Bekker 2005; Luckman & Kavanagh 1998) the ability to detect shifts in ATE using repeat oblique photography depends on increasing the spatial resolution; e.g. if ATE has advanced on the order of ~50 m in a century, the spatial resolution of analysis must be higher than 100 m to detect change using a century-scale photographic record.

Land cover in an oblique photograph can be rasterized through the utilization of a technique pioneered by Stockdale et al. (2015) (henceforth 'the Stockdale method'). The Stockdale method uses software to transform a photograph's perspective from oblique to orthogonal, enabling comparison of land cover between repeat photographs. This chapter will review the Stockdale method, and outline modifications to the method that allow the rasterization of fractional cover from oblique photographs at a resolution of 20 m, thus facilitating ATE monitoring. The validation and error assessment methods proposed by the Stockdale method are employed, while introducing three additional techniques: 1) an analysis of classification agreement in overlapping areas; 2) an application of a general linear model described by the Stockdale method, at a landscape scale; and 3) a validation of fractional cover classifications with airborne lidar. The fractional cover classification from oblique photograph method described in this chapter is the foundation of the subsequent analysis of ATE in chapters three and four.

2.2 Literature Review

2.2.1 Repeat Photography in the ATE

Mountain regions were a frequent subject of early photographers, producing a vast archive of historical photographs from the 1870s onward (Rogers et al. 1984). Repeat photographs of historical images have been used to monitor landscape change as early as 1888, when Sebastian Finsterwalder used oblique photogrammetric techniques to observe glacial retreat in the Alps (Hattersley-Smith 1966). Early use of repeat photography to document vegetative change dates to approximately the same era. A detailed bibliography of studies which employ repeat photography for glacial and

vegetative change is provided by Rogers et al. (1984). Early repeat photography research highlighted two problems with the method: 1) difficulty in accurately recreating the external camera parameters (i.e. camera X, Y, Z coordinates, and the orthogonal axes of the image plane), and 2) inability to measure change area in oblique photographs, given varying spatial scales created by the oblique perspective. While the problem of recreating camera parameters was addressed by Harrison (1974), the issue of varying scale within an oblique photograph has been largely left unaddressed. As a result, many of the early repeat photograph studies are limited to qualitative descriptions of change, rather than quantitative measurements.

Hart and Laycock (1996) give an annotated bibliography of 175 studies which used repeat photography to assess vegetative land cover change in the western United States, adding to the first bibliography of Rogers et al. (1984). The Hart and Laycock bibliography cross-listed studies by state and ecosystem, and include several works which address vegetative change in subalpine regions using repeat photography (Ellison 1954; Gruell 1983; Strickler 1961; Strickler & Hall 1980; Vale 1987; Vankat & Major 1978). These studies illustrate both the utility of using multi-decade photographic records for assessing land cover change and the dependence on quantitative descriptions of change in lieu of a solution to the problem of varying spatial scale. For example, Vale (1987) used 59 photo pairs of Yosemite National Park (1903-1985) to assess land cover change in alpine and subalpine regions; 11 repeat photographs featuring krummholz were compared, with the finding that krummholz only increased aerial footprint in one photograph. However, krummholz patches were described as growing taller in the majority of photographs. Trees at or near treeline were depicted in 22 of the photographs,

and in 21 photographs stand density appears to increase. Vale (1987) also noted that alpine meadows surrounded by forest appeared to experience encroachment by trees, and that isolated instances of lone trees above treeline were more frequent in the 1985 images. In similar research, also conducted at Sequoia National Park, Vankat and Major (1978) reported an apparent increase in cover and density of subalpine stands (mainly *Pinus sp.*, 2900-3700 m), using repeat photography from the period 1912-1977.

The clearest attempt to provide a more quantitative analysis of land cover change in subalpine regions is seen in Roush et al. (2007). This method compared historical and contemporary photographs of Glacier National Park, Montana, through the application of a *fishnet* in a GIS; each fishnet polygon is overlaid on the same region of the historical and contemporary photos. By ensuring that the same two-dimensional area of each image is analyzed, this method uses a standardized classification and comparison of land cover. However, as the fishnet was not wrapped to the topography depicted in the image, thus not orthorectified, it could not be considered truly spatially quantitative. The three-dimensional area in one fishnet polygon may differ dramatically from another, as a function of perspective and slope. Further innovation to the fishnet method by Roush et al. (2007) was required before fully quantitative spatial analysis of planimetrically correct oblique photographs was achieved.

2.2.2 The Stockdale Method

The prior limitations for planimetrically correct quantitative analysis of oblique photography have been overcome with the advent of software like the WSL Monoplotting Tool (WSL-MT, note: WSL is the German acronym for "*Eidgenössische*

Forschungsanstalt für Wald, Schnee und Landschaft" the Swiss Federal Institute for Forest, Snow and Landscape Research). This software produces georeferenced vector data from oblique photographs, using tie points between oblique and aerial photographs and their high resolution topographic data (Bozzini et al. 2012).

The Stockdale method, introduced in Stockdale et al. (2015), is used for two distinct, but related purposes: 1) the method measures accuracy of the georeferenced vector data output from WSL-MT; and 2) the method introduces a procedure to classify and rasterize land cover from oblique photographs, using the WSL-MT. This summary will focus on the accuracy method, reviewing the theory behind the operation of the WSL-MT, and fully describing the error analysis method. The methods section of this chapter will provide a synopsis of the rasterization method, and an overview of how the method was adapted to study ATE.

2.2.3 Monoplotting Theory

Monoplotting, the technique employed by the WSL-MT, is the process of extracting three-dimensional data from a single image (Aumann & Eder 1996). The purpose of monoplotting is to determine the object-space coordinates (i.e. X, Y, Z coordinates) of an object that is depicted in a two-dimensional image. Monoplotting utilizes three related sets of information to extract the object-space coordinates of an imaged objected: the first set contains the external parameters of the camera, including the object-space, X, Y, Z coordinates of the camera, and the rotation angles of the camera along X, Y, and Z axes (i.e. ω, ϕ, κ); the second set contains the internal parameters of the camera, including focal length and principal point; the third set contains the two-

dimension point location of the object on the image plane (Strausz & Doel 2001). A collinearity condition exists between the object-space location of the camera, the two-dimensional point location on the image, and the object-space location of the imaged object; that is, a line can be drawn from the camera origin, through the image plane, to the object in the image (Figure 2.1).

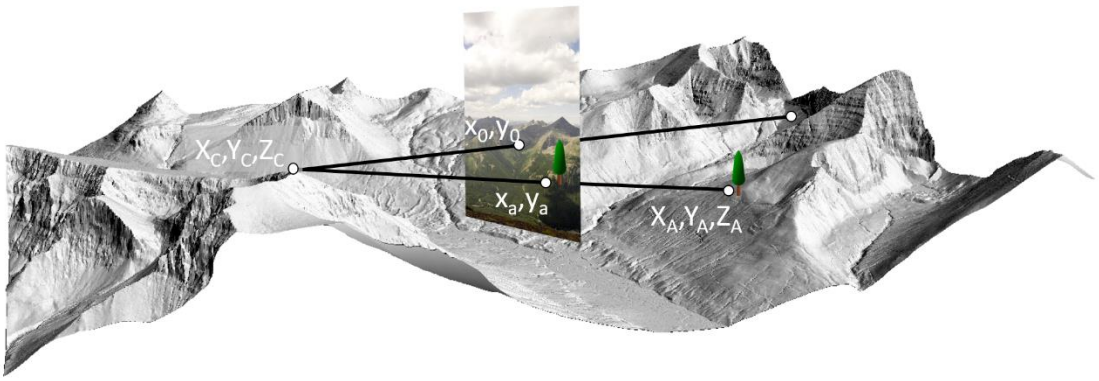

Figure 2.1 - Parameters for the monoplotting collinearity equations (Eq. 2.1 & 2.2), depicted over a three-dimensional hill shade of WCW. Image #7, provided by the Mountain Legacy Project (Trant et al. 2015), is used as an example of two-dimensional image space. Notation provided in text.

The two-dimensional image point location can be expressed in terms of the internal and external camera parameters, and the object-space coordinates of the imaged object, using the following collinearity equations from Strausz and Doel (2001):

$$x_a = x_0 - f \frac{m_{11}(X_A - X_C) + m_{12}(Y_A - Y_C) + m_{13}(Z_A - Z_C)}{m_{31}(X_A - X_C) + m_{32}(Y_A - Y_C) + m_{33}(Z_A - Z_C)} \quad \text{(Eq. 2.1)}$$

$$y_a = y_0 - f \frac{m_{21}(X_A - X_C) + m_{22}(Y_A - Y_C) + m_{23}(Z_A - Z_C)}{m_{31}(X_A - X_C) + m_{32}(Y_A - Y_C) + m_{33}(Z_A - Z_C)} \quad \text{(Eq. 2.2)}$$

Where x_a and y_a are the object's image coordinates, x_0 and y_0 are the central points of the image (i.e. the principal point), f is the focal length, X_A, Y_A, *and* Z_A are the object-

space coordinates of the imaged object, X_c, Y_c, *and* Z_c, are the camera's object-space coordinates, and *m11 - m33* are functions of the rotation angles which are used to transform the image from oblique to orthogonal orientation (see Appendix A of Strausz and Doel (2001) for full derivation of Equations 1 and 2).

While the collinearity calculations that enable repeat photography camera orientation have long been understood (Abdel-Aziz & Karara 1971; Harrison 1974; Thompson 1966), limited computational power prevented oblique to orthogonal transformation methods from becoming wide-spread. As computational power increased, early examples of monoplotting software are seen in OPX-FORM (Doytsher & Hall 1997), the Juke method (Aschenwald et al. 2001), 3D monoplotter (Mitishita et al. 2004), and DiMoTep (Fluehler et al. 2005). One of the more widely used early monoplotting methods, by Corripio (2004), had the user rotate the DEM until it aligned with an oblique image, before fixing control points. While useful, this method was noted for not being intuitive or user-friendly (Bozzini et al. 2012; Stockdale et al. 2015).

The WSL-MT is the most recent attempt at monoplotting software, providing several easy-to-use functions for converting oblique imagery to orthogonal vector data, and vice versa (Bozzini et al. 2012). WSL-MT requires at least two complementary datasets to perform the collinearity calculation: an oblique photograph and a high-resolution DEM (recommended < 2 m). Control points are selected from the image (i.e. pixel coordinates, row number x column number), and matched to object-space control points. Ideally, object-space control points are surveyed using a precision geographic positioning system, but the acquisition of survey points can be cumbersome and is not cost-effective in many environments. If no precision survey points are available, high-

resolution aerial photography can be coregistered with the DEM; easily distinguishable features, such as boulders and single trees, are selected from the aerial imagery, and their object-space coordinates are extracted from the coregistered DEM. It is recommended that control points be placed away from ridges or mountain peaks, as a slight translation of the point can result in the point being projected beyond the horizon (Stockdale et al. 2015).

Once the WSL-MT has calculated a camera calibration, it provides the ability to transform vector data from oblique to orthogonal projections. The *Pixel to World* function transforms data from pixel coordinates to object-space coordinates (e.g. X, Y, Z UTM coordinates). Conversely, the *World to Pixel* function transforms object-space coordinates to pixel coordinates.

2.2.4 Monoplotting Error Analysis

While a handful of publications have used the WSL-MT (Conedera et al. 2013; Kolecka et al. 2015; Scapozza et al. 2014), Stockdale et al. (2015) was the first to test the accuracy of its vectorized output by using an iterative process of angle error reduction. As the user places control points, the accuracy of point placement is assessed through the reduction of angle error. Figure 2.2 illustrates how the user places control points on the two-dimensional image at point *p*, and on the coregistered aerial image/DEM at point *P*. Ray *rp* describes a line from the camera origin (*O*), through the control point on the two-dimensional image (*p*), terminating at the real-world X, Y, Z coordinate (*P*). After a minimum of 5-6 control points have been placed, the user prompts the software to solve the collinearity equations iteratively. Ray rp’ is drawn between the origin and control

points in the resulting camera calibration, as computed by the software. In theory, if both points *p* and *P* were placed perfectly, and no other error was introduced, ray *rp'* would perfectly align with ray *rp*. In practice, the angle between rp and rp', α(rp',rp), shows the magnitude of error for a given control point and is thus referred to as the 'angle error' for that control point (Stockdale et al. (2015). This error may reflect inaccurate control point placement, lens distortion, DEM inaccuracy, or a host of other factors. For camera calibration to be considered adequate, the mean angle error of these registration points should be less than 0.1°.

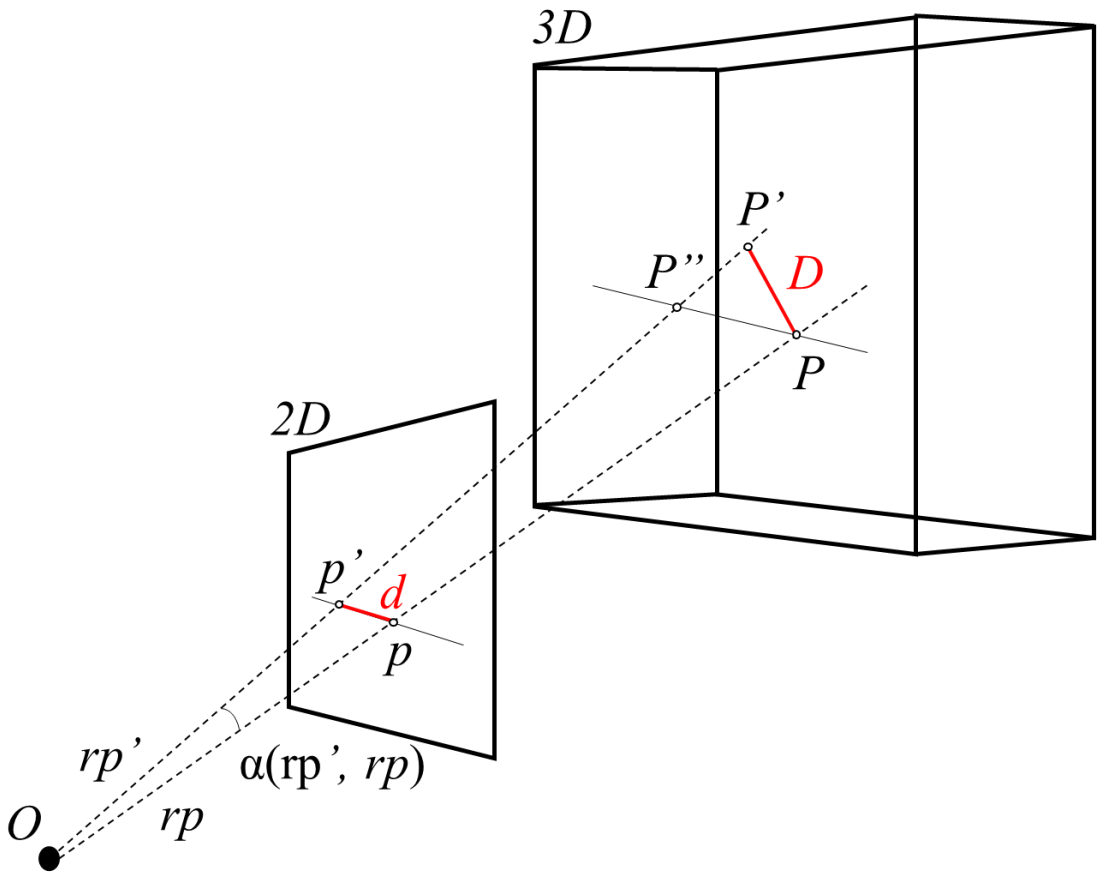

Figure 2.2 - Diagram of angle error and error vector length measurement. Adapted from Stockdale et al. (2015).

Stockdale et al. (2015) propose a standardized method of control point selection which was demonstrated to reduce angle error. Here, the two-dimensional image is divided into three vertical and three horizontal fields, with two or three control points sampled from each field, and a minimum of 21 control points. Following the initial camera calibration, the three control points with the highest angle error are omitted, and the calibration is rerun. Omitted points are referred to as *test points*, and points used for the subsequent calibration are referred to as *registration points*. The process of removing the three test points with the highest angle error is repeated, iteratively, until the six registration points resulting in the lowest angle error remain.

Angle error is a useful metric for assessing camera calibration precision but reveals little about the accuracy of points projected from an oblique to an orthogonal perspective. The Stockdale method tests the accuracy of the WST-MT vector functions by running the object-space coordinates of the discarded test points through the final camera calibration. In effect, this turns each initial, real world coordinate into *P*, and each output point into *P'*. The three-dimensional distance of a line drawn between point *P* and *P'* is measured in a GIS. This distance is referred to as the *error vector length* for that pair of points (i.e. distance *D*, Figure 2.2). Mean error vector length is the average error vector length calculated for all point pairs in a given image.

Systematic shifts in the entire distribution of points can be investigated by looking at the displacement error. To do this, a centroid is generated for both the set of test point coordinates (*P)* and the set of projected test point coordinates (*P'*), within a given image. The three-dimensional distance between these centroids is the *displacement error*. A displacement error that is substantially lower than the mean error vector length suggests

that the error vector length between given pairs of points occurs in a variety of directions and magnitudes, such that they cancel themselves out when examining the whole set. A displacement error that approximates the mean error vector length suggests that the error vector between pairs of test points occurs in similar directions and that the entire set of points is translated in the same direction during projection.

In order to understand factors which contribute to error vector length, Stockdale et al. (2015) modeled vector error length as a function of distance from the camera origin, and *angle of viewing incidence.* This is the angle between the ray connecting the camera origin to the control point and a 10 m ground-line segment, which runs parallel to the ray and is centered on the control point. To model error vector length, Stockdale et al. (2015) executed a general linear model in SPSS 24 (IBM 2016), using the formula:

$$\nu = b + \beta I + \beta D + \beta A \qquad \text{(Eq. 2.3)}$$

where ν the error vector length (m), b is the intercept, I is image number (unitless, used as a random factor), D is the distance to the camera (m), A is the angle of viewing incidence (°), and β is the model coefficient for each parameter (unitless).

2.2.5 Lidar and WSL-MT

The high spatial resolution of airborne lidar makes it a promising candidate for validation of oblique photograph analysis, but at the time of writing, only a single study is known to have validated land cover data generated from the WSL-MT using vegetation measurements from airborne lidar (Kolecka et al. 2015). In that study, lidar-derived estimates of vegetation height and canopy cover were compared to areas of forest succession mapped from oblique photographs, with an overall accuracy of 95%.

The present research compares manual estimates of ATE canopy cover from oblique photography with lidar-derived estimates of fractional cover, at a spatial resolution which is sufficiently high to observe and measure shifts in the ATE over a century scale photographic record (i.e. ~20 m). The rationale for comparing oblique photogrammetric and lidar canopy cover estimates is that temporal change analysis is assumed most effective when the image data being compared are analogous. It is more logical to assess change from contemporary and historical oblique photographs than, say, historical oblique imagery and contemporary lidar. However, lidar is a reliable and widely used technique of contemporary canopy cover assessment, so comparing canopy cover data derived from contemporary oblique photographs and lidar enables long-term change assessments to be placed into a modern context with wide-ranging applicability.

2.3 Methods

2.3.1 Study Area

The study was conducted at the West Castle Watershed (WCW), Alberta, Canada (49.3° N, 114.4° W). WCW is in the headwaters of the Oldman River, on the eastern slopes of the Canadian Rockies, with an area of ~103 km^2, and an elevation range of ~1400-2600 m a.s.l. Aside from a small ski resort and village near the downstream end of the WCW, covering 2.9% of the watershed area, and trails in the valley bottoms, the forested slopes demonstrate limited anthropogenic disturbance, and have not been subject to mountain pine beetle infestation. Consequently, the WCW is an ideal study area for assessing recent natural shifts in the ATE of this part of the Canadian Rockies.

2.3.2 Data

Seven high-resolution oblique photographs of the WCW were selected from a set of 46 provided by the Mountain Legacy Project (MLP). MLP is a collection of over 120,000 historic survey images of the Canadian Rockies (1888 – 1958), of which over 6,000 have been re-photographed in the 21st-century (Trant et al. 2015). The seven selected photographs were chosen to maximize the spatial coverage of the watershed, while also providing areas of overlap for classification error analysis. All photographs were taken in August 2006, and geolocations for photograph origins were provided by the MLP (Figure 2.3, Table 2.1).

An airborne lidar survey of WCW was flown on 18 October 2014 using a Leica ALS70 with a minimal point spacing of 3 pts/m^2 at nominal altitude (1300 m above the mean ground surface elevation). Lidar point cloud processing and fractional cover analysis followed the canopy-to-total returns method described in Hopkinson and Chasmer (2009). Data were classified into ground and non-ground using *Terrascan* (Terrasolid, Finland) and a 1 m DEM was interpolated from the ground classified points and aggregated using mean values to match the 20 m canopy cover classification. For aerial imagery requirement of the WSL-MT workflow, this study used SPOT 6 data (1.5 m, acquired 31 July 2014, © 2014 CNES, Licensed by BlackBridge Geomatics, www.blackbridge.com; purchased by Planet Labs Inc., 2015).

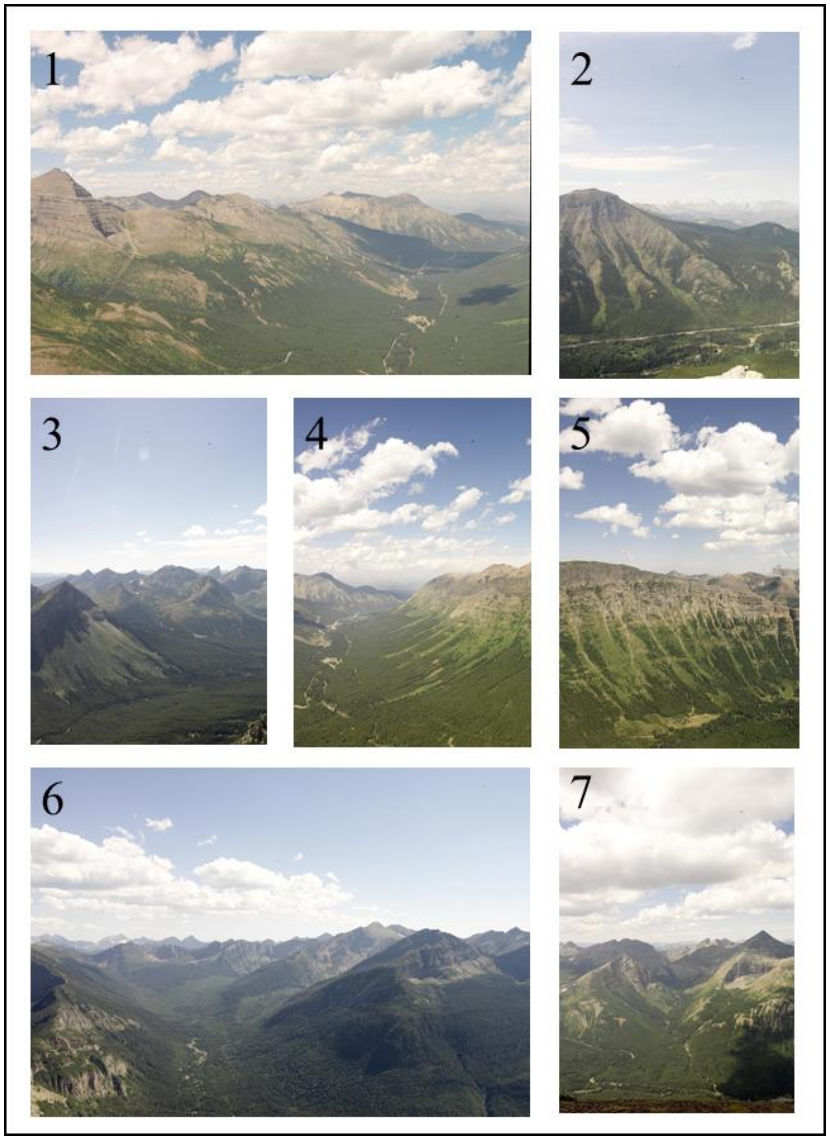

Figure 2.3 - Seven photographs of West Castle Watershed, captured by the Mountain Legacy Project, July 2006.

Table 2.1 - MLP photograph capture data.

Photograph Number	Elevation (m a.s.l.)	Latitude °N	Longitude °W	Photograph Date
1	2295	49° 16′ 3.62′′	114° 22′ 58.97′′	28 July, 2006
2	2216	49° 20′ 14.0′′	114° 23′ 22.81′′	29 July, 2006
3	2390	49° 17′ 7.01′′	114° 20′ 44.21′′	28 July, 2006
4	2283	49° 16′ 4.94′′	114° 22′ 56.77′′	28 July, 2006
5	2283	49° 16′ 4.94′′	114° 22′ 56.77′′	28 July, 2006
6	2390	49° 17′ 7.01′′	114° 20′ 44.21′′	28 July, 2006
7	2462	49° 18′ 7.26′′	114° 22′ 18.63′′	30 July, 2006

2.3.3 Oblique Photograph Registration and Error Modeling

The Stockdale method of iterative angle error reduction was used for each of the seven MLP photographs. For this purpose, 21 control points were placed on each photo, resulting in six registration points and 15 discarded test points after five camera calibrations. Mean error vector length and displacement errors were calculated using the 15 discarded test points from the camera calibrations. Additionally, landscape level measurements of mean error vector length and displacement were completed by aggregating points from all seven images into a single set, using all available test points.

Error vector length was modeled using a general linear model, executed in SPSS 24 (IBM 2016), using Eq. 3. Additionally, an *observation-parameter routine* was constructed (see Appendix A for scripts) which calculates the distance to the camera and angle of viewing incidence for any set of points on the DEM using a Python script in ArcGIS 10.3 (Esri 2014). Measuring the distance and angle parameters allows the modeled error vector length to be applied to any observation grid cell in the watershed.

2.3.4 Canopy Classification

Rasterized canopy cover data were generated from oblique photographs, using WSL-MT and the Stockdale method of angle error reduction. While the WSL-MT typically converts vector data from oblique to orthogonal perspective, a method described by Stockdale et al. (2015) to convert oblique vector data into raster data was adapted and followed here. Camera parameters were exported to ArcGIS 10.3 (Esri 2014), where the 1 m lidar DEM was used to create a viewshed for the image (Figure 2.4b). A 20 x 20 m fishnet (i.e. 400 m^2 grid cells) was overlain and clipped to the viewshed, and grid cells

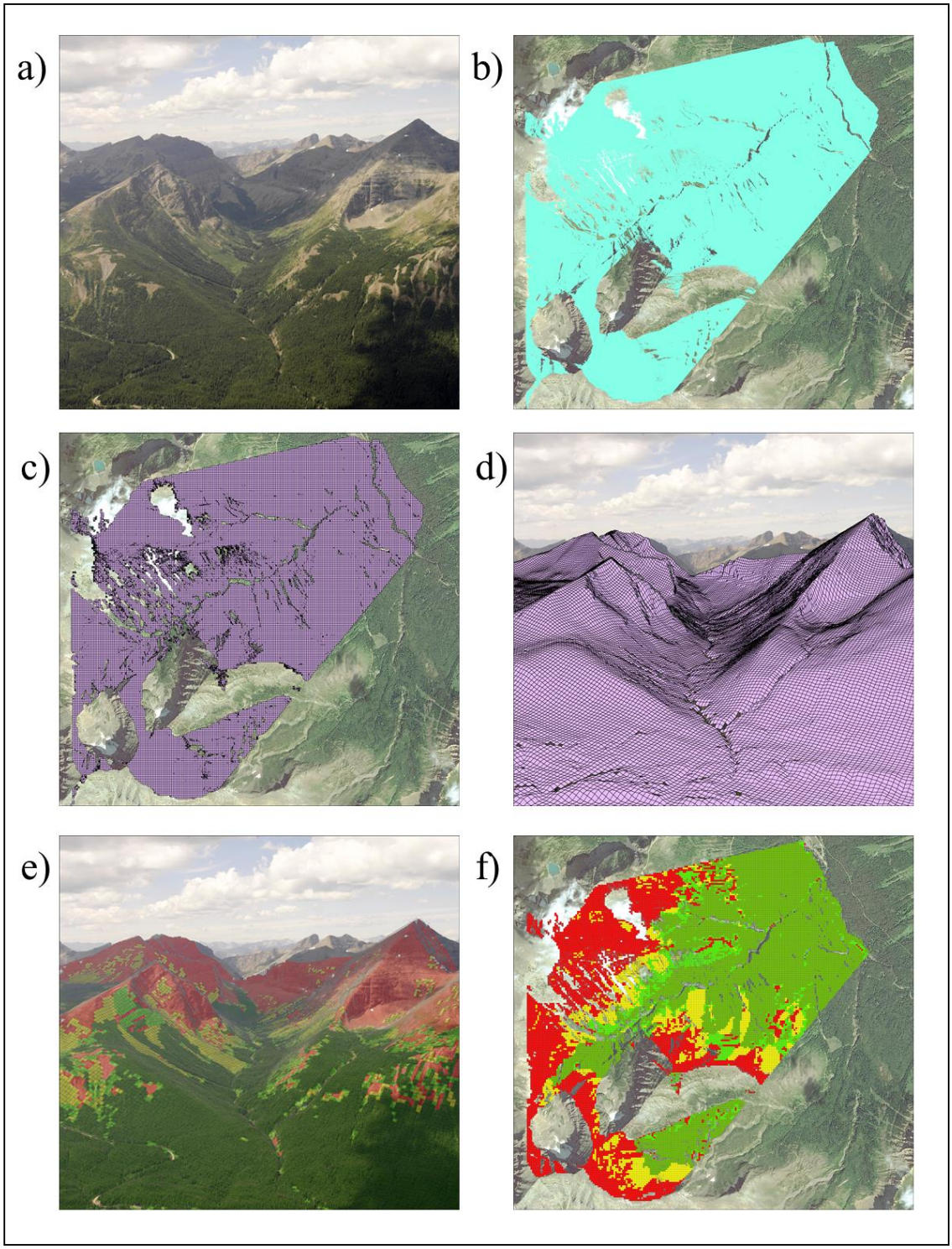

Figure 2.4 - The oblique photograph to raster workflow: a) an oblique image of Mount Haig from MLP; b) orthogonal viewshed of oblique Mount Haig image; c) 20 x 20 m fishnet applied to viewshed; d) obliquely transformed fishnet; e) canopy-cover classified oblique fishnet; f) canopy-cover classified orthogonal raster.

with < 75% coverage (i.e. < 300 m^2) omitted (Figure 2.4c). The *World to Pixel* function of the WSL-MT was used to project fishnet grid cells from UTM coordinates to pixel coordinates, allowing the 20 x 20 m grid cells to be draped over the oblique image (Figure 2.4d). Once in an oblique projection, grid cells were manually assigned into one of six canopy cover classes based on observed canopy openness and texture (Figure 2.4e), and classified oblique images were converted back to orthogonal view for comparative analysis (Figure 2.4f).

Visual estimates of canopy cover from photography are commonplace and can be compared with the lidar-derived fractional cover. The six canopy cover classes are: 1) *No Cover* – grid cells devoid of vegetation; 2) *Low Vegetation* – grid cells appear vegetated, but context and texture suggest shrubs or krummholz, not upright trees > 2 m; 3) *Partial Canopy* – trees are present, but ground is visible in > 50% of the grid cell; 4) *Full Canopy* – trees cover > 50% of a grid cell; 5) *Snow* – snow covers > 50% of a grid cell; 6) *Structure* – any anthropogenic disturbance (e.g. roads, buildings, trails) that is present in the grid cell.

Classification of canopy cover was completed by the author. While it is well-known that manual photograph interpretation is subject to error introduced by misregistration and interpreter bias, which precludes single interpreter analysis, recent studies of fractional cover assessment from aerial imagery have established multi-interpreter agreement using a second interpreter, working on a subset (5-10%) of the data (Nowak & Greenfield 2012; Ucar et al. 2016). A second interpreter classified canopy cover in a random selection of 5% of the observed grid cells, using the same criteria.

Grid cells that extended above ridgelines or the horizon were manually omitted from the analysis, along with any cells that extended beyond the perimeter of the oblique photograph once projected to oblique view; together, these are referred to as *perimeter omissions*. Using the Alberta Vegetation Inventory (Alberta Environment and Parks 2012), vector data for known areas of disturbance (e.g. former cut blocks, oil well pads, roads, ski resort, and a small burn area) were aggregated into a single layer, and any grid cells intersecting with this disturbance layer were omitted; together, these are referred to as *disturbance omissions*. Change in the disturbance area is addressed in chapter four. A summary of the areas of perimeter and disturbance omission can be found in Table 2.2.

Table 2.2 - Areas of perimeter and disturbance omission.

Photograph Number	**Original Area (m^2)**	**Perimeter Omission Area (m^2)**	**% Removed**	**Disturbance Omission Area (m^2)**	**% Removed**
1	13,169,322	346,409	2.6%	2,797,655	21.2%
2	1,632,105	9,729	0.6%	171,929	10.5%
3	8,523,883	194,629	2.3%	31,888	0.4%
4	9,093,506	114,061	1.3%	743,548	8.2%
5	2,486,079	43,052	1.7%	197,918	8.0%
6	15,269,892	569,722	3.7%	4,504,871	29.5%
7	8,679,340	520,110	6.0%	0	-
Weighted Mean	8,407,732	-	3.1%	-	16.8%

2.3.5 Multiple Observations

Photographs with overlapping extents were intentionally selected to test classification correspondence between images. The accuracy of canopy cover classifications was assessed by determining whether the minimum and maximum classification values for each grid cell agreed or disagreed. In cases of disagreement between observations, the canopy cover classification from the image with the lowest

error vector length (as modeled by the *observation-parameter routine*) for that distinct grid cell was selected. The resulting grid cells, each having the canopy cover class with the lowest modeled error, were used for the fractional cover analysis.

2.3.6 Fractional Cover Analysis

Fractional cover was calculated using the LAStools suite (Isenburg 2013); data were height normalized, and *lascanopy* was applied with a height threshold of 2.0 m, and a step of 20 m, in order to match the canopy cover classification grid.

Fractional cover, as a metric, treats canopy cover as a continuous variable (i.e. a percentage, 0-100%). To compare the agreement between fractional cover and manually classified canopy cover, which has discrete, ordinal classes, the measurement of fractional cover was discretized into four classes. Because no logical break points existed *a priori*, three common unsupervised discretization methods were used: equal frequency, equal range, and k-means. We tested agreement between manual interpretation and ordinal, binned classes of fractional cover using Cohen's kappa, weighted linearly (Cohen 1968).

As the results may have been influenced by expected areas of homogenous *full canopy* cover at lower elevations and *no cover* at higher elevations, each analysis was run twice; once using all observed areas, and once restricted to elevations between 1800-2300 m a.s.l., where ATE is expected to cause more variability in canopy cover.

2.4 Results

2.4.1 Multiple Interpreter Results

Overall correspondence between the primary and secondary interpreter was 88.4%, and weighted kappa showed substantial agreement between interpretations (kappa = 0.79, n = 5571, $p < 0.001$). When elevations were restricted to the more variable ATE region, correspondence dropped to 74.1%, with weighted kappa again showing substantial agreement (kappa = 0.73, n = 2161, $p < 0.001$).

2.4.2 Error Reduction Results

Iterative angle error reduction successfully lowered the mean angle error of registration points below the 0.1° threshold (Stockdale et al. 2015) for accurate camera calibration of each image. Average mean angle error for the set of seven photographs was 0.014°, with respective low and high values of 0.009° and 0.025° (Table 2.3). Test points were reserved for testing mean error vector length in each image, but in all seven cases, the WSL-MT omitted points from the projection routine, possibly due to errors in the camera calibration. The total number of available test points was 64. The number of test points per image ranged from 6 to 13. Using the available test points, mean error vector length ranged from 2.0 m to 63.8 m, with a mean of 23.9 m among the seven images. Mean displacement ranged from 0.8 m to 39.5 m, with a mean of 14.4 m among the seven images. In the landscape level analysis of 64 aggregated points, mean error vector length was 21.7 m and displacement was 7.0 m.

2.4.3 Error Model Results

The initial general linear model of vector error length used 64 test points, as described in the previous section. As general linear models assume that the residuals of the dependent variable are normally distributed, vector error length data were tested for normality using a Shapiro-Wilk test, which demonstrated that the data were not normally distributed ($W = 541$, $n = 64$, $p < 0.001$). Two outliers were identified and removed; these outliers had vector error length values of 177.7 m and 192.1 m (the next highest value was 78.0 m) and occurred in different images (image #6 and #3, respectively). The results of the log transformation were adequate to proceed with the general linear model, without violating normality assumptions. The truncated sample of 62 values responded to a common log transformation, with a Shapiro-Wilk test failing to reject normality ($W = 9.65$, $n = 62$, $p = 0.076$). The general linear model yielded the following equation:

$$\log(v) = b + \beta I + 0.000077D + 0.009A \qquad \text{(Eq. 2.4)}$$

All factors were significant at $\alpha = 0.05$, except for D ($f = 1.278$, $p = 0.263$). Using the coefficients from the general linear model and the *observation-parameter routine*, error vector length was modeled for each grid cell in the observation area (Figure 2.5a). In cases of multiple observations, the values from the image with the lowest modeled error were selected (Figure 2.5b). Mean error vector length for the model was 14.6 m, and ranged between 0.9 m and 75.7 m (Table 2.3); these values were comparable to the mean and range of the truncated dataset used to develop the model.

Table 2.3 - Summary of control point accuracy with measurement of error vector length and displacement

Photograph Number	# of Registration Points	Mean Angle Error (°)	# of Test Points	Mean Error Vector Length (+/- SE)	Displacement Error (m)	Mean Distance from Camera (m) (Range)	Mean Angle of Viewing Incidence (°) (Range)
1	6	0.015	8	24.5 (7.9)	11.6	2,954.2 (2,082.6-3,693.0)	26.1 (16.3-45.9)
2	6	0.025	13	22.5 (5.5)	12.9	2,755.0 (2,092.0-3,481.2)	31.8 (18.8-44.7)
3	6	0.014	6	63.8 (24.8)	39.5	2,917.4 (2,506.4-3,273.1)	33.9 (22.6-57.3)
4	6	0.011	8	3.9 (0.6)	1.9	2,892.9 (2,191.2-4,460.6)	33.9 (20.6-50.1)
5	6	0.009	8	2.0 (0.7)	0.8	2,956.7 (2,404.5-3,304.3)	38.8 (14.3-55.4)
6	6	0.014	8	54.9 (19.4)	22.2	3,316.4 (2,578.8-4,058.7)	25.6 (10.6-37.5)
7	6	0.009	13	14.1 (3.9)	11.7	3,547.5 (2,489.9-5,221.1)	31.6 (18.6-49.5)
Mean		**0.014**	**9.3**	**23.9 (9.0)**	**14.4**	**3,048.6**	**31.7**
Landscape			**64**	**21.7 (4.3)**	**7.0**		
			62	**16.5 (2.3)**	**5.9**		
Model Error Vector Length			**119,306**	**14.6 (<0.1)**	**0.9-75.7**		

2.4.4 Canopy Classification

The first step in canopy classification was the manual omission of grid cells appearing over ridge lines, or outside the extent of oblique photographs, which reduced the area of observation by a mean 2.6% (Table 2.2). Next, areas which intersected with the disturbance layer (aggregated polygons of known cut blocks, infrastructure, oil well pads, and small fires) were omitted, which reduced the area by an additional 11.1%. This step resulted in the largest areas of omission, particularly in image #1, where the ski resort was omitted, and image #6, where a large area of historic cut blocks was omitted. On average, 86.3% of each image was preserved. Given the low frequency of *snow* and *structure* classifications, these canopy cover classifications were removed from the analysis. These classes are further considered in chapter four.

2.4.5 Multiple Observation Results

Multiple observations due to overlapping of images occurred in an area of 10.5 km^2, or 27.2% of the total observed area (Table 2.4). No area in the watershed was observed in more than three different images (Figure 2.6a). Comparison of multiple observation areas shows that 78.4% of the grid cells agreed between observations, while at least one classification value disagreed in 21.6% of cases (Figure 2.6b, Table 2.4).

2.4.6 Fractional Cover Results

Agreement between manual and fractional cover classes was generally consistent across discretization methods; accuracy ranged from 43.3-47.0%, and weighted K values

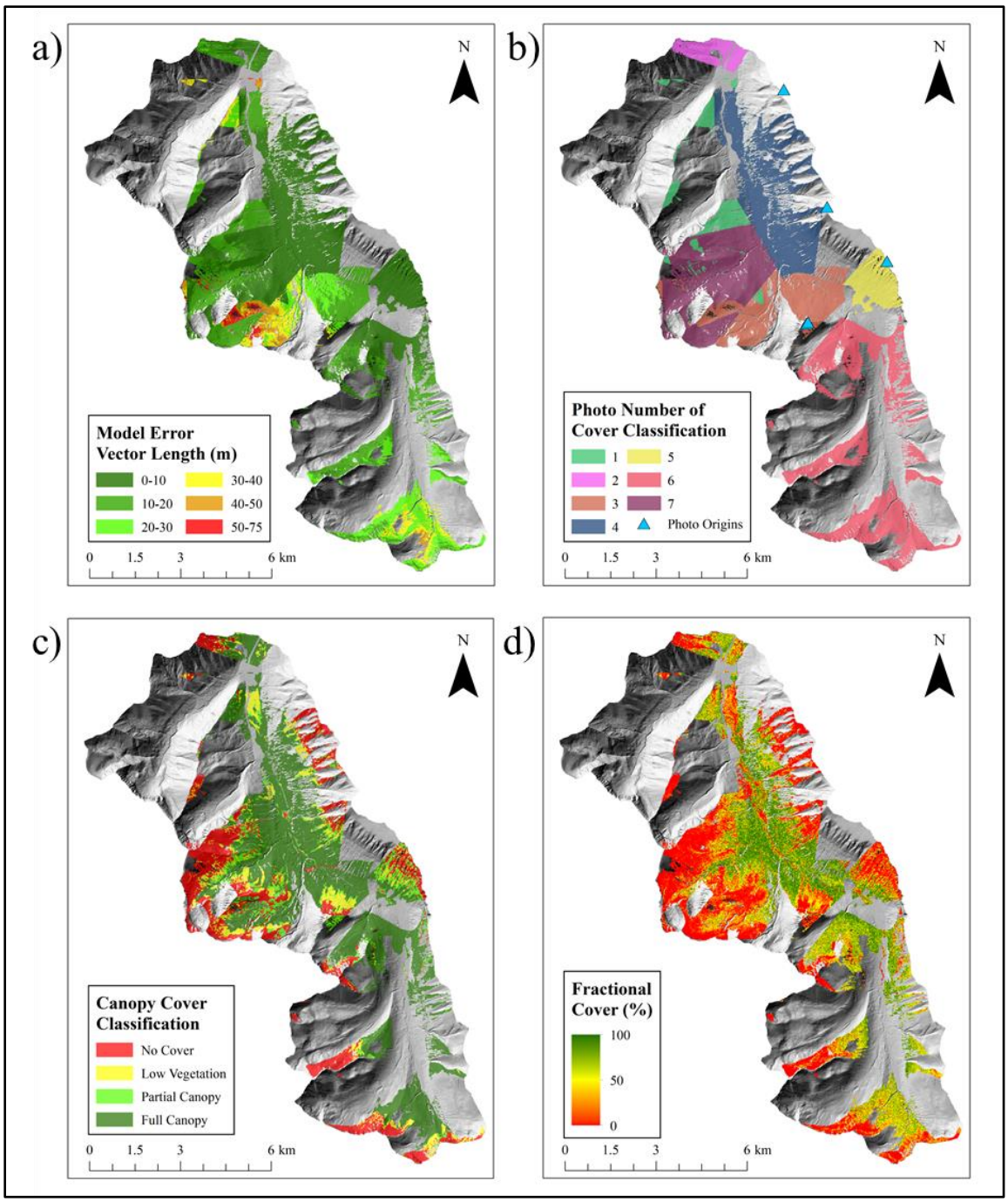

Figure 2.5 - Canopy classification results at the WCW area of interest: a) minimum error vector length; b) number of the photograph with the lowest modeled error; c) four-class manual canopy cover classification; d) lidar-derived fractional cover.

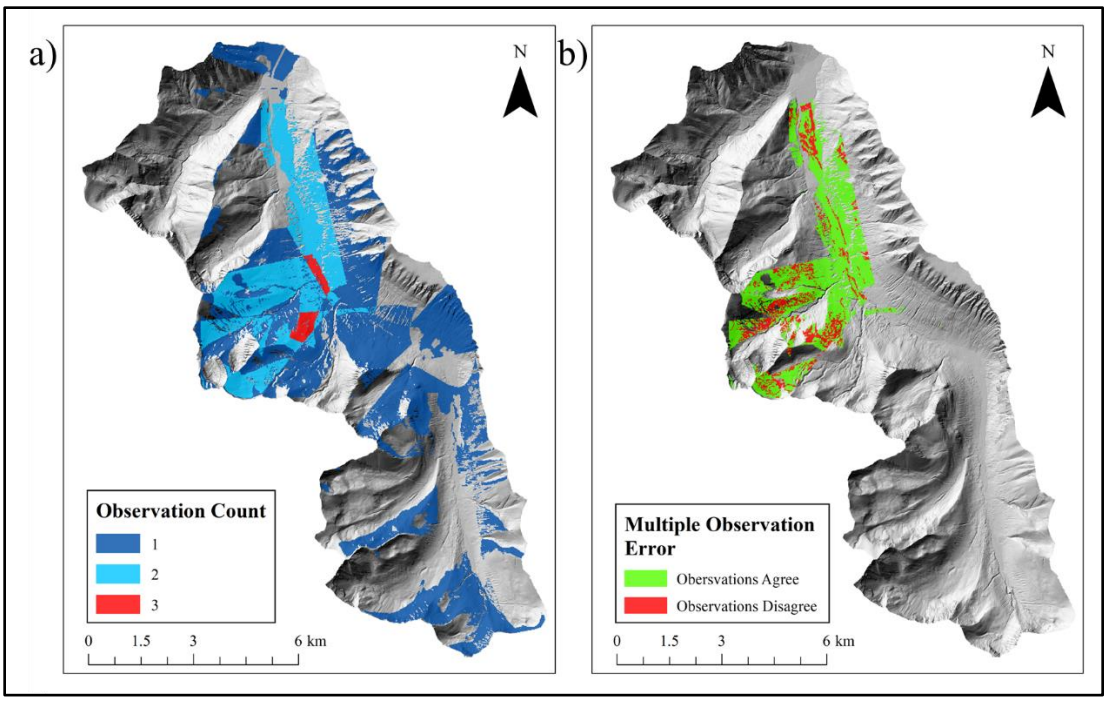

Figure 2.6 - Multiple observations: a) areas covered by either 1, 2, or 3 different oblique images; b) areas with multiple observations that either agreed or disagreed between 2 or 3 images.

Table 2.4 - Agreement of multiple observations.

Number of Observations	Area (km^2)	Percent of Observed Area
1	28.1	72.8%
2	9.8	25.4%
3	0.7	1.8%
Agree	8.3	78.4%
Disagree	2.3	21.6%

showing moderate agreement (kappa = 0.42-0.43, n = 115,438, $p < 0.001$) (Figure 2.7, Table 2.5). In the ATE, accuracy was only slightly reduced from the full watershed analysis, ranging from 39.4-46.0%, with weighted K values showing fair agreement (kappa = 0.35-0.36, 44,169, $p < 0.001$) (Table 2.5).

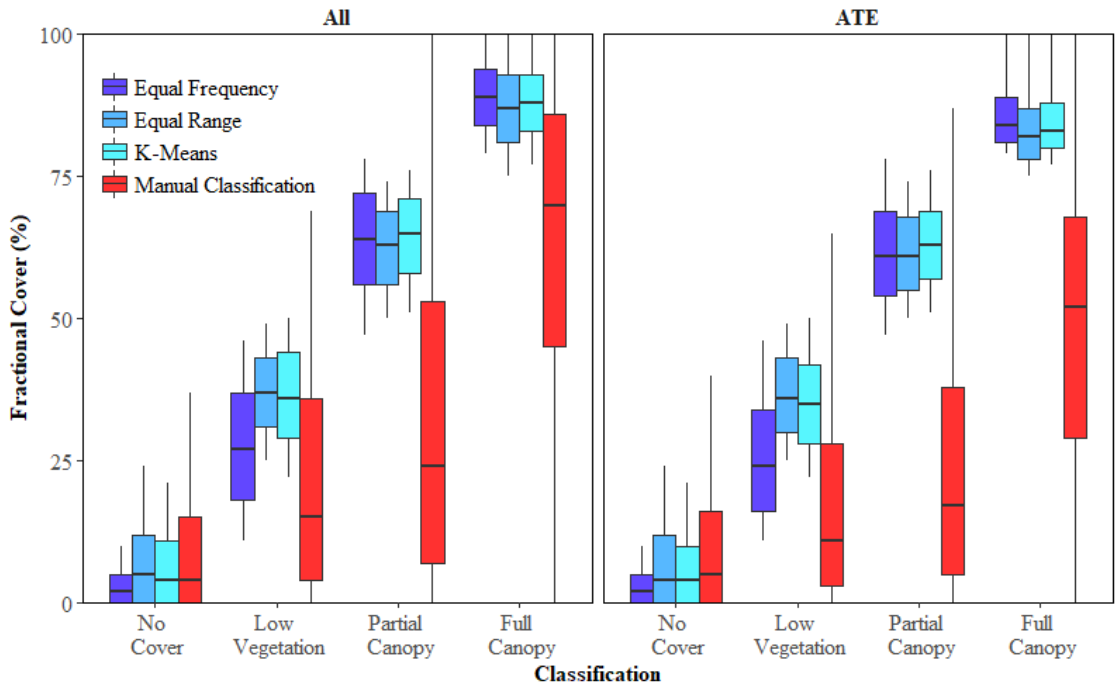

Figure 2.7 - Lidar-derived fractional cover values, discretized using three methods (i.e. equal frequency, equal range, and k-means); the boxplot depicts interquartile range for each of these groups, and compares their fractional cover distributions with those from manual cover classifications.

Table 2.5 - Agreement between manual classifications and discretized fractional cover.

	All			ATE		
Method	**Agreement**	**kappa**	**p-value**	**Agreement**	**kappa**	**p-value**
Equal Frequency	43.3%	0.420	< **.000**	39.5%	0.350	< **.000**
Equal Width	47.0%	0.428	< **.000**	46.0%	0.357	< **.000**
K-means	45.5%	0.418	< **.000**	46.0%	0.350	< **.000**
Manual Breaks	64.7%	0.539	< **.000**	52.4%	0.471	< **.000**

2.5 Discussion and Conclusions

The analysis presented in this chapter indicated that fractional cover across the ATE was reliably discriminated from oblique imagery at a resolution of 20 m. Mean error vector length and displacement error were both higher than error values calculated in

Stockdale et al. (2015). Mean error vector length was 23.9 m and landscape level displacement error was 7.0 m, while Stockdale et al. (2015) found errors of 14.4 m and 2.9 m, respectively. Following the removal of two outliers, mean error vector length and displacement error were reduced to 16.5 m and 5.9 m.

Several possibilities exist for the larger error observed in the present study. Stockdale et al. (2015) had a larger sample size of test points (n = 121), which resulted from fewer omissions in test point projection from WSL-MT. These omissions may have reflected higher error vector lengths than those seen in processed test points, making actual error vector length in the present study higher than reported. The range of values for *distance to camera* and *angle of viewing incidence* may have contributed to error differences. Average angle of viewing incidence in Stockdale et al. (2015) was 22.4°, but was 31.7° in the present study. Interestingly, the larger slope contributed to error vector length in the general linear model reported in this study (positive coefficient of *A* in Eq. 2.4), but would have reduced error vector length in the model of Stockdale et al. (2015) (negative coefficient of *A*). Distance to camera was not reported in Stockdale et al. (2015), and cannot be compared. Another potential cause of the discrepancy between error estimates is that aerial imagery used for control point selection in the previous study Stockdale et al. (2015) was at a resolution of 0.5 m, a roughly 3x higher resolution than the 1.5 m SPOT 6 data used in the present study. Higher resolution aerial imagery could have improved control point placement, reduced angle error, and contributed to a lower mean error vector length.

Regardless of the discrepancy, in the present study, mean error vector length was comparable to canopy cover grid cell resolution and displacement error remained

substantially below this resolution, demonstrating that surfaces can be rasterized from oblique photographs at a resolution of 20 m. This spatial resolution is an important threshold to reach for the application of the method to ATE observations, as it corresponds to the area of most forest mensuration plots (400 m^2), and permits cataloging of changes in the ATE given the expected rate of advance over the century scale observation period permitted by repeat photography.

Comparison of grid cells with multiple observations showed that canopy cover classification disagreed in 21.6% of cases. Disagreement cases were resolved using modeled error vector length, which produced values comparable to those in the observed error vector length; observed mean error vector length for the 62 test points used for model development was 16.5 m, with a range of 1.9-78.0 m, while modeled values had a mean of 14.6 m and a range of 0.9-75.7 m (Table 2.3). Stockdale et al. (2015) found that image number (*I*), distance to the camera (*D*), and angle of viewing incidence (*A*) all contributed significantly to the model, but in the model presented in this chapter, the factor of distance to the camera (*D*) was not significant. This may have been a result of different distance ranges between the two studies. Collectively, the results demonstrated that models of error vector length were useful in resolving cases of disagreement in oblique photograph classification. Angle of viewing incidence was considered the primary factor affecting displacement error, but this finding may have been contingent on the underlying distributions of slope in each study area.

Manual classifications of fractional cover from the oblique photographs were, in part, validated using lidar-derived fractional cover. Fractional cover distributions from manual classifications had increasing median values with each ordinal class (Figure 2.7)

in both the full watershed and ATE restricted analyses. While accuracy between the discretized fractional cover classes and the manual classes was generally low (< 47.0%) it is worth considering that this may have resulted from the fact that the discretization methods used were theoretical, and did not necessarily reflect real-world groups of fractional cover. For example, if lidar-derived fractional cover values are arranged in order, and partitioned into bins with frequency ratios proportional to those seen in the manual classifications, accuracy of 64.7% is reached (see Table 2.5, *Manual Breaks*). While this method is not a defensible validation, as it assumes that the manual classifications are the truth, it does demonstrate that the results of this analysis rely on partition points that are in some ways arbitrary.

With an abundance of repeat oblique photography in the Canadian Rockies (Trant et al. 2015), future research which combines quantitative analysis of oblique photography with lidar-derived forest structure data can increase the spatial resolution and temporal extent of ATE monitoring. These improvements are necessary as we continue to explore the impacts of climatic change on forested mountain ecosystems and downstream water resources.

Chapter 3 - Correlation Between Canopy Cover Change and Terrain Attributes in the ATE

3.1 Introduction

Alpine treeline ecotone (ATE), the transition zone between closed canopy forest and alpine tundra, occurs where tree growth is limited by thermal thresholds at high elevations (Körner 1998; Körner & Paulsen 2004). At continental scales, the approximate elevation of ATE is predicted by the *growth limitation hypothesis*, which suggests an inverse relationship exists between latitude and ATE elevation (Körner 1998) as a function of temperature in the growing season (Körner & Paulsen 2004). However, at landscape scales, modulating factors suppress treeline below this thermal limit, causing local variability in treeline elevation (Holtmeier & Broll 2005; Körner 2003a; Malanson et al. 2011). These modulating factors can include: physiological stressors, like moisture limitation (Elliott & Cowell 2015) and wind exposure (Broll & Holtmeier 2010); disturbances, like rockslides (Butler et al. 2007), avalanches (Walsh et al. 1994), and fires (Stine & Butler 2015); geomorphic conditions (Butler et al. 2007; Resler 2006); and numerous others factors (for detailed list, see Holtmeier (2009)). The relative influence of these modulating factors on ATE has been shown to vary by spatial scale (Case & Duncan 2014; Holtmeier & Broll 2005; Weiss et al. 2015). Less attention has been given to the potential for modulating factors to interact or covary, which may lead to a multi-scale, synergistic suppression of ATE below thermal elevation limits.

For an example of how modulating factors might be correlated, consider two often-cited factors, moisture limitation and fire disturbance, and their relationship to subalpine topography. Heating experiments in trees at ATE elevations have demonstrated

that moisture limitation both inhibits conifer seedling recruitment (Kueppers et al. 2017) and reduces carbon gain (Moyes et al. 2015). Direct observations of suppressed treeline on warm, dry aspects have also been linked to moisture limitations. Germino et al. (2002) found that survival of Engelmann spruce (*Picea engelmannii)* seedlings at treeline was reduced by 48% on south-facing aspects, and observed that recruitment success was highly correlated to annual precipitation. Elliott and Cowell (2015) demonstrated that interactions between temperature and precipitation were responsible for increased recruitment pulses on north-facing slopes during drought periods, leaving recruitment on south-facing aspects suppressed.

Fire is a natural disturbance agent in the ATE (Colombaroli et al. 2010; Stueve et al. 2009), and effects of fire on subalpine regions are potentially increasing with climate change (Cansler et al. 2016). Like moisture limitation, fire may also disproportionately affect warm, dry aspects. Rogeau and Armstrong (2017) demonstrated that fire return intervals for subalpine fir (*Abies lasiocarp*a) and Engelmann spruce stands in the Canadian Rockies bear evidence of topographic effects, particularly in subalpine areas. They showed that south-facing aspects were more than twice as likely to burn, while fire return intervals decreased by 33% with every 100 m of elevation gain. Consequently, cool, high-elevation aspects showed longer fire return intervals. This pattern was observed over a broad region of southern Alberta, suggesting the pattern is independent of prevailing wind or specific fire events.

If two distinct modulating factors correlate to the same topographic variable, as moisture limitation and fire disturbance appear to correlate with warm aspects, then it is necessary to develop the means to: 1) distinguish between their effect on ATE in relation

to each other; and 2) determine if there are interaction effects between factors. Change analysis is useful in this situation, given the long life-span of trees, and the potential for establishment patterns to lag decades behind causative factors (Körner 2003a). For example, a single observation of contemporary ATE with suppressed southern aspects would not readily indicate the cause of variations, but within a historical context, vegetation patterns might correlate to fire-exposure, moisture deficit, or other disturbance.

One of the challenges with assessing topographic effects on land cover change in the ATE is that the rate of change may vary, from rapid pulses of advance and catastrophic die-off (Elliott & Cowell 2015; Luckman & Kavanagh 1998), to more gradual upslope advance and downslope recession (Bekker 2005). ATE must therefore be observed at a high spatial resolution, in order to differentiate gradual processes from rapid ones. In the Canadian Rockies, there is evidence of both upslope advance and downslope recession in the ATE over the past 300 years. Luckman and Kavanagh (1998) found massive die-off of Engelmann spruce on south-facing aspects, that was coincident with a five-year period of extremely cold summers in the late 1600s. Bekker (2005) reported a subalpine fir advance rate of 0.28-0.62 m yr^{-1} along and upslope transect. Back-calculating from the reported values in Bekker (2005), a 100 year record would have seen ~45 m in upslope advance, which corresponds to a ~5 m increase in elevation, and a ~44 m planimetric change in cover (note: slope was not reported in Bekker but transect length and elevations were. Simple trigonometry showed that average slope was low, at 6.79°. Similar rates of change in steeper slope areas would increase the altitudinal gain, and reduce the planimetric area in which the change occurred).

Unfortunately, a trade-off exists between spatial resolution and temporal extent in ATE observation methods (Danby 2011). Multitemporal remote sensing can monitor vegetative land cover change at spatial resolutions required to correlate with topographic variables (10-100 m) (Stueve et al. 2009), but observations of ATE using passive optical satellite imagery, like Landsat TM (Allen & Walsh 1996; Walsh et al. 1994) can only extend back to the 1970-80s. Aerial photographs are similarly useful for treeline change monitoring (Danby & Hik 2007; Stueve et al. 2009), but aerial photography records only extend to the late 1940s and early 1950s for much of Canada. Conversely, ATE observation records with very long temporal extents often have poor spatial resolution, prohibiting topographic analysis. For example, palynological records extend thousands of years before present, with some exceeding 10,000 years (Tinner & Theurillat 2003), but these observations can only provide a spatial resolution equivalent to the seed distribution distance (> 100 m).

Dendrochronological records have offered the best combination of high spatial resolution (< 10 m) and high temporal extent (~1000 yr). Tree-ring records are often used in ATE studies (Bekker 2005; Elliott & Cowell 2015; Mamet & Kershaw 2012; Sakulich 2016). The spatial resolution and temporal extent of dendrochronological studies are both high, but the spatial extent is limited by onerous collection methods and the large sample size required to cover enough sites for topographic analysis (Elliott & Cowell 2015; Rogeau & Armstrong 2017).

The need for ATE observations that provide high spatial extent and resolution and long temporal range can be addressed with repeat photography. This method has been widely used to assess land cover change in the ATE: patterns of ATE advance in eastern

slope regions of the Canadian Rockies have been described using repeat photography (Butler & DeChano 2001; Butler et al. 1994; Klasner & Fagre 2002); high resolution photographs were used to identify shrub advance in the Swedish Scandes (Kullman & Öberg 2009); and for a description of land cover change in the Ural Mountains (Moiseev & Shiyatov 2003). While the temporal extent of repeat photographs, 100 years or more in cases, is useful for studies of change in the ATE, the method has been mostly restricted to qualitative analysis, given the previous inability to standardize spatial scale across oblique imagery. Roush et al. (2007) attempted a quantitative spatial analysis of ATE by draping a polygon *fishnet* over repeat photographs, in order to standardize the observation units in both historical and contemporary photographs, but spatial scale still varied between polygons, limiting this techniques usefulness for spatial analysis.

Recent technological advances have enabled fully quantitative spatial analysis of repeat photographs, using the WSL Monoplotting Tool (WSL-MT, note: WSL is the German acronym for "Eidgenössische Forschungsanstalt für Wald, Schnee und Landschaft", the Swiss Federal Institute for Forest, Snow and Landscape Research), which produces georeferenced vector data from oblique photographs using tie points between oblique and aerial photographs, and high resolution topographic data (Bozzini et al. 2012). Stockdale et al. (2015) introduced a technique to monitor land cover change, over a period of 100 years, at a spatial resolution of 100 m. McCaffrey and Hopkinson (2017), see also chapter two, used this technique to establish that fractional cover classes could be assessed from oblique imagery, at a spatial resolution of 20 m. Both experiments were conducted on photo pairs from the Mountain Legacy Project, a collection of over 120,000 historic survey images of the Canadian Rockies (1888 – 1958), of which over

6,000 have 21st-century repeat photographs available under creative commons license (Trant et al. 2015).

3.1.1 Research Goals

Given that the technique described in McCaffrey and Hopkinson (2017) provides the ability to assess fractional cover from oblique photographs, this method will be used to assess vegetative change in repeat photographs of a watershed in the Canadian Rockies. The goal of this research is two-fold: 1) to identify patterns of change in the ATE, and establish whether the technique could be used to observe correlation between change magnitude and topographic variables (elevation, slope, and aspect); 2) to compare the effect of a modulating factor, fire disturbance, on the relationship between change and topography. This research is intended as a proof of principle that repeat photography can be used to monitor change in the ATE, and that this can be accomplished at a spatial resolution which is sufficient to identify correlations between change and topography.

3.2 Methods

3.2.1 Study Area

The study was conducted over the West Castle Watershed (WCW), Alberta, Canada (49.3° N, 114.4° W). WCW is in the headwaters of the Oldman River, on the eastern slopes of the Canadian Rockies, with an area of ~103 km^2, and an elevation range of ~1400-2600 m a.s.l. Aside from a small ski resort and village near the downstream end of the WCW (2.9% of the watershed area), and trails in the valley bottoms, the forested slopes demonstrate limited anthropogenic disturbance, and have not been subject to

mountain pine beetle infestation. Consequently, the WCW is an ideal study area for assessing recent natural shifts in the ATE of this part of the Canadian Rockies. Dominant species at ATE elevation in WCW are subalpine fir and Engelmann spruce.

3.2.2 Repeat Photographs

Repeat photographs were provided by the Mountain Legacy Project (Trant et al. 2015). The historical images were taken in the summer of 1914 by Morrison Parsons Bridgeland, a well-known Dominion Land Surveyor. The precise dates of the historical photographs are unknown, but they were likely collected over the span of a few days. The broad expanse of the Canadian Rockies which Bridgeland surveyed in the summer of 1914 made return visits to WCW unlikely (MacLaren et al. 2005), and snow cover at high elevations is consistent across the photographs, suggesting acquisition within a few days. The repeat photographs were taken by the Mountain Legacy Project, over a three-day period in July of 2006, 92 years after the Bridgeland survey. Details of the repeat photographs are provided in Table 3.1.

Table 3.1 - Collection data for seven MLP photographs.

Photograph Number	Elevation (m a.s.l.)	Latitude °N	Longitude °W	Photograph Date
1	2295	49° 16´ 3.62”	114° 22´ 58.97”	28 July 2006
2	2216	49° 20´ 14.00”	114° 23´ 22.81”	29 July 2006
3	2390	49° 17´ 7.01”	114° 20´ 44.21”	28 July 2006
4	2283	49° 16´ 4.94”	114° 22´ 56.77”	28 July 2006
5	2283	49° 16´ 4.94”	114° 22´ 56.77”	28 July 2006
6	2390	49° 17´ 7.01”	114° 20´ 44.21”	28 July 2006
7	2462	49° 18´ 7.26”	114° 22´ 18.63”	30 July 2006

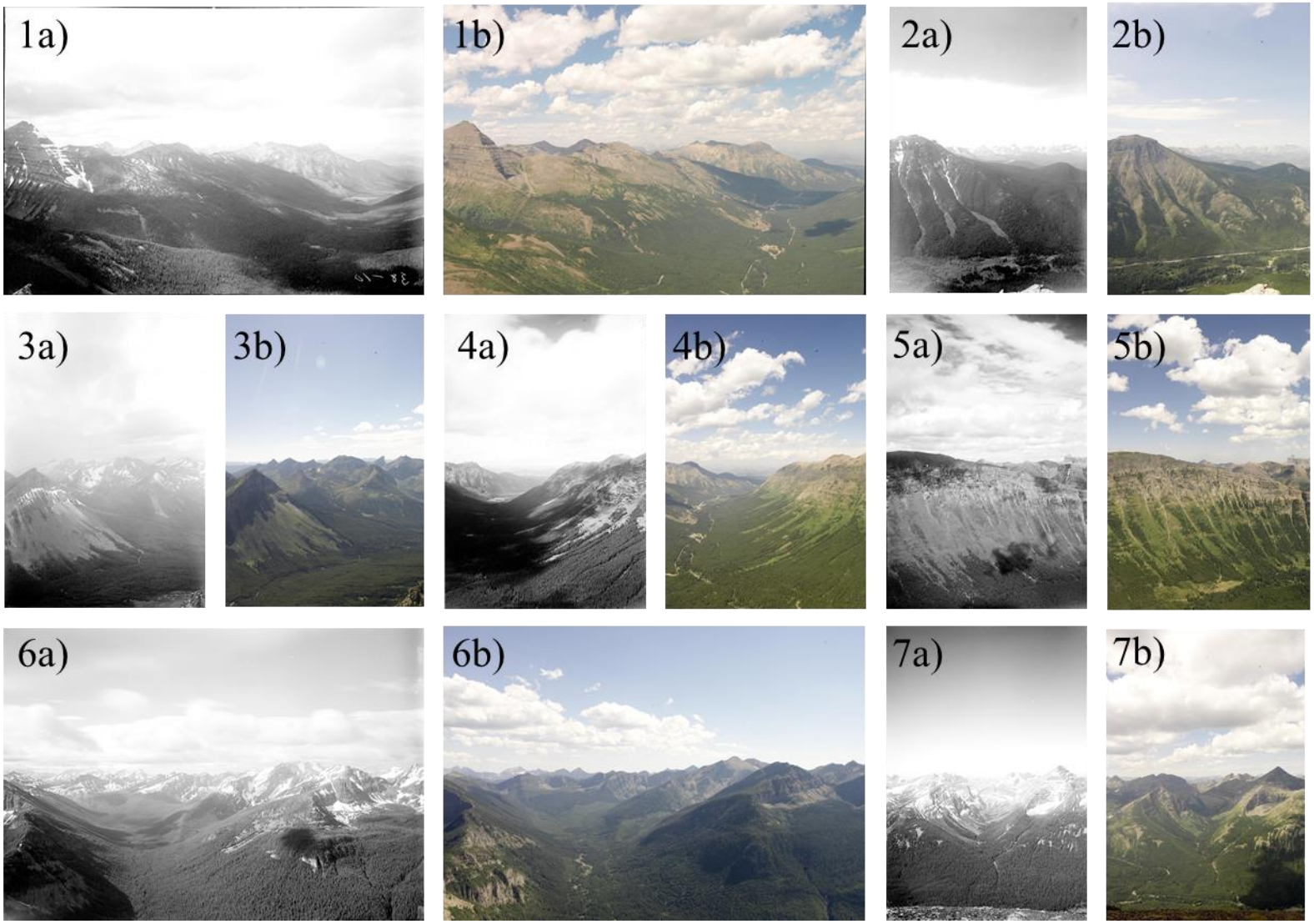

Figure 3.1 - Seven repeat photograph pairs of WCW; a-series by M.P. Bridgeland, 1914, courtesy of Library and Archives Canada; b-series copyright Mountain Legacy Project, 2006.

Photograph pairs were selected to maximize the spatial coverage of the observed area of WCW (Figure 3.1). McCaffrey and Hopkinson (2017) showed that the observation area was covered by multiple images in 27.2% of cases, and canopy cover classification disagreed in 21.6% of these cases. A general linear model, describing positional error as a function of distance to the camera and angle of viewing incidence, can be used as a decision criterion in cases of multiple observations (McCaffrey & Hopkinson 2017). When canopy cover classifications disagreed, the value from the image with the lowest modeled error was used for all analyses described in the present research.

3.2.3 Canopy Classification

Canopy cover was extracted from oblique photography with the WSL monoplotting tool (Bozzini et al. 2012), using a novel method described in detail in chapter two and McCaffrey and Hopkinson (2017). The method utilizes an oblique photograph rasterization technique, introduced by Stockdale et al. (2015), combined with a function of the WSL monoplotting tool (WSL-MT) which allows vector data to be transformed from oblique to orthogonal perspectives. An orthogonal fishnet vector of an area of interest was constructed at the desired step of the raster output (20 m). The fishnet was then transformed to an oblique perspective and overlaid on the oblique image, where land cover was manually assigned to each grid cell (previous work showed inter-operator agreement of manual fractional cover classification to be 88%). Finally, the fishnet vector was returned to an orthogonal perspective, where it was converted to a raster. This method circumvents the problem of varying spatial scale in the oblique image, allowing quantitative spatial analysis to be performed on the resulting raster.

The WSL-MT performs oblique to orthogonal vector transformation following camera calibration, which was achieved by pairing control points between oblique photographs and a high resolution DEM (< 2 m) that was co-registered with aerial imagery. For the DEM requirement, a 1 m DEM was used, which was collected from an airborne lidar survey in October 2014. For the aerial imagery requirement, a SPOT 6 image of WCW was used (1.5 m, acquired July 31, 2014, © 2014 CNES, Licensed by BlackBridge Geomatics; acquired by Planet Labs Inc., 2015). In the absence of high resolution topographic and aerial data from 1914, the analysis relied on the camera calibration from the 2014 lidar DEM and 2006 SPOT image being applied to the 1914 oblique photographs. This approach was deemed reasonable, as no extreme changes in topography (e.g. rock slides, slumping) are apparent between the 1914 and 2006 datasets.

Following calibration, a 20 m fishnet (400 m^2 grid cell area) was applied to the seven oblique images. Any fishnet grid cell that intersected with less than 75% of the viewshed (i.e. < 300 m^2) was omitted from the analysis (note: because these data were eventually rasterized, and each raster represented an area between 300-400 m^2, canopy cover and change is reported by grid cell count rather than surface area). Once in an oblique projection, grid cells were manually assigned into one of six canopy cover classes based on observed canopy openness and texture. The six canopy cover classes were: 1) *No Cover* – grid cells devoid of vegetation; 2) *Low Vegetation* – grid cells appear vegetated, but context and texture suggest shrubs or krummholz, not upright trees > 2 m; 3) *Partial Canopy* – trees are present, but ground is visible in > 50% of the grid cell; 4) *Full Canopy* – trees cover > 50% of a grid cell; 5) *Snow* – snow covers > 50% of a grid

cell; 6) *Structure* – any anthropogenic structure or non-vegetated land cover is present in the grid cell (e.g. buildings, roads, and trails).

Given the focus on vegetative land cover change, further analysis focused on the first four, ordinal classes of vegetation (*no cover* through *full canopy*). Any grid cells having *snow* or *structure* in either 1914 or 2006 were omitted from analysis. The *snow* class was removed due to uncertainty of vegetation beneath the snow. Recent lidar measurements of snow depth in the valley have shown late-season accumulation in excess of 5 m in some areas (Kelsey Cartwright, personal communication, June 2017), suggesting that snow cover may be concealing any of classes 1-4. Without knowing what was underneath the snow, the conservative approach was to omit these areas from analysis. The anthropogenic *structure* class was omitted because the processes causing vegetative land cover to change were distinct from the processes being studied. Additionally, the method used in this analysis looks at the magnitude of change as the difference between the ordinal canopy cover classes; because anthropogenic structures do not fit in these ordinal categories, their use in assessing change is limited. 7.2% of the total observed area was affected by the removal of snow cover, and 2.9% by the removal of anthropogenic structures (Table 3.2).

3.2.4 Anthropogenic Disturbance

Holtmeier and Broll (2005) noted that regional land cover in the ATE is regulated by orographic and climatic processes only in the absence of anthropogenic influence on the landscape. As one of the goals of the research was to distinguish land cover change in various disturbance types, a method of distinguishing between vegetative change in

anthropogenically modified areas and undisturbed areas was required. The Alberta Vegetation Inventory (Alberta Environment and Parks 2012) was produced from interpretation of aerial photographs, and identifies several types of former and current human disturbance, including former oil well pads, historical cut-blocks, settlements (including the Castle Mountain Ski Resort), and roads. These areas were aggregated into a single layer of anthropogenic disturbance so that topographic and other factors which affected land cover change could be considered independently of human activity.

Clarification should be made as to why areas of anthropogenic disturbance are considered separately from anthropogenic structures as an end-member land cover class. Regions that have anthropogenic structures as end-member classes reveal nothing about vegetative change; these regions were removed regardless of whether they occurred inside or outside of the identified anthropogenic disturbance layer. What is of interest is the ability to distinguish vegetative change in areas that have experienced human interference from vegetative change driven by other processes.

3.2.5 Fire Disturbance

Historical wildfires in the WCW were identified in order to examine topographic correlates of change, independently of the effect of fire. Two major historical fires in the area occurred in the interval between the oblique photograph observations, in 1934 and 1936. The extents of the historical fires were delineated in 2005, using a combination of visual evidence from a 1949 aerial photograph survey and descriptions from historical fire reports (Wildfire Management Branch - Alberta Agriculture and Forestry 2017) (Figure 3.2). A qualitative check of historical and contemporary forest boundary was

performed using the same repeat photographs from the MLP, but fire extent was not directly delineated from those images (Rogeau, personal communication, February 2017).

More detailed attributes of these fires, such as intensity and cause, are unknown. Fire suppression in early 20th-century was common practice, yet it is known that the Government of Alberta did not engage in fire suppression in the 1930s and 1940s, for reasons related to the Great Depression and the Second World War (Rogeau et al. 2016). However, historic accounts suggest that upwards of 180 men from nearby mining towns fought the 1936 fire (Murphy 2006). It is unclear if these fire-fighting techniques introduced topographic bias. Fire suppression techniques did not affect the fire return interval of subalpine forests in the region (Rogeau et al. 2016).

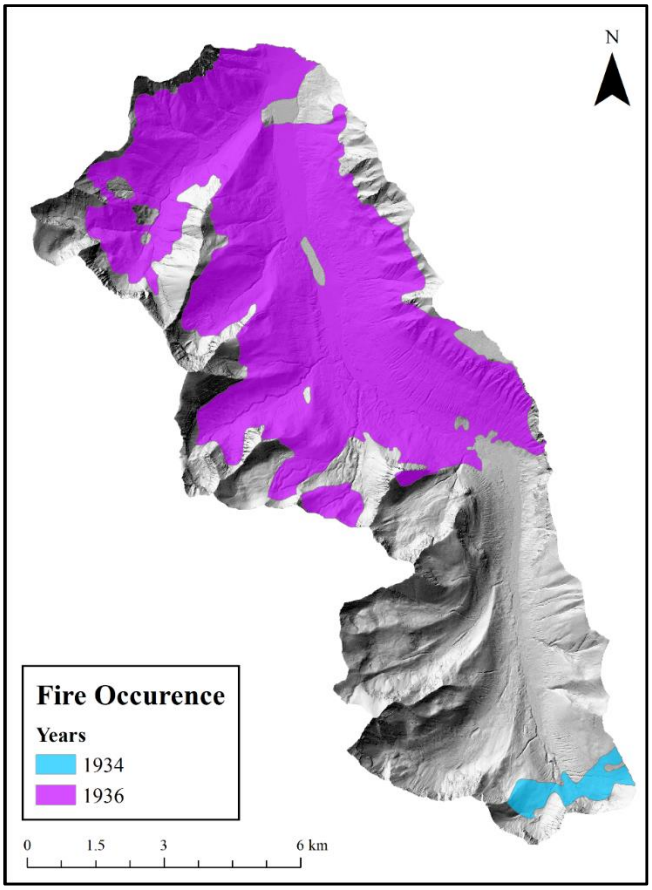

Figure 3.2 - Historic fire occurrence in West Castle Watershed.

3.2.6 Topographic Analysis of Change

The four ordinal classes of canopy cover *(1 - no cover, 2 - low vegetation, 3 - partial canopy, 4 - full canopy)* were used to categorize vegetative change between 1914 and 2006 (Figure 3.3 & Figure 3.4). For each 20 m grid cell, the difference between the 2006 cover class and the 1914 cover class was used to generate a change class (Figure 3.5). For example, if canopy cover in 2006 was *no cover* (1), and canopy cover in 1914 was *full canopy* (4), then the change class for that area was 1 - 4 = -3. Given four vegetative classes, the number of possible change classes was seven (2n - 1). The seven change classes were: -3 (high mortality), -2 (medium mortality), -1 (low mortality), 0 (no change), +1 (low succession), +2 (medium succession), +3 (high succession).

In preparation of the topographic analysis, a 1 m DEM was aggregated to 20 m and coregistered to the change classes: for elevation, the mean value of the 1 m cells was used for its corresponding 20 m raster; for slope, the degree angle of slope was calculated from the 1 m DEM, and the mean of degree values was used for the 20 m raster; for aspect, azimuth was calculated on the aggregated 20 m DEM, and discretized in eight intercardinal direction bins of 45° each: N = 337.5-22.5°, NE = 22.5-67.5°, E = 67.5-112.5°, SE = 112.5-157.5°, S = 157.5-202.5°, SW = 202.5-247.5°, W = 247.5-292.5°, NW = 292.5-373.5°.

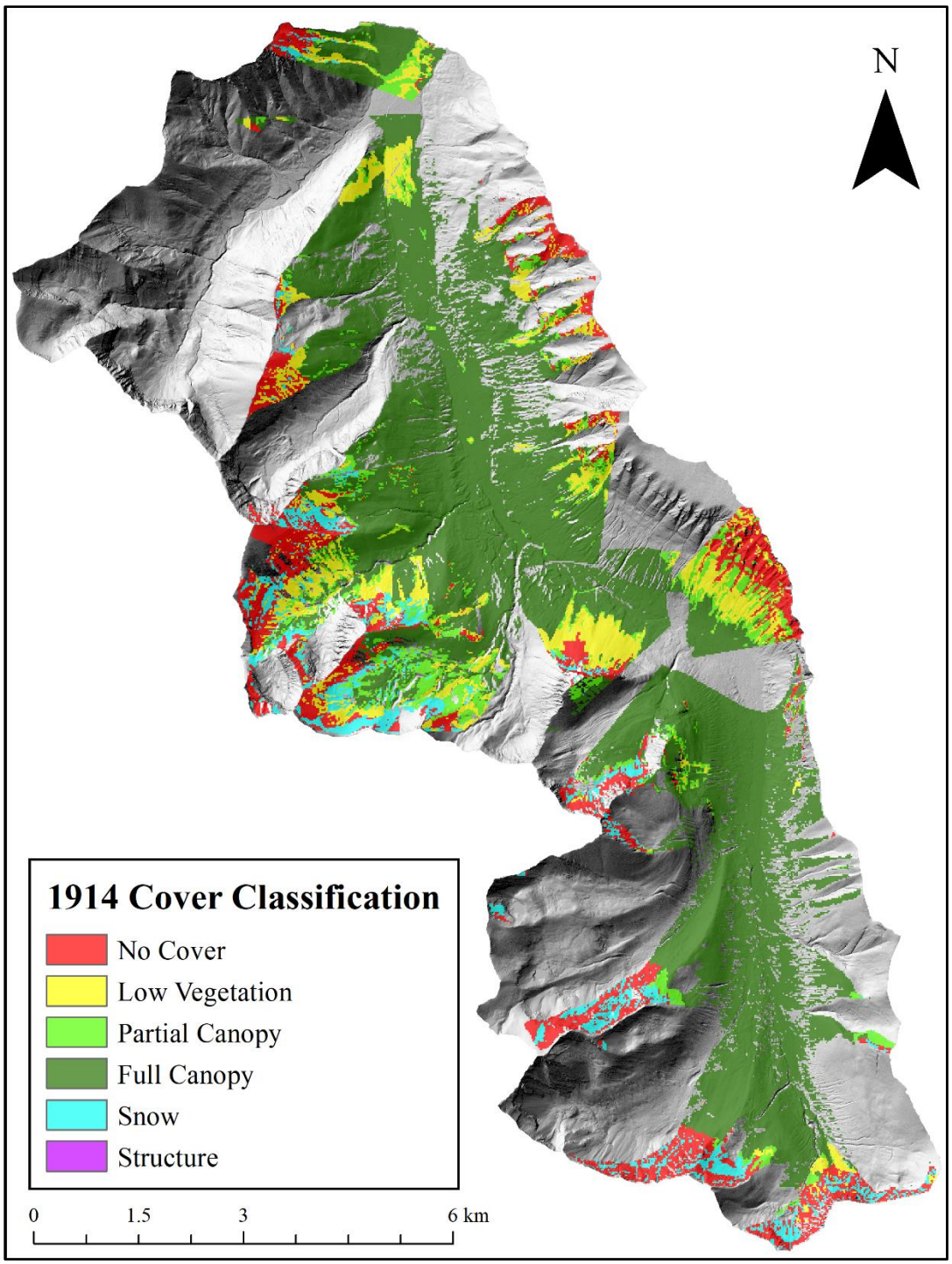

Figure 3.3 - 1914 canopy cover classification.

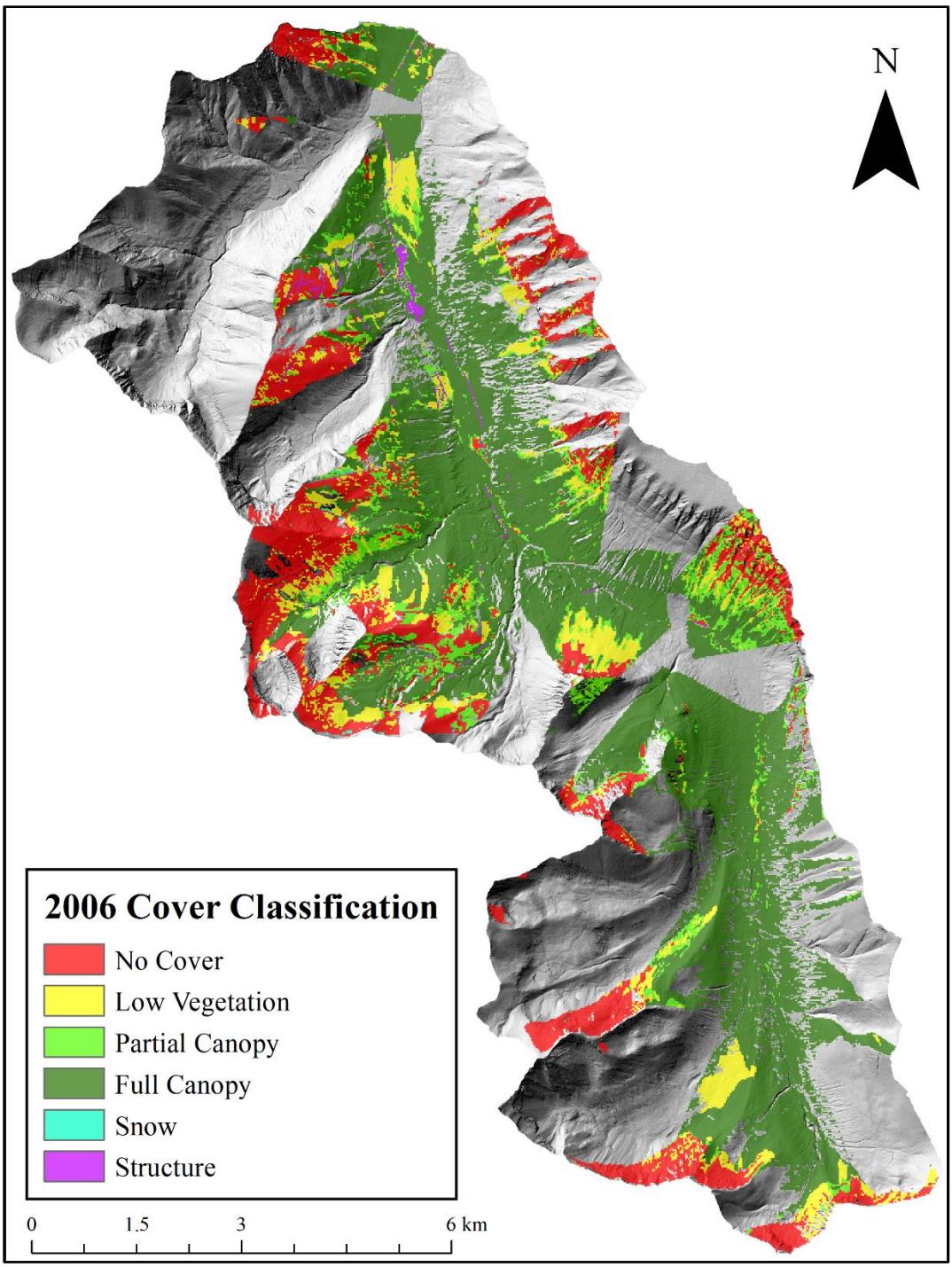

Figure 3.4 - 2006 canopy cover classification.

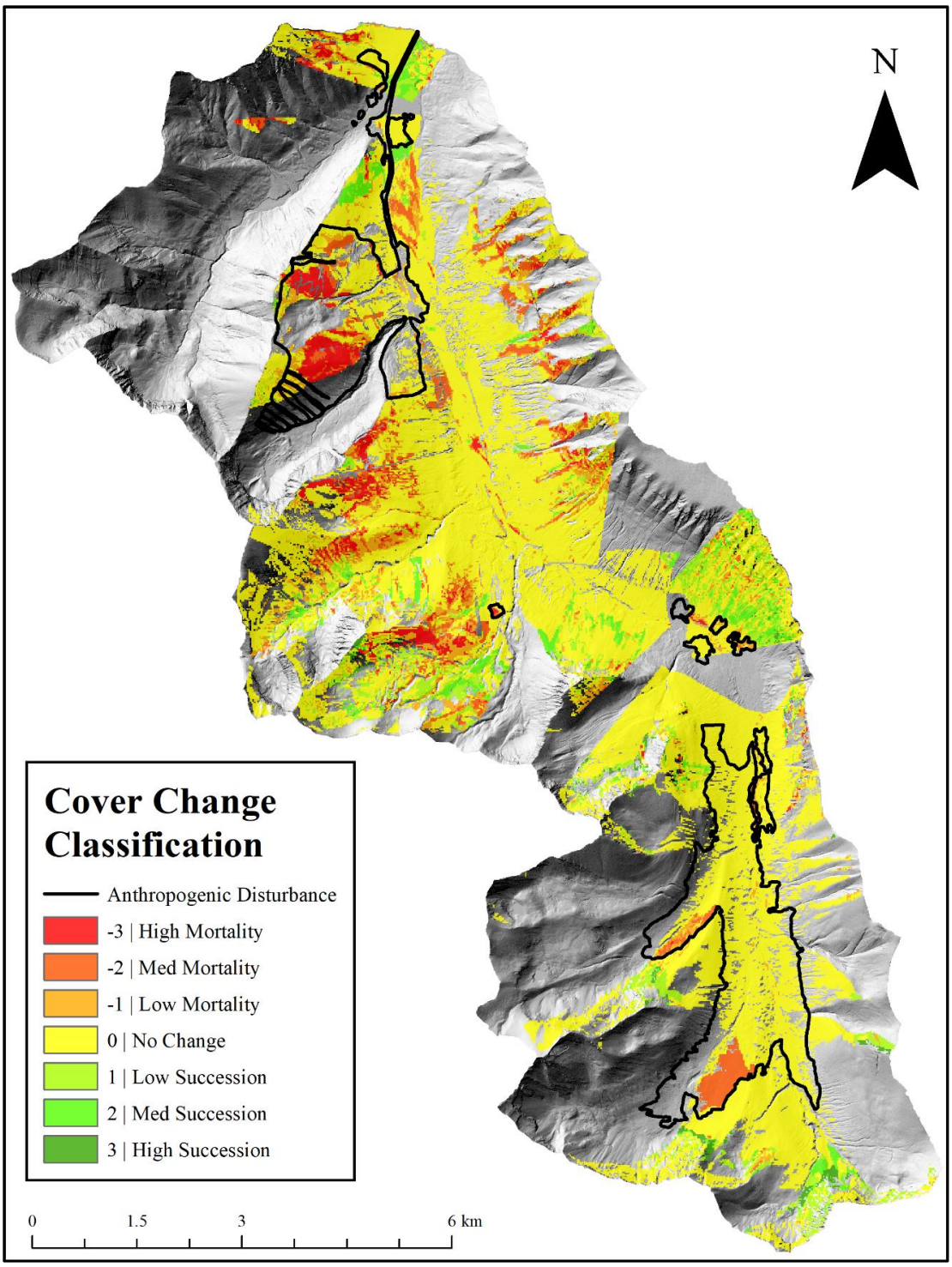

Figure 3.5 - Cover change classification for 92- year period 1914-2006.

For the continuous variables elevation and slope, distributions within each of the seven change classes were investigated. One-way ANOVA tested whether any of the seven classes mean values differed from the others. For both elevation and slope comparisons, Welch's t-test was used on each of the 20 pairwise combinations of seven change classes to establish which classes differed from each other. Note that Welch's test corrects for both unequal variance between distributions and unequal sample size (Lumley et al. 2002). A Bonferroni correction was applied to the t-tests to account for multiple comparisons by lowering the alpha value of the test.

For the nominal aspect variable, the 20 m DEM was sampled to establish the expected frequency of the eight aspects in the WCW. The observed frequency of aspect, within each change class, was compared to the expected frequency with a chi-square goodness-of-fit test.

All topographic analyses were completed solely outside of the anthropogenic disturbance area (see Figure 3.5).

3.2.7 Interaction Between Topography and Fire

In an effort to distinguish fire-related changes to vegetation cover from other factors that may be correlated to topography, change cover data were separated by fire exposure. The 1934 and 1936 fire extents were aggregated into a single layer. The distribution of topographic variables within each change cover class was contrasted between fire-exposed and non-fire-exposed areas in the time interval 1914-2006.

3.3 Results

3.3.1 Canopy Cover in 1914 and 2006

In both anthropogenically disturbed and non-disturbed areas, *full canopy* was the largest class (Figure 3.6), but the proportion of this class declined between 1914 and 2006. The decline was more pronounced in anthropogenically disturbed areas (93.6% to 71.6%) than in non-disturbed areas (59.0% to 57.5%) (Table 3.2). The proportion of the *no cover* class increased sharply over the same period, from 1.1% to 10.2% in disturbed areas, and 14.9% to 22.3% in undisturbed areas. The extremely low sample sizes for both *snow* and *structure* classes further justified their removal from the analysis. As the 1914 observation had limited snow cover (6.7%), it could be argued that removal of this class might bias the distribution of topographic variables in the subsequent analysis. Of particular concern would be if this late-season snow cover selectively covered certain aspects, changing the distribution of aspect across observed areas. A Pearson's chi-squares goodness-of-fit test showed that the proportion of eight aspect classes in the removed snow class was not statistically different than the proportion of aspect classes in areas with elevation greater than 1800 m a.s.l. ($X^2 = 0.615$, df = 7, p = 0.999), removing this concern.

3.3.2 Change Classes

In both disturbed and non-disturbed areas, the dominant change cover class was *no change* (Figure 3.7 & Table 3.3). In anthropogenically disturbed areas, the mortality classes outnumbered the succession classes by more than an order of magnitude (4,598 to 237). In the non-disturbed areas, the frequency of a change class decreased with

increasing magnitude of mortality or succession, but mortality and succession occurred with more even frequency (13,630 to 11,192).

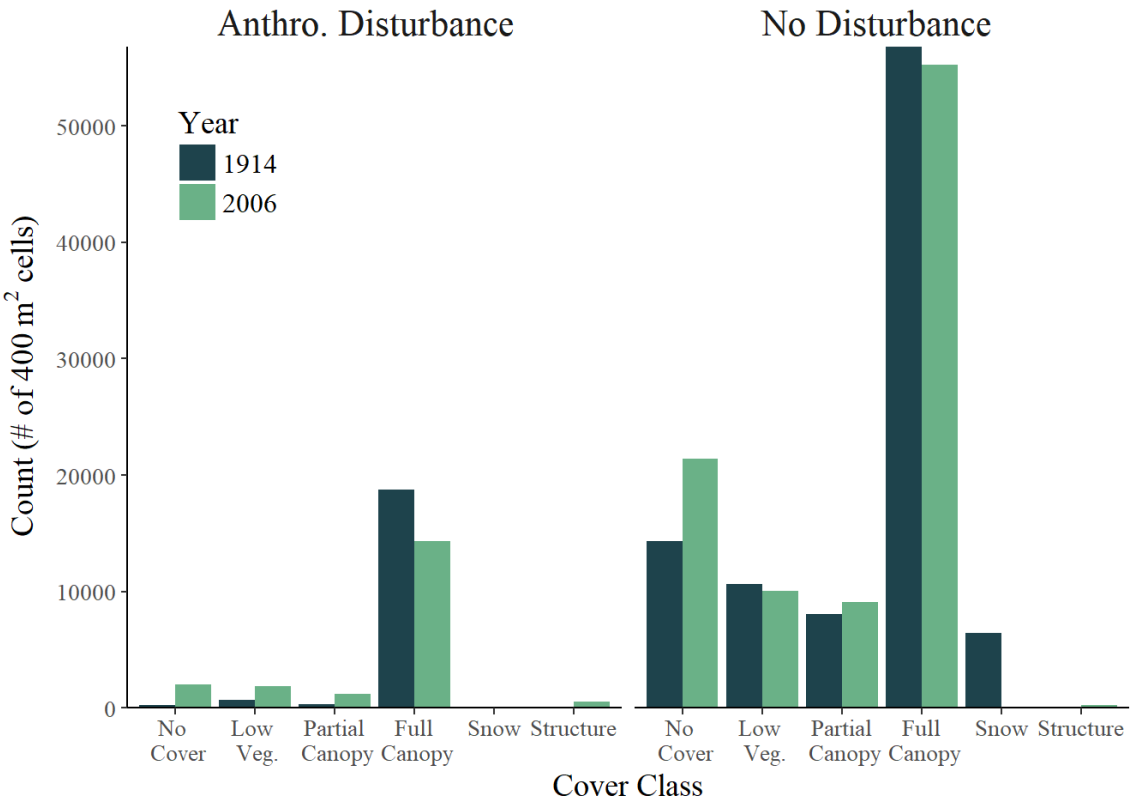

Figure 3.6 - Cover class count.

Table 3.2 - Cover class count and percentage for regions with anthropogenic disturbance and no disturbance.

	Anthro. Disturbance				**No Disturbance**			
	1914		**2006**		**1914**		**2006**	
	# of cells	**% Total**	**# of cells**	**% Total**	**# of cells**	**% Total**	**# of cells**	**% Total**
No Cover	230	1.1	2,045	10.2	14,360	14.9	21,422	22.3
Low Vegetation	656	3.3	1,900	9.5	10,626	11.0	10,056	10.5
Partial Canopy	297	1.5	1,229	6.1	8,074	8.4	9,069	9.4
Full Canopy	18,781	93.6	14,348	71.6	56,780	59.0	55,274	57.5
Snow	94	0.5	0	0.0	6,463	6.7	95	0.1
Structure	0	0.0	530	2.6	0	0.0	258	0.3

Figure 3.7 - Change class count.

Table 3.3 - Change class cell count, factored by aspect and exposure to fire.

	Change Class						
	-3	**-2**	**-1**	**0**	**1**	**2**	**3**
Disturbance							
No Disturbance	2,433	3,809	7,388	64,618	7,055	3,356	781
Anthro. Disturbance	1,354	1,738	1,506	1,4687	163	69	5

3.3.3 Topographic Correlations

3.3.3.1 Elevation

One-way ANOVA showed that the mean elevation of at least one of the change classes was significantly different from the remaining groups ($F= 743.16$, $df = 6$, $p < 0.001$). The result of the pairwise t-tests showed that, of the 20 possible pairwise

combinations, 19 showed significant differences (Table 3.4). Only one change class pair showed no significant difference; *medium mortality - medium succession*. The highest mean elevations were observed in the *high mortality* and *high succession* classes, and the lowest mean elevation was in the *no change* class (Figure 3.8), indicating that the magnitude of change, for both mortality and succession, covaried with elevation. To test this effect, change classes were pooled by absolute value (e.g. -3 combined with 3, -2 combined with 2), and a Spearman rank test was performed. The results showed that magnitude of change was significantly correlated with elevation ($r = 0.174$, $p < 0.001$), though the correlation was weak.

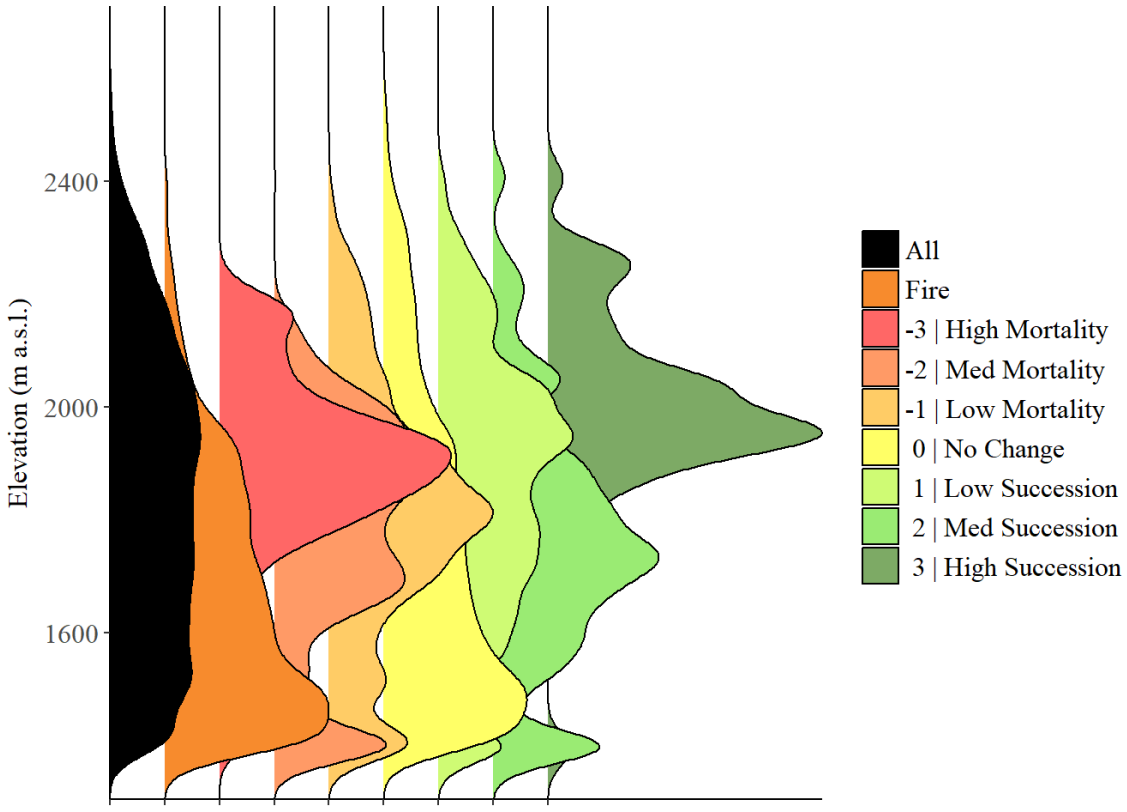

Figure 3.8 - Elevation distributions in WCW, normalized with a probability density function; all terrain, fire-exposed terrain, and change categories.

Table 3.4 - Results of elevation t-test between change classes.

	Change Class					
	-3	-2	-1	0	1	2
-2	-24.042	-	-	-	-	-
	< 0.001	-	-	-	-	-
-1	-20.153	6.643	-	-	-	-
	< 0.001	**< 0.001**	-	-	-	-
0	-42.218	-10.400	-22.928	-	-	-
	< 0.001	**< 0.001**	**< 0.001**	-	-	-
1	-7.627	18.686	13.900	39.454	-	-
	< 0.001	**< 0.001**	**< 0.001**	**< 0.001**	-	-
2	-24.636	-2.525	-8.754	5.790	-19.643	-
	< 0.001	0.244	**< 0.001**	**< 0.001**	**< 0.001**	-
3	13.569	30.010	27.219	39.397	19.105	30.610
	< 0.001	**< 0.001**	**< 0.001**	**< 0.001**	**< 0.001**	**< 0.001**

3.3.3.2 Slope

In the slope analysis, one-way ANOVA showed that the mean slope of at least one of the change classes was significantly different from the remaining groups ($F= 213.69$, $df = 6$, $p < 0.001$). The result of the pairwise t-tests showed that, of the 20 possible pairwise combinations, 17 showed significant differences (Figure 3.9 & Table 3.5). Three group pairs showed no significant difference*; high mortality – high succession*, *medium mortality – low mortality*, and *medium mortality – low succession*. The highest mean slope values were seen in the *high mortality* and *high succession* classes, while the lowest was in the *no change* category. To test the effect, change classes were again pooled by absolute value, and a Spearman rank test was performed. The results showed that magnitude of change was significantly correlated to slope ($r = 0.126$, $p < 0.001$), though the correlation was weak.

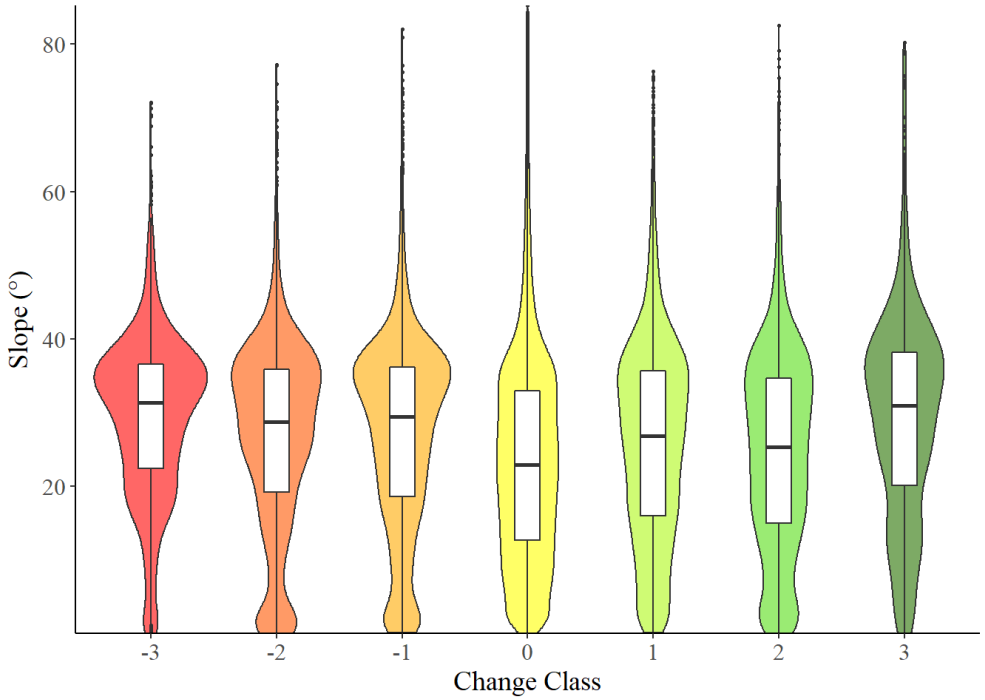

Figure 3.9 - Slope distribution of change class.

Table 3.5 - Results of slope t-test between change classes.

		Change Class					
		-3	**-2**	**-1**	**0**	**1**	**2**
-2	t	-8.609	-	-	-	-	-
	p	< **0.001**	-	-	-	-	-
-1	t	-8.727	1.097	-	-	-	-
	p	< **0.001**	1.000	-	-	-	-
0	t	-24.947	-14.348	-21.092	-	-	-
	p	< **0.001**	< **0.001**	< **0.001**	-	-	-
1	t	-12.396	-2.926	-4.793	13.790	-	-
	p	< **0.001**	0.072	< **0.001**	< **0.001**	-	-
2	t	-14.204	-6.250	-8.061	4.742	-4.204	-
	p	< **0.001**	< **0.001**	< **0.001**	< **0.001**	< **0.001**	-
3	t	-0.064	4.710	4.350	11.106	6.297	8.120
	p	1.000	< **0.001**	< **0.001**	< **0.001**	< **0.001**	< **0.001**

3.3.3.3 Aspect

Aspect change classes were examined both by frequency and by proportion. As a function of the orientation of the valley, overall aspect counts varied dramatically; SW, E, and NE aspect had higher occurrence, while S, SE, and NW aspects had lower occurence (Figure 3.10). As discussed previously, the frequency of *no change* classes was dramatically higher than that of areas that experienced mortality or succession. From a frequency perspective, SE, SW, and E aspects had high net mortality. Net succession frequencies were fairly evenly distributed, with slightly higher frequency of *low* and *medium succession* classes on SW aspects.

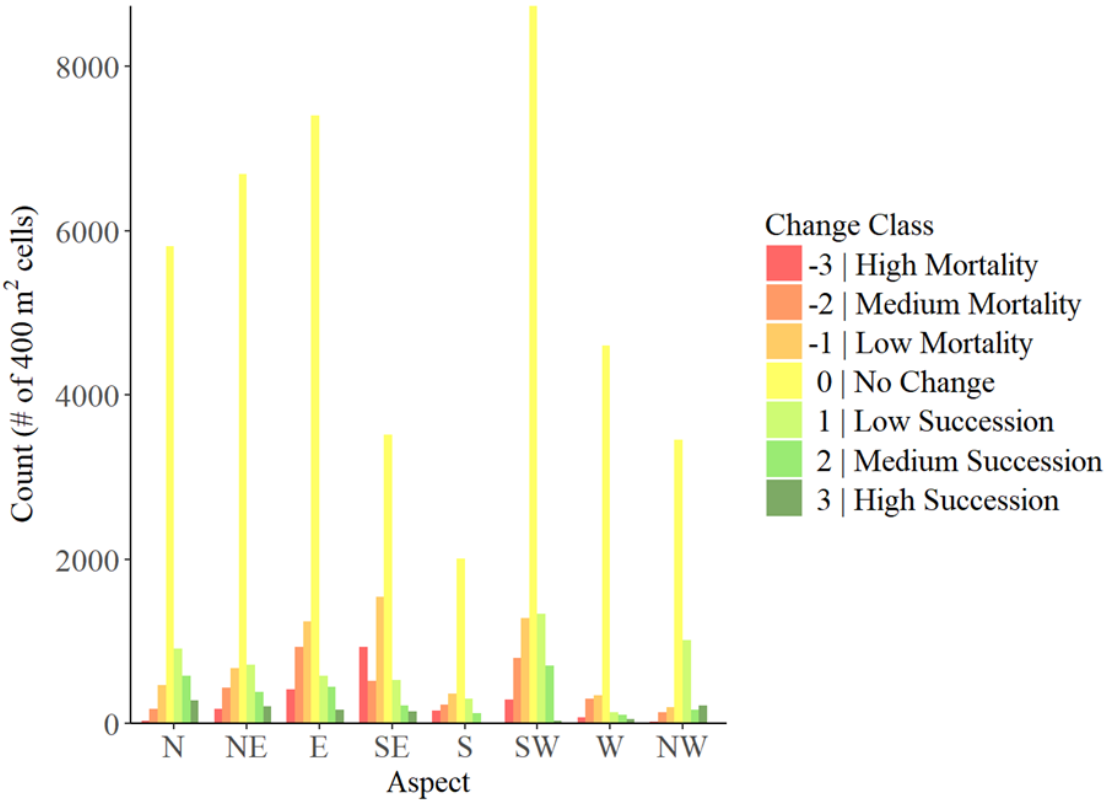

Figure 3.10 - Change class count by aspect.

Table 3.6 - Aspect change class summary, factored by fire.

		Change Class						
Aspect		**-3**	**-2**	**-1**	**0**	**1**	**2**	**3**
N	Fire	28	177	468	4,962	680	577	165
	No Fire	8	36	130	5,807	913	290	279
	Total	36	213	598	10,769	1,593	867	444
NE	Fire	181	435	678	6,104	715	385	88
	No Fire	8	25	111	6,691	672	252	205
	Total	189	460	789	12,795	1,387	637	293
E	Fire	410	933	1,237	7,401	508	449	30
	No Fire	22	29	253	6,119	578	197	171
	Total	432	962	1,490	13,520	1,086	646	201
SE	Fire	932	513	1,544	3,514	529	223	20
	No Fire	144	37	214	1,928	247	68	149
	Total	1,076	550	1,758	5,442	776	291	169
S	Fire	158	229	368	2,003	297	123	1
	No Fire	91	88	64	664	20	9	7
	Total	249	317	432	2,667	317	132	8
SW	Fire	287	796	1,279	8,734	1,336	708	35
	No Fire	11	49	145	934	85	63	14
	Total	298	845	1,424	9,668	1,421	771	49
W	Fire	70	302	340	4,437	131	108	16
	No Fire	46	28	204	4,601	134	43	49
	Total	116	330	544	9,038	265	151	65
NW	Fire	25	132	200	1,689	117	135	13
	No Fire	12	9	153	3,451	1,016	165	223
	Total	37	141	353	5,140	1,133	300	236

When within change class proportions of aspect were compared to the expected distribution of aspects in the WCW, striking patterns emerge. In N and NW aspects, the proportion of succession classes is notably higher than the expected proportion, and

mortality classes are notably lower (Figure 3.11). On S and SE aspects, the inverse is true, with mortality classes being over represented. The results of the chi-squared test show that significant differences are caused by even slight differences in proportions; 46 out of 56 (82.1%) of the change class/aspect cases showed significant differences from expected proportions Table 3.7.

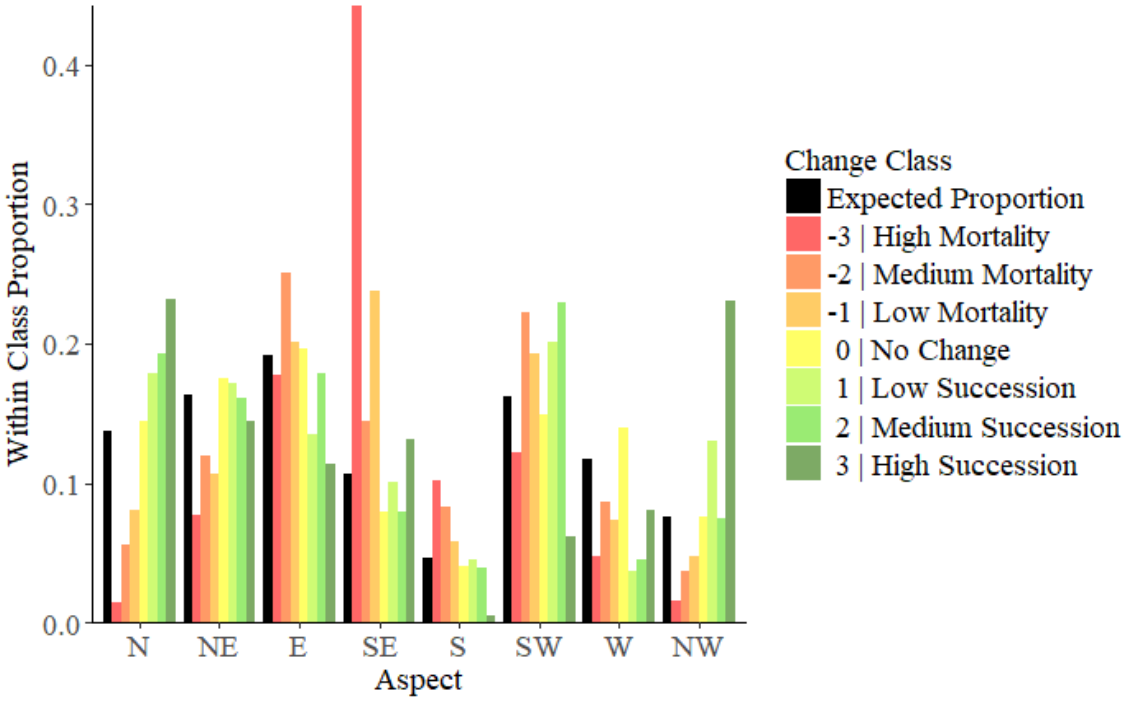

Figure 3.11 - Proportion of change classes by aspect.

Table 3.7 - Results of chi-squared test of aspect proportions.

	Change Class						
	-3	-2	-1	0	1	2	3
N	307.5	212.1	196.8	28.6	101.4	90.0	59.2
	< 0.001	**< 0.001**	**< 0.001**	**< 0.001**	**< 0.001**	**< 0.001**	**< 0.001**
NE	130.1	52.6	171.7	64.5	3.4	0.1	1.9
	< 0.001	**< 0.001**	**< 0.001**	**< 0.001**	0.066	0.728	0.163
E	3.3	85.9	4.4	6.1	147.0	4.2	30.7
	0.069	**< 0.001**	0.037	**0.013**	**< 0.001**	**0.041**	**< 0.001**
SE	2863.3	55.9	1327.0	530.7	2.6	27.5	5.1
	< 0.001	**< 0.001**	**< 0.001**	**< 0.001**	0.109	**< 0.001**	**0.024**
S	177.1	121.3	26.7	34.4	0.1	3.3	29.6
	< 0.001	**< 0.001**	**< 0.001**	**< 0.001**	0.702	0.070	**< 0.001**
SW	27.8	101.1	52.0	71.2	81.5	114.1	58.0
	< 0.001	**< 0.001**	**< 0.001**	**< 0.001**	**< 0.001**	**< 0.001**	**< 0.001**
W	114.1	34.8	136.6	311.9	434.0	169.8	10.2
	< 0.001	**< 0.001**	**< 0.001**	**< 0.001**	**< 0.001**	**< 0.001**	**< 0.001**
NW	127.0	81.2	81.9	0.0	301.4	0.1	268.0
	< 0.001	**< 0.001**	**< 0.001**	0.963	**< 0.001**	0.806	**< 0.001**

3.3.4 Fire

The fires of 1934 and 1936 combined, burned 63.2% of the observed area in WCW. Fire burned a disproportionately larger area of S, SE, and SW aspects, compared to the distribution of aspects in the watershed (Figure 3.12). The SW aspect was particularly affected, which is notable as it is the dominant wind direction in WCW.

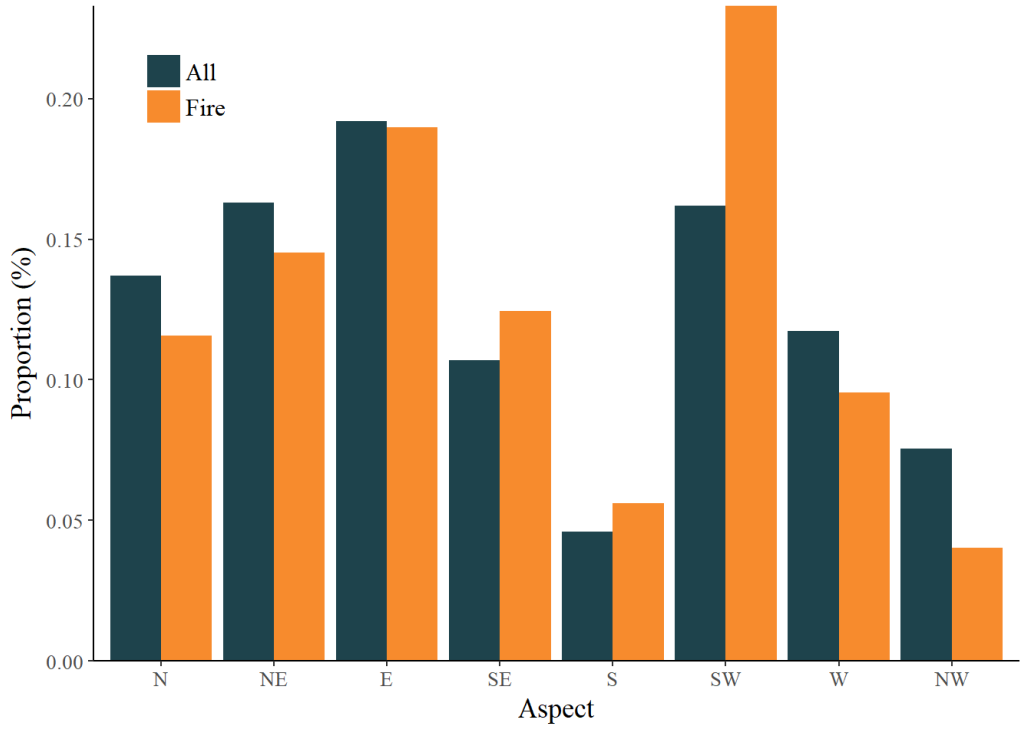

Figure 3.12 - Distribution of aspects in WCW compared to distribution of aspect in fire-exposed areas.

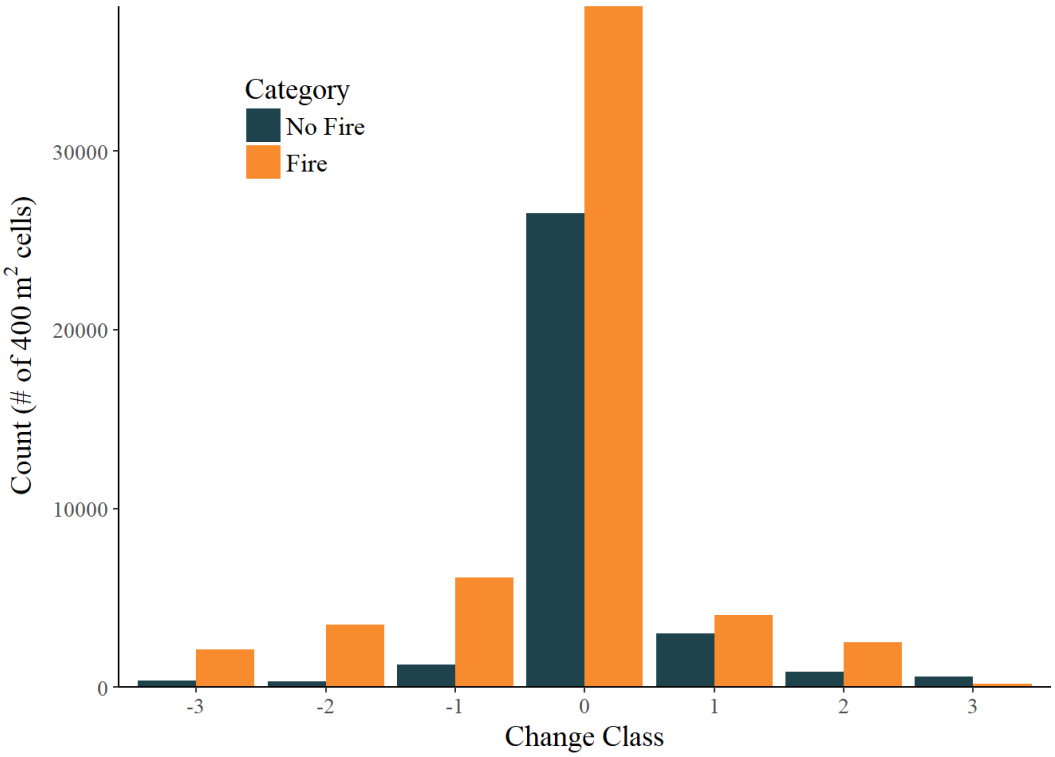

Figure 3.13 - Change class frequency by fire exposure.

Observed mortality and succession varied by exposure to fire (Figure 3.13). The majority of mortality was seen in fire-exposed areas. The rate of mortality within fire-exposed areas was four times higher than the rate in non-fire-exposed areas (Table 3.8, 20.7% to 5.8%). Net succession was also higher in fire-exposed regions (6,740 to 4,452), but after accounting for the difference in area between fire-exposed and non-fire-exposed regions, the within region rate of succession was higher in non-fire-exposed regions (13.5% to 11.9%).

3.3.4.1 Elevation

Mean elevation of fire-exposed areas was lower than mean elevation of non-fire-exposed areas in every change class (Figure 3.14). This is as expected, given the decreasing probability of fire with increasing elevation (Rogeau & Armstrong 2017). While factoring by fire showed between group differences in elevations, the significant correlation between change magnitude and elevation was preserved in both fire-exposed cases ($r = 0.340$, $p < 0.001$), and non-fire-exposed cases ($r = 0.110$, $p < 0.001$).

3.3.4.2 Slope

In a majority of change classes (-3 through 1), mean slope was lower in fire-exposed area than in non-fire-exposed areas (Figure 3.15). This was expected, given reduced burn frequency at high elevations, and the positive relationship between elevation and slope with hypsometry. In *medium* and *maximum succession* classes, fire-exposed areas had slightly higher mean slope than non-fire-exposed areas. The significant

Table 3.8 - Frequency of change classes by fire-exposure.

		Mortality					Succession					
		-3	-2	-1	All Mort.	0	1	2	3	All Succ.	Total	%
No Fire	**Count**	342	301	1274	1917	26515	3021	840	591	4452	32884	36.8%
	%	1.0%	0.9%	3.9%	5.8%	80.6%	9.2%	2.6%	1.8%	13.5%		
Fire	**Count**	2091	3508	6114	11713	38103	4034	2516	190	6740	56556	63.2%
	%	3.7%	6.2%	10.8%	20.7%	67.4%	7.1%	4.4%	0.3%	11.9%		

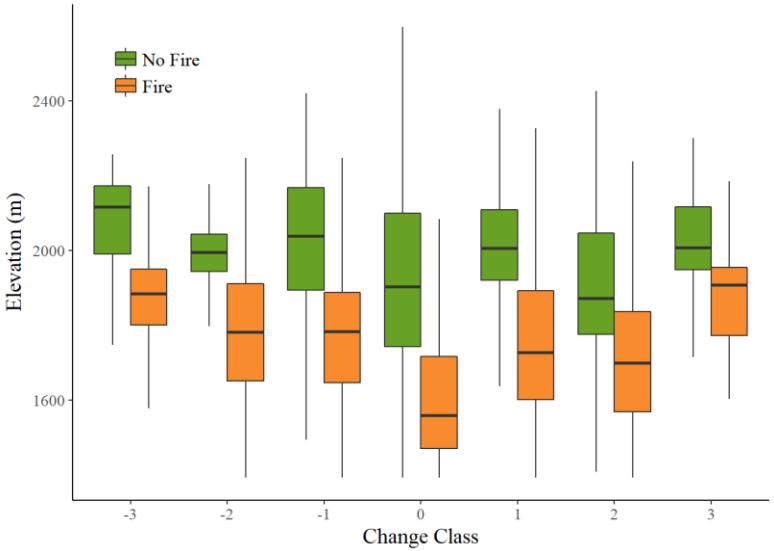

Figure 3.14 - Change class elevation factored by fire exposure.

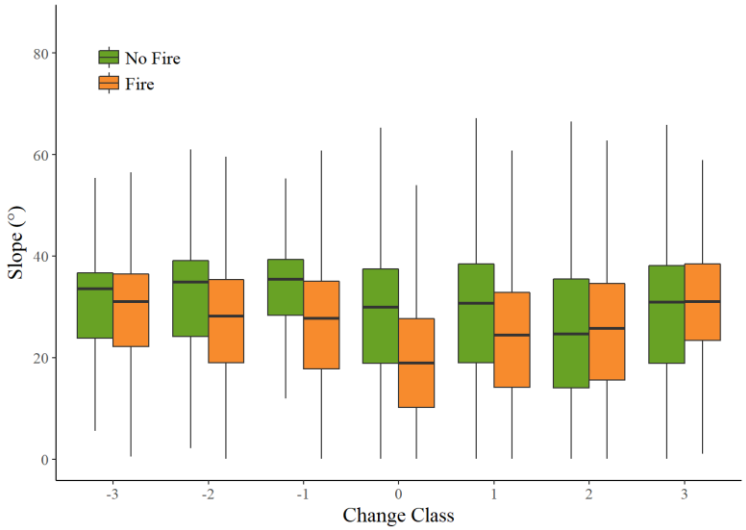

Figure 3.15 - Change class slope factored by fire exposure.

correlation between change magnitude and slope was preserved in both fire-exposed cases ($r = 0.244$, $p < 0.001$), and non-fire-exposed cases ($r = 0.027$, $p < 0.001$).

3.3.4.3 Aspect

Analysis of aspect showed that the high overall frequency of mortality on fire-exposed areas occurred primarily on SE, E, and SW aspects (Figure 3.16, Figure 3.17, & Table 3.6). In areas that experienced succession, high frequency of succession classes was seen on N, NE, and E aspects, in both fire-exposed and non-fire-exposed areas. Succession was frequent on SW, fire-exposed aspects but limited on SW, non-fire-exposed aspects. Conversely, succession was limited on NW, fire-exposed aspects, but frequent on NW, non-fire-exposed aspects.

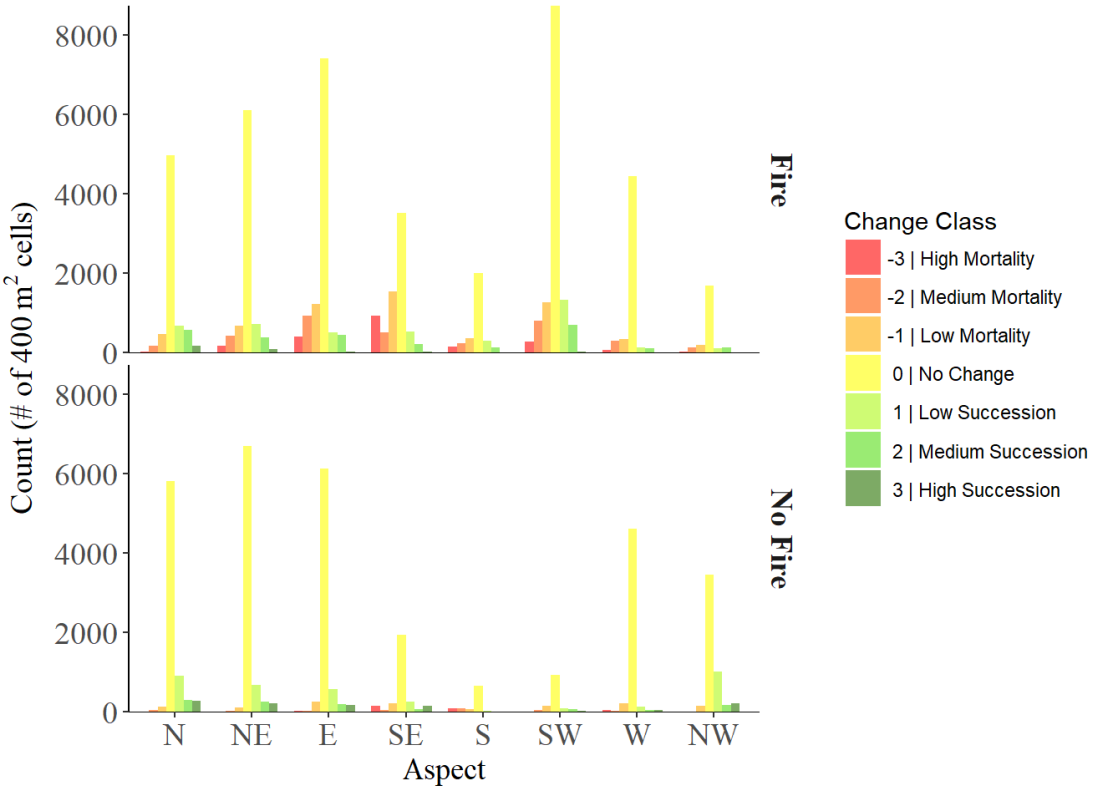

Figure 3.16 - Count of change class, factored by aspect and fire-exposure.

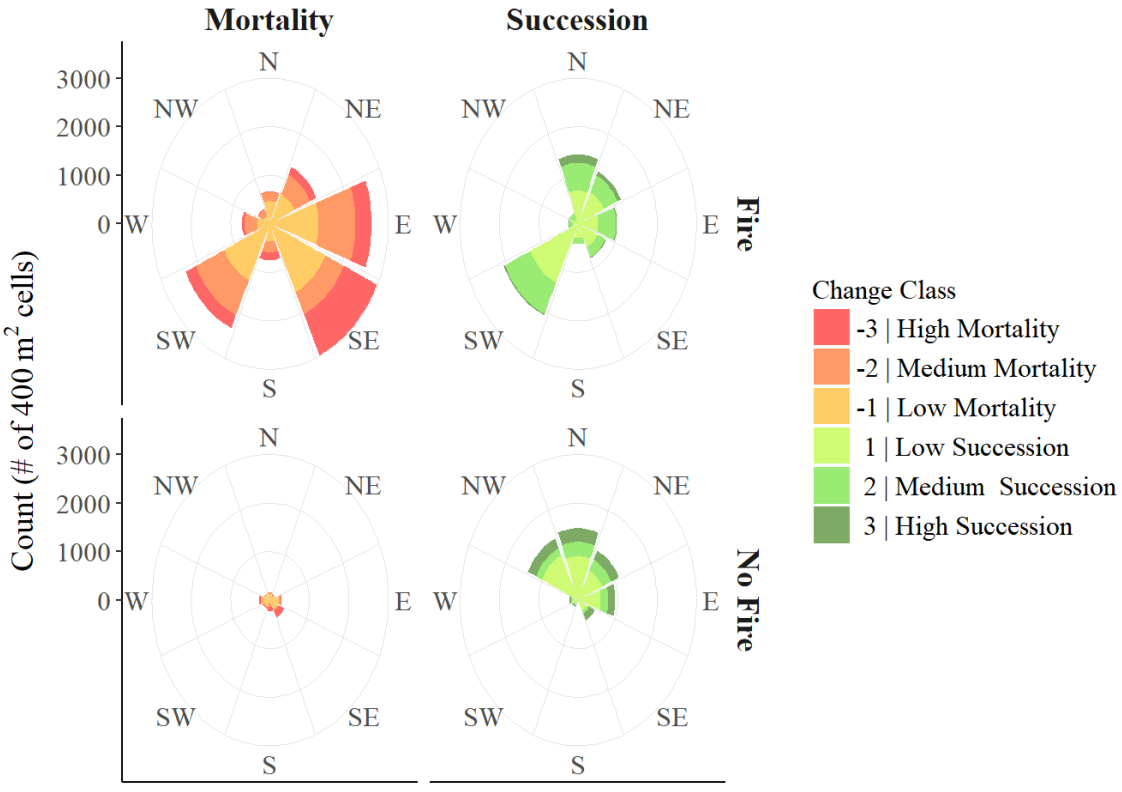

Figure 3.17 - Mortality and succession, factored by exposure to fire.

3.4 Discussion and Conclusions

The primary research objective was to to identify change in ATE canopy cover using the WSL-MT, and to establish whether the technique could be used to identify correlations between change and topography (elevation, slope, and aspect). This objective was met: canopy change was classified into seven ordinal classes of change, ranging from high mortality to high succession. Correlations were observed between topography and the degree of canopy change.

Degree of change correlated positively with elevation; the highest within-class mean elevations occurred in the *high mortality* and *high succession* classes, and the

lowest mean elevation was in the *no change* class. These high degree change classes covered a smaller area than low degree changes. While low degree changes occurred over a range of elevations, high degree change was almost entirely restricted to elevations greater than 1800 m, which coincide with the lower extent of ATE (see change class hypsometry in Figure 3.8). This finding is consistent with the expectation that, as a transitional boundary that occurs as a function of elevation, canopy cover at ATE would be subject to a high level of variability (Harsch et al. 2009; Körner 2012; Tranquillini 1979).

Similarly, analysis of slope angle showed that the highest within-class mean slope occurred in the *high mortality* and *high succession* classes, and the lowest mean slope was in the *no change* class. The probability density functions in Figure 3.9 suggest that, in most classes, the likelihood of change increases in terrains > 30°. Treelines in high slope areas are known to be subject to mechanical disturbances by avalanches (Butler & Walsh 1994; Walsh et al. 1994), which introduces the prospect that treelines in WCW may be orographically regulated (Holtmeier & Broll 2005). Cyclical patterns of disturbance and regrowth may explain the high degree of both mortality and succession seen in high slope areas. However, Butler et al. (1994) found that in a nearby site in Glacier National Park (GNP), avalanche-regulated treelines were stable over a 70+ year repeat photograph record, showing no cycle of disturbance and advance. If the observed slope pattern in WCW is a result of cyclical processes, then this discrepancy between WCW and GNP must be investigated.

Aspect was also correlated to canopy cover change. Greater than expected proportions of succession occurred on N and NW aspects, while higher than expected

proportion of mortality occurred on S and SE aspects. Similar aspect effects have been reported in a number of studies of ATE dynamics (Bader & Ruijten 2008; Dang et al. 2015; Elliott & Cowell 2015; Greenwood et al. 2014). However, the proposed mechanisms of these aspect effects are often site-specific, and vary by study region. These include: differences in lapse rates among aspects (Dang et al. 2015); diurnal cycles of cloud cover causing preferential aspects in equatorial rainforests (Bader & Ruijten 2008); and aspect specific patterns of snow accumulation affecting the functional length of the growing season (Elliott & Cowell 2015).

The secondary research objective was to investigate the effect of a modulating factor, fire disturbance. This analysis demonstrated that correlations between canopy change and topography differed when factored between fire-exposed areas and non-fire-exposed areas.

The observed topographic distribution of fire in WCW agreed with expectations based on the topographic distribution of fire return intervals (FRIs) in the region (Rogeau & Armstrong 2017); for every 100 m of elevation gain in subalpine regions of the Canadian Rockies, the probability of burning decreases 33%. This effect was observed in WCW, as the hypsometry of fire-exposed areas was biased towards lower elevations when compared to the hypsometry of the valley (Figure 3.8). The distribution of fire-exposed aspects in WCW also agrees with the observation of Rogeau and Armstrong (2017), that south-facing, subalpine aspects are twice as likely to burn as north-facing aspects. In WCW, warm aspects (S, SE, SW) displayed higher than expected proportions of fire exposure, with SW aspects being highly over represented (Figure 3.12). This is notable, as wind direction in WCW is predominantly from the SW.

Fire-exposed areas had lower mean elevations in all change classes, but the majority of canopy cover change was seen in these areas. In Figure 3.8, we see that elevations > 1900 m accounted for a proportionally small region of fire-exposed areas, and yet the highest degree of change was seen at those elevations. The positive correlation between change degree and elevation is maintained in fire exposed areas (Figure 3.14), suggesting that post-fire mortality and re-establishment are potentially affected by factors that covary with elevation.

The slope of fire-exposed areas was generally lower than non-fire-exposed areas. High terrain slopes can accelerate the spread of fire (Werth et al. 2011), but this effect was outweighed by the extent of the WCW fire that occurred on the low slopes of the valley bottom. In two cases, *medium* and *high succession* classes, slopes were greater in fire-exposed areas than in non-fire-exposed areas. Stueve et al. (2009) made a similar observation, showing that slope was one of the factors that predicted re-establishment of subalpine fir following disturbance by fire. In that study, 75% of establishment occurred on slopes with angles between 40-60°. Stueve et al. (2009) reasoned that this intermediate slope range was steep enough to avoid competition by shrubs during re-establishment, but shallow enough to avoid frequent disturbance by rockslide and avalanche. That explanation is inconsistent with the present finding, as areas with slopes above 30° saw a high proportion of both mortality and succession.

Finally, correlation between aspect and canopy cover change appears to be associated with fire-exposure. In total, 58% of all observed mortality occurred on SW, SE, and E aspects in fire-exposed areas. While aspect effects have been observed in a number of ATE change studies (Bader & Ruijten 2008; Dang et al. 2015; Elliott &

Cowell 2015), no universal control for these effects has been proposed. There are several site-specific mechanisms which may explain the observed aspect effect in WCW.

One hypothesis is *moisture limitation*: water stress levels may have been a significant barrier to recruitment following a burn. It is known that seedling recruitment of subalpine fir and Engelmann spruce is inhibited on warm-aspects in the ATE, primarily as a function of water stress caused by high temperature and solar radiation (Germino et al. 2002). Insolation is high on south- and west- facing aspects (Agee 1996), causing reduced FRIs. In a post-fire environment, insolation would increase due to reduced interception and increased gap fraction in the burned canopy. This increased insolation could have caused aspect specific mortality on warm aspects in WCW, particularly the SW aspect.

Stueve et al. (2009) reported that aspect predicted post-fire recruitment of subalpine fir, with cool, north-facing aspects having rates of establishment twice as high as on south-facing aspects. Post-fire erosion may also contribute to mortality. In a study conducted in a watershed adjacent to WCW, Silins et al. (2009) found that total suspended sediment levels were eight times higher in fire-exposed areas, an effect that was exaggerated by steep terrain at high elevations. High levels of erosion in fire-exposed, subalpine areas may suppress the moisture retention capacity of the soil and exacerbate other obstacles to recruitment. The hypothesis that warm, dry conditions prevented post-fire recruitment is consistent with known climatic history of the region. The early 20th-century is noted as being a historically warm period in the eastern slopes of the Canadian Rockies, with dendroclimatic records showing the periods from 1917-1936 and 1939-1958 as having the highest temperature anomalies since the 1400s

(Luckman and Wilson 2005). In fact, one of these reconstructions listed 1936, the year of the Pass Creek fire in WCW, as the second warmest year in the ~1000 year record (Luckman & Wilson 2005).

An alternative hypothesis for the observed aspect effect is *wind influence*. The warm, dry Chinook winds which occur on the lee slopes on the Canadian Rockies are known to accelerate the spread of wildfire (Werth et al. 2011). Observed wind direction in WCW is predominantly from the SW. Werth et al. (2011) note that Chinooks from the SW often follow the passage of weak low-pressure systems over the Rocky Mountains, and can result in large crown fires. Thus, fire behavior may explain the greater proportion of area burned and higher mortality observed on SW aspects. The effects of wind influence may also explain the high occurrence of succession observed on SW aspects. Bekker (2005) shows that the upslope advance of ATE can occur in finger like projections which result from high rates of establishment in areas sheltered from wind. The resulting advance moves in a wind-ward to lee-ward direction, which in WCW would maximize the effect on SW aspects.

In conclusion, this research demonstrated that there are correlations between topography and canopy cover change in the ATE, and that an interaction may exist between these topographic controls and exposure to fire. While this research is limited to observations within a single watershed, the described pattern of land cover change suggests that it is appropriate to generate hypotheses about the interaction of factors that modulate ATE and their topographic controls. Future research would benefit from investigating these interactions using the multi-scale approach that has recently contributed to understanding ATE dynamics (Case & Duncan 2014; Weiss et al. 2015).

The MLP dataset used in our method is ideal for multi-scale investigation of change in the ATE; the spatial extent of MLP photographs ranges from individual meadows (~100 m), to valleys (~10 km), at sites which can be several hundred kilometers apart. The method provides the ability to observe ATE at a spatial resolution and temporal extent which is sufficient to identify topographic correlates of change, which is an important step in understanding interactions between modulating factors.

Chapter 4 - Historic Change in the Alpine Treeline Ecotone Using A Random Forest Model

4.1 Introduction

In the alpine treeline ecotone (ATE) tree growth is limited at high elevations by low air temperature (Körner & Paulsen 2004). Heterogenous tree cover in the ATE is generally attributed to patterns of climate, topography, and response to disturbance (Butler et al. 2007; Holtmeier & Broll 2005; Weiss et al. 2015), but it is understood that the absolute limit to tree growth at the upper boundary of ATE is thermal (Körner 1998). Increases in atmospheric temperature are expected over the 21st-century, and the effects of warming on mountain ecosystems may be amplified by elevation-dependent processes (Pepin et al. 2015). The potential for atmospheric warming to increase the elevation of treelines globally has been a matter of debate (Grace et al. 2002; Harsch et al. 2009). Some models predict a linear increase in the elevation of ATE, correlating to increases in atmospheric temperature (Schwörer et al. 2014). Other models suggest that ATE elevation will remain static (Paulsen & Körner 2014), or that advance may be limited by geomorphic barriers (Macias-Fauria & Johnson 2013). Ultimately, the ability to predict what effect, if any, a warming climate will have on ATE position will rely on the accuracy of models of ATE dynamics.

Most models of change in the ATE are generated by using recent climate history and local topography to explain the present location of ATE, then extrapolating future ATE limits under anticipated climate warming scenarios (Bader et al. 2008; Macias-Fauria & Johnson 2013; Paulsen & Körner 2014). Alternatively, ATE dynamics can be understood by observing historical change and associating advance or recession with the climatic and topographic conditions under which the change occurred (Dang et al. 2015;

Elliott 2012; Greenwood et al. 2014; Leonelli et al. 2016; Liang et al. 2016; Lloyd & Graumlich 1997; Yadava et al. 2017). But attempts to model future change, or to use modeling to describe historic change are both potentially problematic. As Körner (1998) notes, modeling the relationship between climate and vegetation generally suffers from three fundamental problems: 1) auto-correlation between different climate factors, 2) averaging procedures, and 3) uncertainty over whether past or present conditions are reflected in current vegetation patterns.

Auto-correlation is a problem, as models of change are often reliant on proxies of historic or future climate in place of direct observations (Macias-Fauria & Johnson 2013). While these proxies are sufficient for coarse scale models, ATE processes can occur at landscape and microsite scales (Holtmeier & Broll 2005), where climatic conditions are difficult to assess in lieu of direct observations. For example, temperature and precipitation gradients occur in mountain areas as a function of adiabatic lapse rates. Separating the relative effect of temperature versus precipitation using modeled values, rather than direct observations, is likely to be difficult as it would be expected that the variables are highly correlated.

Averaging procedures are also problematic, as the range of a climatic variable is often as important as the mean. For example, diurnal temperature fluctuations have been shown to inhibit seedling establishment in the ATE (Germino et al. 2002), yet these fluctuations are not captured in the mean monthly temperature records which correlate to treeline position globally (Körner & Paulsen 2004).

Finally, explanations of current ATE position which rely on recent (i.e. ~30yr) climate records lack some credibility, as they may not reflect environmental conditions at

the time of establishment, given the long life of most trees (Körner 2003a). Air temperature, insolation, and moisture availability are critical to plant development in early stages, and are also subject to high variability over the life-span of a tree. This means that conditions at the time of establishment may outweigh current conditions in the ability to predict tree presence or absence in a given location (for elaboration on this idea, see the discussion of "the plants eye view" of ATE in Malanson et al. (2009)).

This chapter adds to the body of research that attempts to understand ATE dynamics through modeling historic change. It adapts a previously published model of ATE change in the Canadian Rockies (Macias-Fauria & Johnson 2013), and trains that model on the change classes described in chapter three.

4.2 Literature Review

The oldest records of ATE dynamics are generally from temperate regions, and show correlations between climate and ATE position throughout the Holocene (Heiri et al. 2006; Lloyd & Graumlich 1997; Schwörer et al. 2017; Schwörer et al. 2014). Schwörer et al. (2017) used paleobotanical records to show that in the Canadian Cordillera, the position of subalpine fir (*Abies lasiocarpa*) and Engelmann spruce (*Picea engelmennii*) was primarily correlated to summer temperature throughout the Holocene. In that research, study sites did not have concurrent ATE advance in response to increases in atmospheric temperature, suggesting local variations in topography or geomorphology may have modified ATE position. Dendrochronological records have been used to estimate the relative effects of temperature and moisture availability on ATE position, with evidence from the Sierra Nevadas indicating treeline elevation decreasing

during periods of extended drought, ~750-850 BP (Lloyd & Graumlich 1997). These inferences about ATE position in previous millennia often lack the spatial resolution to determine site-specific impacts of climate and topography. One exception is found in Schwörer et al. (2014), who developed a dynamic vegetation model of climatic and topographic conditions surrounding a lake in the Swiss Alps, at a resolution of 25 x 25 m, adjusting model parameters until conditions at 9800 BP were simulated; results suggested dry conditions with increased seasonality. But while paleobotanical and dendrochronological records provide excellent temporal range, other methods must be used to provide the spatial resolution needed to model the specific effects of topography on ATE position.

Records of ATE dynamics in the 20th-century are abundant and typically collected using remote sensing (aerial or satellite imagery), dendrochronology, or long-term plots (Harsch et al. 2009). In a meta-analysis, Harsch et al. (2009) identified 103 publications which describe long term records of treeline position (both ATE and latitudinal treeline) at 166 sites around the world, between 1900-2008. Approximately 52% of these sites saw some form of treeline advance, and the only two studies that reported treeline recession were associated with disturbances. Linear regression with climate records revealed that many of these increases were associated with increases in atmospheric temperature. This finding is in line with multi-scale models that have emphasized the primacy of temperature in determining ATE position at a coarse scale (latitudinal or continental), while demonstrating local variation that is often topographically mediated (Case & Buckley 2015; Paulsen & Körner 2014; Weiss et al. 2015).

When topographic factors are considered, variables like slope, curvature, or compound topographic index have all been cited as factors regulating landscape-scale ATE position (Bader & Ruijten 2008; Case & Buckley 2015; Macias-Fauria & Johnson 2013). Topographic variables may influence mechanical disturbance (rockslide and avalanche), moisture accumulation, microsite formation, pedogenesis, erosion, and geomorphic conditions, all of which have the potential to affect the position of ATE.

Among topographic variables, aspect is strongly associated with heterogeneity in treeline landscapes (Bader & Ruijten 2008; Dang et al. 2015; Elliott & Cowell 2015; Greenwood et al. 2014). ATE advance can occur preferentially on one aspect in a landscape, with proposed mechanisms of this effect varying by location. Dang et al. (2015) found that in the Chinese Qinling Mountains, ATE advance occurred predominantly on north-facing slopes. This is surprising, considering that northern slopes of the region are cooler. Dang et al. (2015) note that a warming trend in lapse rates has been shown to occur at a faster rate on northern slopes, suggesting the aspect effect is a result of air mass movement. In a model of ATE in the Ecuadorian Andes, Bader and Ruijten (2008) found that treeline was higher on western slopes. They hypothesized this was a result of diurnal cycles of cloud cover in the rainforest; clear mornings led to excess insolation on eastern slopes, resulting in drying or photoinhibition. In dendrochronological records of treeline advance along a 1,000 km latitudinal transect of the American Rockies, Elliott and Cowell (2015) showed that pulses of treeline advance were more pronounced on northern aspects than on southern aspects during periods of drought. While this may seem paradoxical, it must be considered that drought in this context does not mean a reduction in summer precipitation, but rather a reduction in snow

accumulation and a subsequent lengthening of the growing season. While not all research demonstrates an aspect effect on ATE dynamics (Leonelli et al. 2016), it is evident that ecologically relevant variables that are affected by aspect can cause asymmetric treeline change, and that the nature of this aspect effect is site specific.

A rarely considered way in which aspect may impact heterogeneity in the ATE is through interactions with fire disturbance. Fire return intervals in the Canadian Rockies have varied by aspect throughout the Holocene, with south-facing aspects seeing more frequent fires (Mustaphi et al. 2013). Rogeau and Armstrong (2017) show that south-facing aspects in the front ranges of the Canadian Rockies are more than twice as likely to burn as north-facing aspects. Aspect may not only impact fire frequency in the ATE, but also post-fire patterns of re-establishment and mortality in the ATE. In a study site on Mount Rainier, Washington, Stueve et al. (2009) used aerial imagery from the period 1970-2003 to analyze topographic effects on ATE advance following a fire that occurred in 1930. They found that tree establishment rates were twice as high on north-facing aspects than on south-facing aspects. These findings introduce the possibility that the underlying climatic and topographic variables which lead to low fire return interval on southern aspects may be correlated, and potentially causally related, to environmental variables which influence ATE position.

The aspect effect described in Stueve et al. (2009) supports similar observations made in the West Castle Watershed (WCW), in the Canadian Rockies (chapter three). Using an oblique photography analysis, ATE change was assessed between 1914 and 2006. As in Stueve et al. (2009), the region experienced wildfires in 1934 and 1936. Distinct topographic patterns of ATE change were observed, and differences emerged

when these patterns were factored by exposure to fire. High rates of mortality (i.e. downslope ATE recession) were seen in south-facing areas that had been exposed to fire between observation periods. North-facing aspects experienced high rates of succession (i.e. upslope ATE advance). These observations led to questions about the interaction between fire exposure, aspect, and ATE position. The research highlighted the need to better understand the effect of topographic and climatic variables on post-fire tree establishment in the ATE.

4.3 Objectives

The primary objective of this chapter is to develop a model of historic canopy cover change in the WCW. To do so, this chapter adapts a modeling technique form Macias-Fauria and Johnson (2013) which uses proxy values for climatic, topographic, and disturbance variables to predict changes in canopy cover. The accuracy of these predictions is tested using the method of Macias-Fauria and Johnson (2013).

The secondary object of this chapter is to test the findings Macias-Fauria and Johnson (2013) with respect to the ranked importance of the climatic, topographic, and disturbance variables in their ability to explain ATE dynamics in the Canadian Rockies. Using a model trained on contemporary ATE position, Macias-Fauria and Johnson (2013) suggested that ATE advance would primarily be obstructed by geologic barriers under future warming scenarios. It is important to test these assumptions using historical observations of ATE dynamics, such as those from WCW.

The final objective of this chapter is to explore the potential for ranked variable importance to disentangle the climatic and topographic factors leading to the apparent

interaction between fire-exposure and aspect, described in Stueve et al. (2009) and in chapter three. To that end, the modeling procedure repeated in separate analysis which are restricted to areas below ATE, and areas at and above ATE. Ranked variable importance is compared between these areas, to determine if the processes driving change in the ATE are distinct from those driving change at lower elevations.

4.4 Methods

4.4.1 Study Area and Data

This research was conducted using a land cover change dataset from the WCW, described in chapters two and three. Located in the Canadian Rockies, the WCW is ~103 km^2 in area, with elevation ranging from 1400-2600 m. ATE occurs between ~1800-2300 m a.s.l. and is dominated by subalpine fir and Engelmann spruce.

The land cover change dataset was generated using fractional cover estimates from repeat oblique photography (McCaffrey & Hopkinson 2017). The repeat photographs, provided by the Mountain Legacy Project (Trant et al. 2015), contain pairs of photographs from a 1914 survey of the Canadian Rockies and repeat photographs from 2006. With the aid of a high-resolution DEM and monoplotting software, spatial information was extracted from the oblique photographs and projected to an orthogonal view. Differences between the 1914 and 2006 land cover were observed (for details, see chapter two and three). The result was a dataset which classified change into one of seven categories: high, medium, and low mortality, high, medium, and low succession, and no change (Figure 4.1). A total of 89,440 grid cells were classified, 20 x 20 m each, representing ~36% of the WCW area.

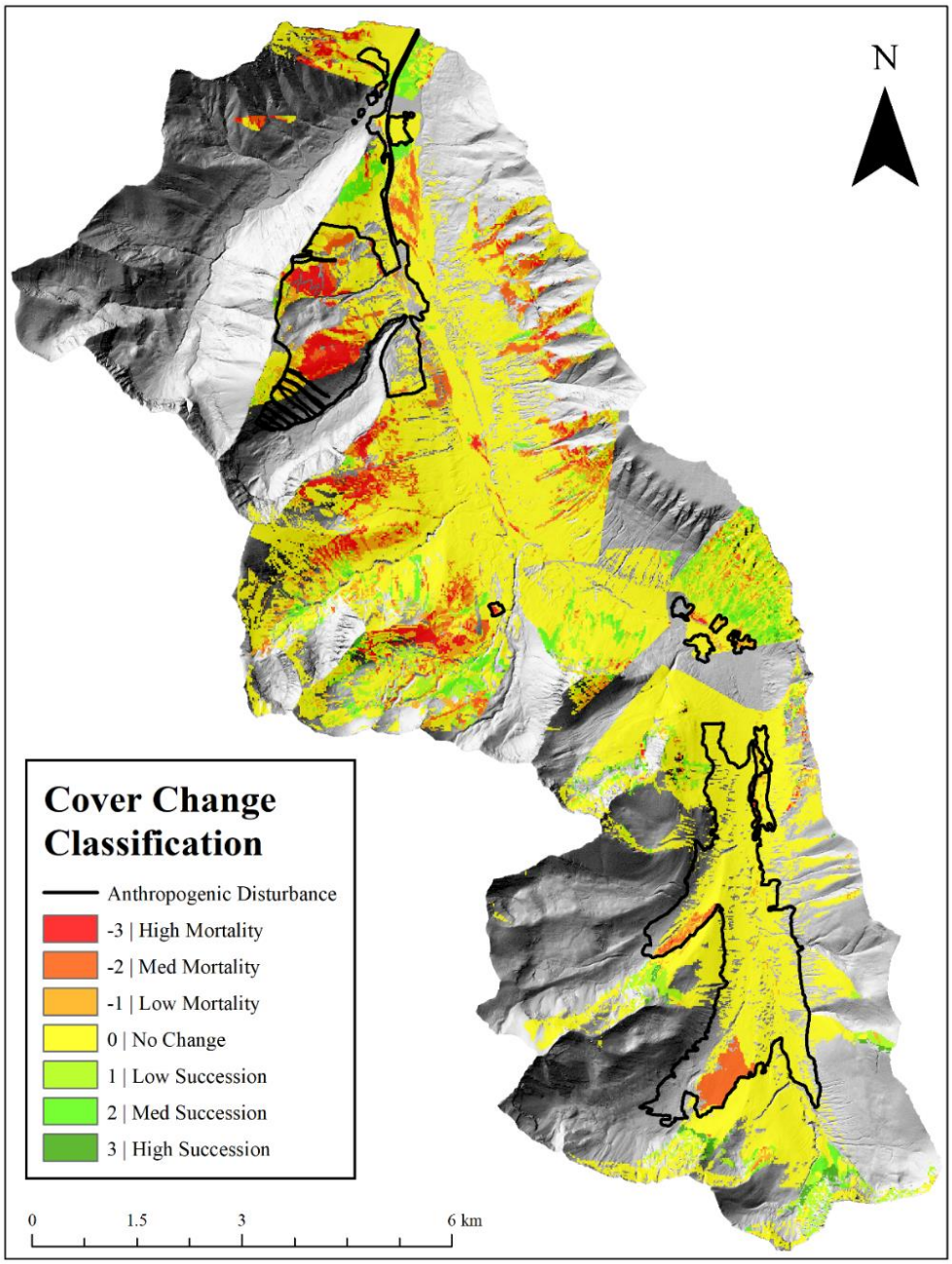

Figure 4.1 - Land cover change in WCW. Areas of anthropogenic disturbance, bounded in black lines, were omitted from training data in the present model.

4.4.2 Random Forest

Random forest is a classification and modeling algorithm that uses bootstrapped decision trees based on random samples of multivariate data (Breiman 2001). The technique provides strong predictive capability, while also demonstrating the ability to rank the relative importance of classification variables in ecologically relevant ways (Cutler et al. 2007). Recently, random forest analysis was used to investigate variability of *Nothofagus* treeline in New Zealand (Case & Buckley 2015). The analysis used 17 topographic and climatic variables, showing that in addition to the expected effects of precipitation and moisture gradients, regional differences in topo-climate were able to explain up to half of the variance in treeline position.

Random forest has also been used to predict the response of ATE to climate change in the Canadian Rockies (Macias-Fauria & Johnson 2013). Similar to Case and Buckley (2015), this work used variable importance ranking to understand the relative influence of climate, topography, and geology/geomorphology on contemporary ATE position. When historic climate values were substituted with warming projections, geologic and geomorphic barriers to upslope tree establishment became apparent, with ATE advance largely restricted to gentle, colluvium-mantled slopes.

The random forest model presented by Macias-Fauria and Johnson (2013) predicts ATE change in the Kananaskis Valley, a site that shares many characteristics with the WCW, including similar elevation range, climate, area, species mix, and topography. As such, the present work attempted to closely replicate the climate and topography proxy variables used by Macias-Fauria and Johnson (2013), and also adopted their modeling procedure. If upslope ATE advance is limited primarily by geology, any

advances observed over the 20th-century in WCW may have already hit geologic barriers. In this case, geology would have high variable importance rank in the present study, as it did in Macias-Fauria and Johnson (2013). Similarly, if historic upslope advance were restricted to colluvium, as Macias-Fauria and Johnson (2013) predict future upslope advance will be, then the importance of surficial geology will rank high in the model.

To date, no known studies have used random forest for classification of historical change in the ATE.

4.4.3 Topographic Variables

Five topographic variables were used to investigate potential correlations in ATE change: elevation, slope, aspect, curvature, and compound topographic index (Table 4.1). All topographic variables were calculated using a 1 m digital elevation model (DEM), generated from airborne lidar flown on October 18, 2014. Topographic conditions in 2014 are an accurate representation of conditions in 2006, as there were no notable geomorphic disturbances (landslides, etc.) in the intervening period.

Elevation was gridded at 1 m resolution, then aggregated to match the 20 m land cover change dataset, using mean values. Slope values were calculated on the 1 m DEM using the *slope* function in ArcGIS 10.3 (Esri 2014), then aggregated to 20 m resolution, again using mean values. The 1 m DEM is expected to produce greater estimations of slope, compared to slopes calculated on the 20 m, aggregated DEM (Kienzle 2004). Aspect was calculated on the 20 m grid, as averaging azimuth values in an aggregation process may have led to errors. Aspect was classified into nine categorical values, based on 45° bins, eight for the intercardinal directions (N = 337.5-22.5°, NE = 22.5-67.5°, E =

67.5-112.5°, SE = 112.5-157.5°, S = 157.5-202.5°, SW = 202.5-247.5°, W = 247.5-292.5°, NW = 292.5-373.5°) and one for flat surfaces without slope.

Table 4.1 - Summary of variables used in random forest model of ATE change.

Variable	Abbreviation	Unit	Mean	Std dev.	Min	Max
Continuous						
Topographic						
Elevation	ELEV	m	1843.20	263.24	1391.52	2624.44
Compound Topographic Index	CTI	unitless	5.86	2.07	1.46	23.16
Curvature	CURV	unitless	0.00	2.24	-62.62	69.99
Slope	SLOPE	°	26.42	13.59	0.00	87.38
Climatic						
Annual Precipitation	ANNPREC	mm	1477.41	279.38	901.04	2298.08
Annual Solar Radiation	ANNSOLR	Wh/m^2	1103737.10	233753.55	169984.64	15990846.00
Annual Temperature	ANNTEMP	°C	2.01	1.07	-1.12	3.93
Summer Potential Evapotranspiration	JJAPET	mm/day	1.27	0.22	0.16	1.58
Summer Precipitation	JJAPREC	mm	255.02	34.53	195.68	357.95
Summer Solar Radiation	JJASOLR	Wh/m^2	505483.39	80525.16	69832.80	652794.63
Summer Temperature	JJATEMP	°C	10.97	1.06	7.83	12.77
Categorical						
Aspect	ASPECT	9 classes: N,NE,E,SE,S,SW,W,NW,Flat				
Fire	FIRE	2 classes: Fire Exposed, Non-Fire-Exposed				
Geological Formation	SUBGEO	9 classes: Phillips Formation, Gateway Formation, Sheppard Formation, Purcell Lava, Siyeh Formation, Grinnell Formation, Appekunny Formation, Altyn Formation, Waterton Formation				
Surficial Geology	SURFGEO	5 classes: Bedrock, Colluvial Deposit, Fluvial Deposit, Glaciofluvial Deposit, Moraine				

Curvature refers to the convexity or concavity of a DEM grid cell, in relation to neighboring cells. It is calculated by fitting a fourth order polynomial to the 3 x 3 window around a DEM grid cell; positive values indicate convexity and negative values represent concavity (Zevenbergen & Thorne 1987). Curvature was calculated on the 20 m DEM, using the *curvature* function in ArcGIS 10.3. This function calculates standard curvature, which combines both profile and plan curvature.

Compound topographic index (CTI), is an index of the ratio of upstream area to slope (Beven & Kirkby 1979). In ATE research, CTI has been used as a proxy for both

cold air pooling (Case & Duncan 2014) and soil accumulation (Schwörer et al. 2014). CTI is measured using the formula:

$$CTI = \ln (A / \tan \beta) \quad (1)$$

Where A is the contributing upslope area, and β is the slope in degrees. These variables were calculated in ArcGIS 10.3, using the *flow direction* and *flow accumulation* functions for A, the *slope* function for β.

4.4.4 Geologic Variables

It has been demonstrated that soil properties, surficial geology, bedrock type, and mountain architecture all have a significant effect on the position of ATE (Fagre et al. 2007; Macias-Fauria & Johnson 2013). To account for potential geologic barriers to change in the ATE, two geologic variables were included in this model: surficial geology and bedrock type. For surficial geology, areas of bedrock, colluvial deposits, fluvial deposits, glacio-fluvial deposits, and moraine were categorized using data from the Alberta Geological Survey (Fenton et al. 2013). For bedrock types, nine geologic formations in the WCW were identified using the Lexicon of Canadian Stratigraphy (Glass 1990) and digitized from a historic geologic map of the region (Geological Survey of Canada & Price 1961).

4.4.5 Climatic Variables

Seven climatic variables were used to model change: precipitation (annual and JJA), temperature (annual and JJA), solar radiation (annual and JJA), and potential evapotranspiration. Given the geographic similarity in the research areas, this study

followed the methods of Macias-Fauria and Johnson (2013) to develop precipitation and temperature model inputs. In alpine areas, steep gradients in temperature and precipitation are caused by lapse rates, which generally result in cooler temperatures and increased precipitation with increased elevation. To create proxy values that spatially distribute the anticipated effect of lapse rates, Macias-Fauria and Johnson (2013) adapted a method from Randin et al. (2009): 1) historic normal values (30-year) for temperature and precipitation were collected from three meteorological stations, within 32 km of their study site in the Canadian Rockies; 2) using locally observed temperature and precipitation enhancement rates (Cullen & Marshall 2011), monthly averages were normalized to sea-level (i.e. the residual if elevation is equal to 0), 3) residual temperature and precipitation values were interpolated, at 'sea-level', using inverse distance weighting (IDW), 4) using a DEM of the study area and the definition of the linear regression of lapse rate, temperature and precipitation values were calculated for each grid cell according to elevation, then adjusted by either adding or subtracting the value from the interpolated residual surface.

One issue with the Randin et al. (2009) method used by Macias-Fauria and Johnson (2013) is that the lapse rates described by Cullen and Marshall (2011) were from observations made between 2005-2009. Macias-Fauria and Johnson (2013) applied these to climate records for a period between 1971-2000. Given that the present study seeks to identify climatic variables associated with historic change in the ATE, a longer observation period was required (1914-2006). Five Environment Canada meteorological stations were identified within 20 km of the WCW (West Castle, Spionkop Creek, Gardiner Creek, Castle, and Carbondale Lo). While these stations provided adequate

elevation range to calculate lapse rates, the temporal coverage did not extend earlier than 1958. The search radius was extended to 50 km, and stations with the longest temporal coverage were selectively added. These historic records came from three nearby towns (Coleman, Beavers Mines, and Pincher Creek Town). The addition of the towns provided adequate temporal coverage, but they were located at low elevations compared to the study site. Using monthly mean temperature and monthly precipitation totals, annual and summer (JJA) averages for temperature and precipitation were calculated.

If a record did not contain all 12 months in a calendar year, that year was omitted from annual average calculation. Similarly, if a record did not contain all three summer months (June, July, and August), the year was omitted from summer average calculation. Sporadic temporal coverage caused the Carbondale Lo site to be omitted entirely, leaving seven meteorological stations, summarized in Figure 4.2, Figure 4.3, and Table 4.2.

Following the Randin et al. (2009) method, data from the seven meteorological stations were used to regress a line between elevation and either temperature or precipitation. In all cases, elevation was significantly correlated to average annual and summer values for temperature and precipitation (Table 4.3). The lapse rates for both annual and JJA temperature were -4.0°C / 1 km, were comparable to regional values reported in Cullen and Marshall (2011), (-4.2°C and -5.0°C respectively).

Table 4.2 - Summary of Meteorological Station Attributes

Station Name*	Latitude	Longitude	Elevation (m)	Years on Record	Dist. to WCW (km)
Castle	49.40	-114.33	1360	1958-2007	7.8
Westcastle	49.28	-114.37	1524	1999-2007	0.0
Pincher Creek Town	49.52	-113.97	1154	1893-1963	36.6
Spionkop	49.22	-114.08	1861	1998-2007	17.3
Gardiner	49.37	-114.52	1920	1998-2007	5.1
Coleman	49.63	-114.58	1341	1912-1997	32.5
Beaver Mines Town	49.47	-114.18	1257	1912-2007	21

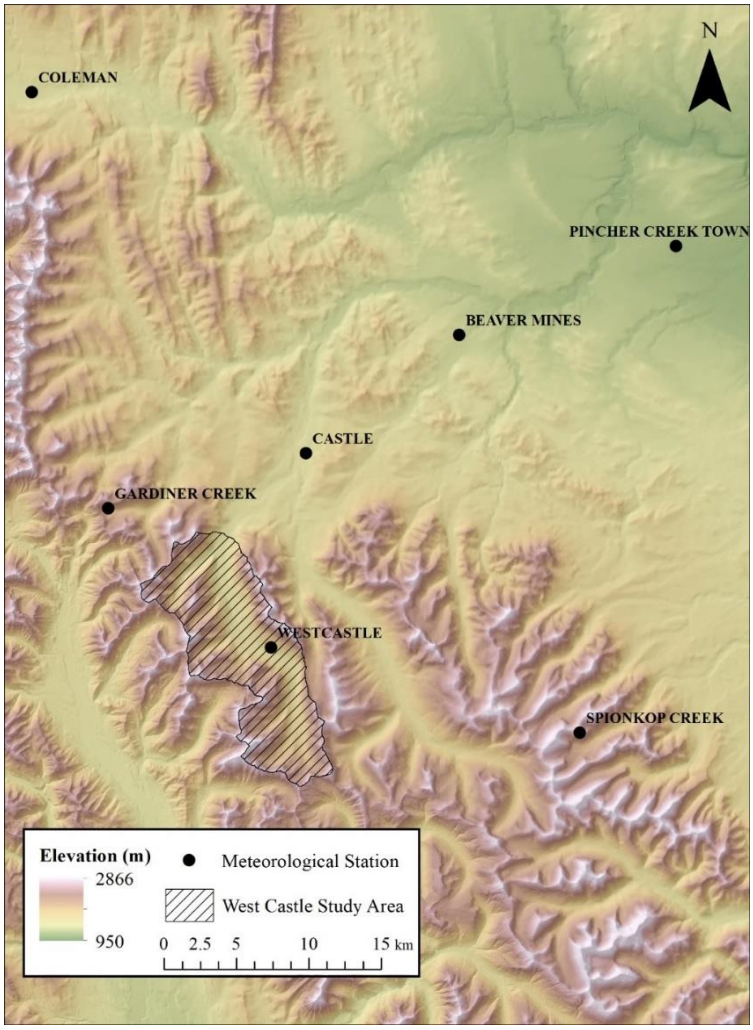

Figure 4.2 - Meteorological Stations in the West Castle Region

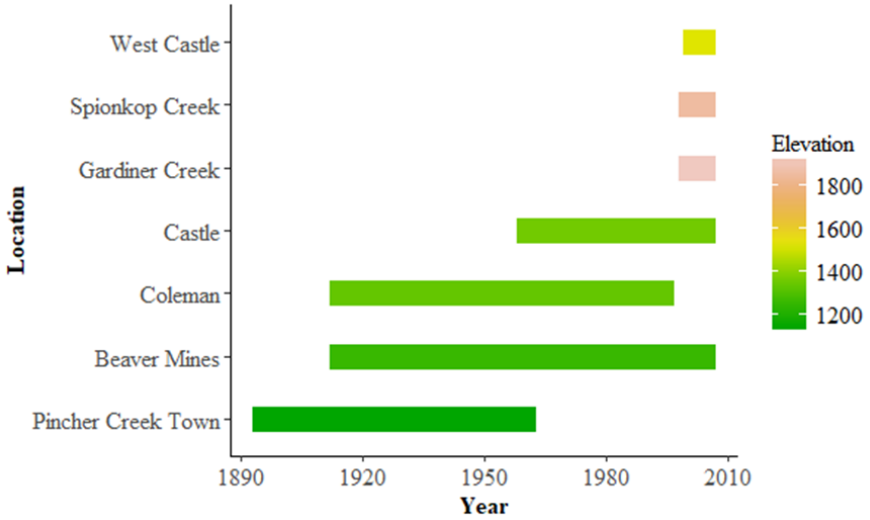

Figure 4.3 - Meteorological Station Elevation and Years on Record

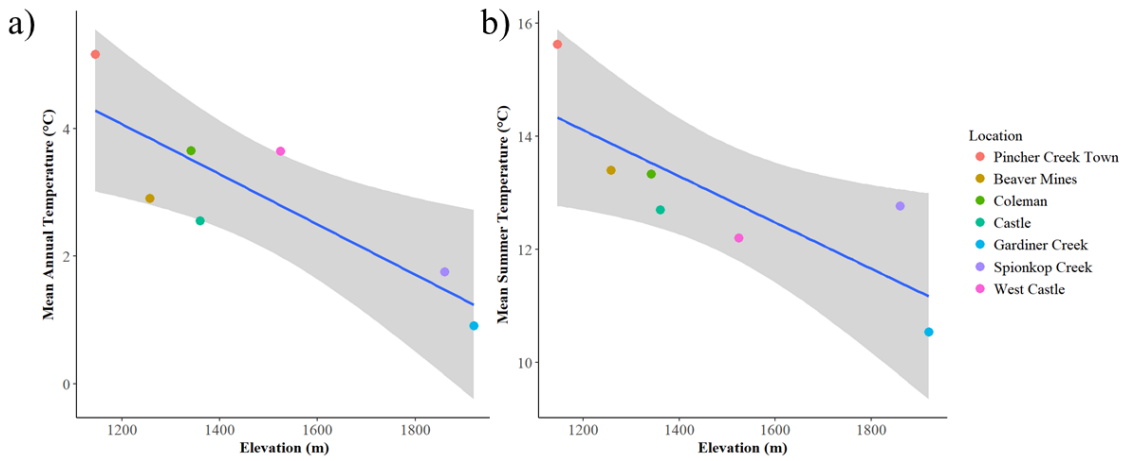

Figure 4.4 - Annual and Summer (JJA) Temperature Lapse Rates

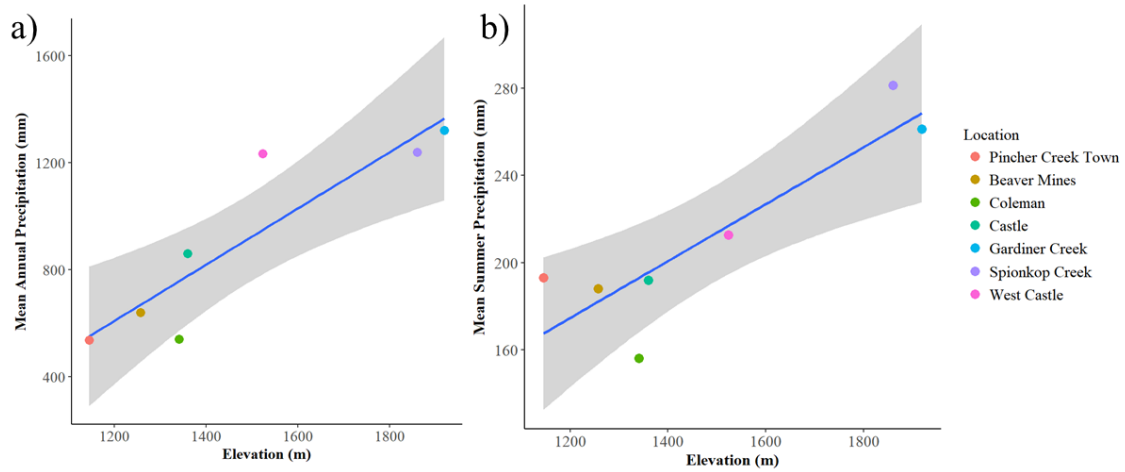

Figure 4.5 - Annual and Summer (JJA) Precipitation Enhancement

Table 4.3 - Results of Lapse Rate Regression

	slope	**y-intercept**	**R^2**	**F**	**p-value**
Annual Precipitation	1.050	-650.29	0.77	20.73	0.006
Summer Precipitation	0.130	18.20	0.74	17.81	0.008
Annual Temperature	-0.004	8.79	0.65	12.25	0.017
Summer Temperature	-0.004	19.01	0.74	17.81	0.008

Solar radiation was calculated in ArcGIS 10.3 using the *area solar radiation* tool on the 20 m DEM. Solar radiation was modeled at 30-minute intervals, with all monthly totals summed for an estimate of annual insolation, and JJA totals summed for summer insolation.

Potential evapotranspiration (PET) values were modeled using the method of Oudin et al. (2005), which gives comparable results to Penman-Monteith calculations in rainfall-runoff models, but can be implemented when values for wind speed and humidity are unreliable. This method of PET calculation was based on the models of Jensen and Haise (1963) and McGuinness and Bordne (1972), which use the general form:

$$PE = \frac{R_e}{\lambda\rho}\frac{T_a + K_2}{K_1} \quad if\ T_a + K_2 > 0 \qquad (2)$$
$$PE = 0 \quad otherwise$$

where PE is the rate of potential evapotranspiration (mm day $^{-1}$), R_e is extraterrestrial solar radiation (MJ m^{-2} day^{-1}), λ is latent heat flux (2.45 MJ kg^{-1}), ρ is the density of water (1000 kg m^{-3}), T_a is the mean daily air temperature (°C). The fixed parameters K_1 (°C) and K_2 (°C) scale the importance of T_a, and set a threshold at which $PE = 0$. Oudin et al. (2005) empirically determined 100 and 5 to be the optimal values for K_1 and K_2, which are the values used in this study. Average summer potential evapotranspiration values were modeled by calculating average daily JJA solar radiation (total JJA solar radiation in Wh/m^{-2}, divided by number of days in summer, converted to MJ m^{-2} day^{-1}) for R_e, and using the average JJA temperatures (calculated from the previously described lapse rate analysis) for T_a.

4.4.6 Disturbance Variables

Two disturbance types were accounted for in the model: wildfire and anthropogenic disturbance.

Two wildfires affected the WCW in the period between the 1914 and 2006 oblique photographs which were used to generate the change dataset. The Pass Creek Fire of 1936 mainly affected the northern extent of the WCW, covering 45.2% of the area of the watershed. A smaller fire occurred in 1934 and was restricted to the southern-most slope, covering only 1.5% of the watershed. Fire extents were delineated using historic descriptions, and aerial imagery from 1949 where the remnant fire scars were still visible (Wildfire Management Branch - Alberta Agriculture and Forestry 2017). These fires occurred at the height of the Great Depression, it is believed that the Province of Alberta had very few resources to contain them (Rogeau et al. 2016). However, historical accounts suggest that up to 180 men from nearby mining towns spent the summer fighting the fire (Murphy 2006). It is unknown if these fire-control procedures would have had any effect on the topographic extent of the fire. As a result of the lack of information regarding fire source and intensity, fire disturbance is treated as a binary input to the model, with areas classified as being either fire-exposed or non-fire-exposed.

Finally, areas of WCW featuring anthropogenic disturbance between observations were identified and omitted. The Alberta Vegetation Inventory (Alberta Environment and Parks 2012) was used to aggregate disturbances including former oil well pads, historical forestry cut-blocks, a small ski resort (Castle Mountain), and roads. These features were excluded from model training, and were not included in the extent of the model prediction.

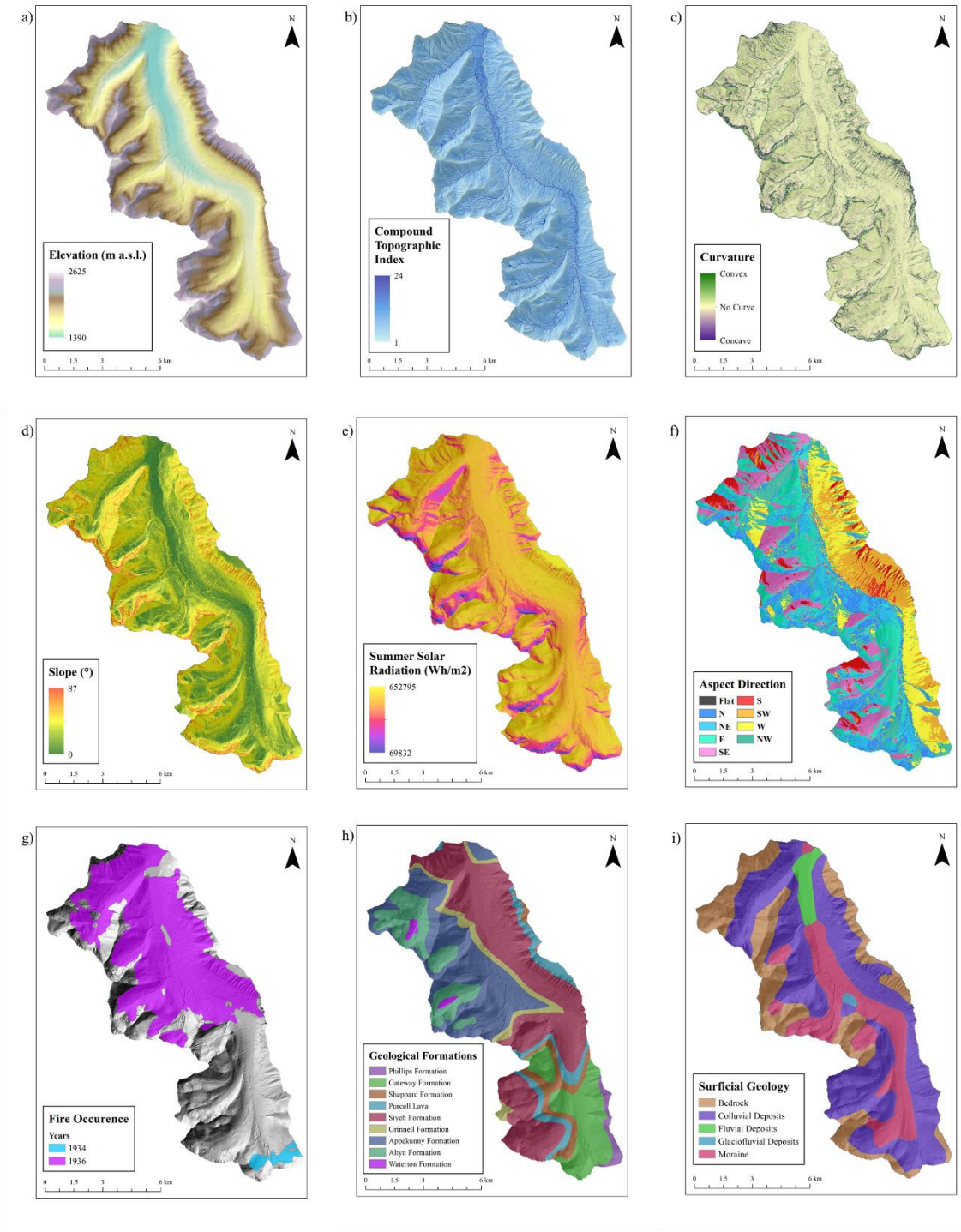

Figure 4.6 - Nine variables used in the random forest model: a) elevation, b) compound topographic index, c) standard curvature, d) slope, e) summer solar radiation, f) aspect, g) fire occurrence, h) bedrock geology, i) surficial geology.

4.4.7 Model Execution

The topographic, geomorphic, climatic, and disturbance variables listed in Table 4.1 were used as model inputs for classification of land cover change in R v3.2.3 (R Core Team 2017) using the *randomForest* package (Liaw & Wiener 2002). A correlation matrix for the continuous variables was generated using the *corrplot* package (Wei & Simko 2016), and groups of variables that were highly correlated ($|r| > 0.60$) were reduced to a single, representative variable.

Canopy cover change in unobserved areas was predicted using the method of Macias-Fauria and Johnson (2013). The model was run 11 times, each time with a random sample of 50% of the training data used as input variables (see Appendix A for scripts). After each model run, the results using that specific sample of training data were used to generate a prediction of land cover change for the whole extent of WCW, including the area of the watershed that was not observed in the initial oblique photography (note: anthropogenic disturbance areas were omitted from both training and prediction datasets, as they are a result of processes independent of historical ATE change). An odd number of model runs was used, so that once 11 predictive surfaces had been generated, the median value for each grid cell could be joined to make a final prediction raster (Macias-Fauria & Johnson 2013). Model accuracy was assessed by clipping the extent of the training data from the prediction raster, and comparing against the observed land cover change in a confusion matrix, using the *caret* package (Williams et al. 2017). Additionally, the out-of-bag assessment of error (overall accuracy when the 50% random sample is trained to predict the remaining 50% of the data) was recorded for each of the 11 runs.

Variable importance was compared by cataloging the mean decrease in Gini coefficient (MDG) for each variable, in each model run, and taking the mean MDG value among the 11 runs as the final MDG for each variable. Ranked variable importance is compared to the results of Macias-Fauria and Johnson (2013).

Finally, in an attempt to disentangle the climatic and topographic factors leading to the apparent interaction between fire-exposure and aspect in the ATE, a second analysis compared variable importance between the ATE and lower elevations. The training dataset was split in two; areas where elevation > 1800 m, which include ATE and alpine areas, are referred to as *high* e*levation*, and areas < 1800 m are referred to as *low* e*levation.* The value of 1800 m was selected as a break point, as it fell approximately between the median elevation of the training data (1742 m) and the median elevation for the extent of WCW (1838 m). The previous analyses were repeated with 11 model runs, confusion matrix accuracy assessment, and ranking of variable importance using MDG.

4.5 Results

Three groups of highly correlated continuous variables were identified (Figure 4.7, Table 4.4). In the first group, annual precipitation, annual temperature, summer precipitation, summer temperature, and elevation were found to be highly correlated ($|r| = 0.85 – 1.00$). These correlations reflected the results of Macias-Fauria and Johnson (2013), which also failed to prevent auto-correlation in the proxy variables developed using the method of Randin et al. (2009). In the second group, annual solar radiation, summer potential evapotranspiration, and summer solar radiation were found to be highly correlated ($|r| = 0.85 – 0.96$). In the third group, summer potential evapotranspiration and slope were found to be highly correlated ($|r| = 0.65$). Following the method of Macias-

Fauria and Johnson (2013), one variable was selected from each of the highly correlated groups (elevation, summer solar radiation, and slope), with the other variables omitted.

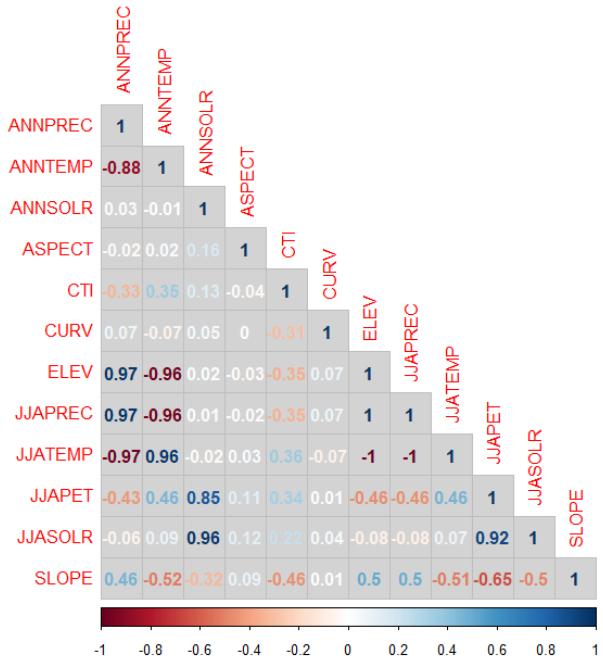

Figure 4.7 - Correlation matrix of continuous variables.

Table 4.4 - Correlated variable groups.

	Group 1	Group 2	Group 3
Correlated Variables	ANNPREC ANNTEMP ELEV JJAPREC JJATEMP	ANNSOLR JJASOLR JJAPET	JJAPET SLOPE
Selected Variable	ELEV	JJASOLR	SLOPE

Using the remaining nine variables (Figure 4.6), the median prediction raster was compared to the training data. Overall accuracy was significant (0.840, n = 89,440, $p < 0.001$), and kappa showed moderate agreement at 0.577. The training data had high representation of the *no change* cover class, which is evident from the high sensitivity

value of *no change* compared to other variables. Conversely, specificity was much lower for *no change* than for the other change variables. To understand the effect of the large *no change* sample on measures of accuracy, sensitivity, and specificity, a second confusion matrix was

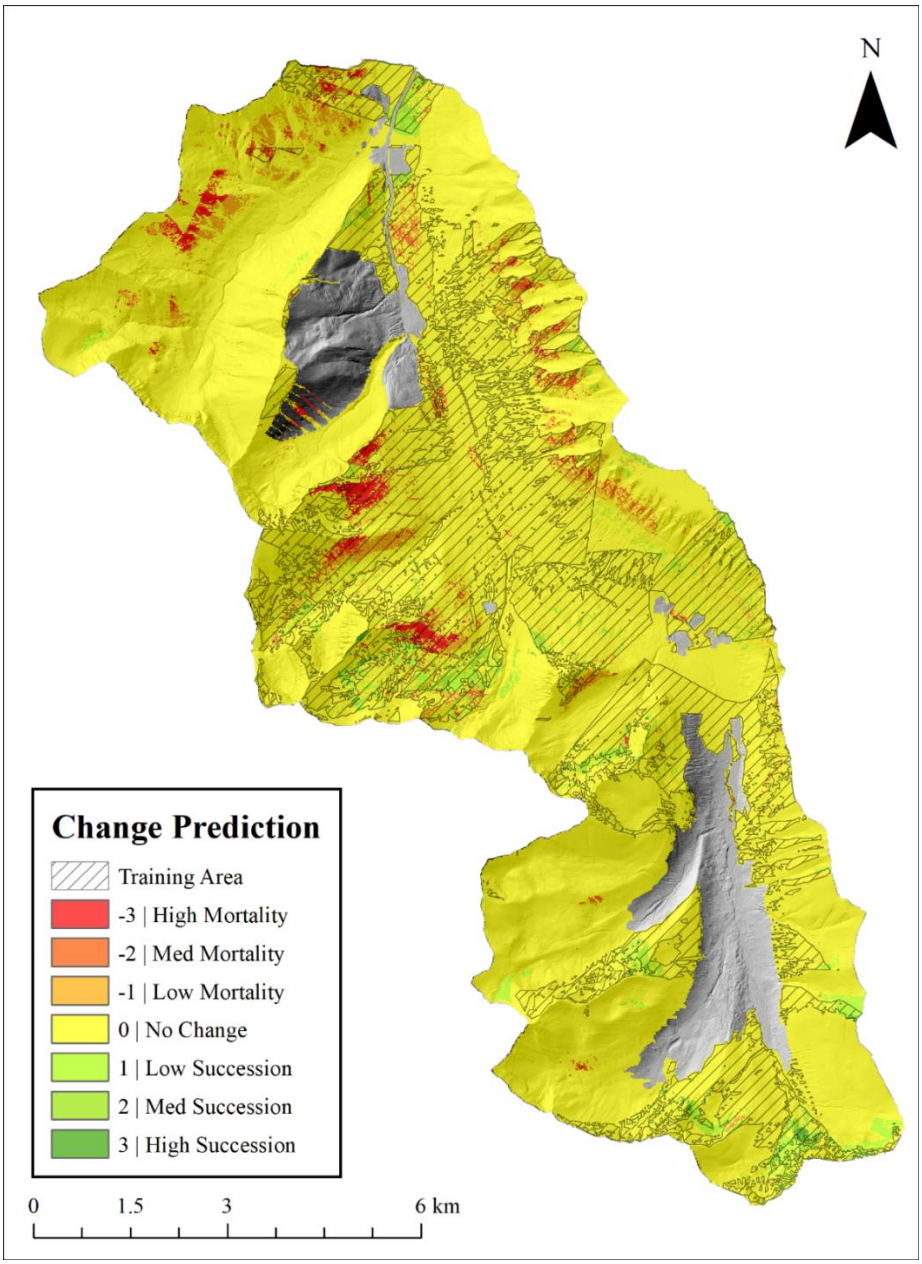

Figure 4.8 - Result of canopy change spatial extension into unobserved areas of WCW. Grey areas are omitted anthropogenic disturbance.

Table 4.5 - Within-training-data confusion matrix and accuracy assessment.

Prediction	Reference								Including 0		Excluding 0	
									Sensitivity	Specificity	Sensitivity	Specificity
	-3	**-2**	**-1**	**0**	**1**	**2**	**3**					
-3	1381	149	155	107	12	1	0		0.568	0.995	0.841	0.972
-2	58	1500	82	83	25	11	0		0.394	0.997	0.778	0.984
-1	198	244	3325	262	90	46	4		0.450	0.990	0.910	0.936
0	790	1880	3729	63802	3530	1758	316		0.988	0.516	-	-
1	3	32	82	271	3322	123	70		0.471	0.993	0.943	0.967
2	2	4	13	62	71	1411	18		0.420	0.998	0.883	0.990
3	0	0	1	5	4	6	373		0.478	0.999	0.803	0.999
								Accuracy	0.840		0.883	
								Kappa	0.577		0.850	

constructed with *no change* values omitted. Sensitivity increased, and specificity remained high. Out-of-bag estimates of error showed 75.8% overall accuracy when training on a 50% random sample of the data, 11 times.

Prediction of canopy change class in unobserved areas was generated using the full training sample area (Figure 4.8). While this spatial extension was not validated, the out-of-bag estimate of error from the model training (i.e. 75.8%) provides the best assessment of model predictive accuracy on naïve data.

Variable ranking showed that elevation had the highest MDG, followed by the other continuous variables (summer solar radiation, slope, CTI, and curvature) (Figure 4.9, Table 4.6). The lowest MDG was seen in the categorical variables (bedrock geology, aspect, surficial geology, and fire exposure).

Table 4.6 - Confusion Matrix Accuracy Results.

	Accuracy	95% CI	n	p-value	Kappa
All	0.840	0.838 - 0.843	89 440	< 0.001	0.577
High Elev.	0.761	0.756 - 0.764	38 014	< 0.001	0.490
Low Elev.	0.826	0.823 - 0.829	51 426	< 0.001	0.300

Table 4.7 - Variable Importance MDG Values.

Variable	All	High Elev.	Low Elev.	Difference (High Elev. – Low Elev.)
FIRE	472.18	478.59	152.28	326.32
SUBGEO	991.52	643.29	416.94	226.35
JJASOLR	2413.21	1403.11	1204.39	198.72
ASPECT	988.08	590.13	416.54	173.58
CURV	1870.38	1108.34	977.3	131.04
CTI	1996.19	1167.64	1059.17	108.47
SURFGEO	521.44	352.2	287.43	64.76
SLOPE	2249.92	1272.1	1280.58	-8.47
ELEV	3435.21	-	-	-

The second analysis, based on elevation partition, showed that *high elevation* areas resulted in model accuracy of 0.761, n = 38,014, p < 0.001, and kappa = 0.490. *Low elevation* areas had model accuracy of 0.826, n = 51,426, p < 0.001, and kappa = 0.300. Order of variable importance was generally consistent across both conditions, with summer solar radiation and slope having high MDG (Figure 4.9, Table 4.7). The categorical variables remained below the continuous variables in order importance. The largest difference in MDG between the *high elevation* and *low elevation* training samples was observed in the fire exposure variable.

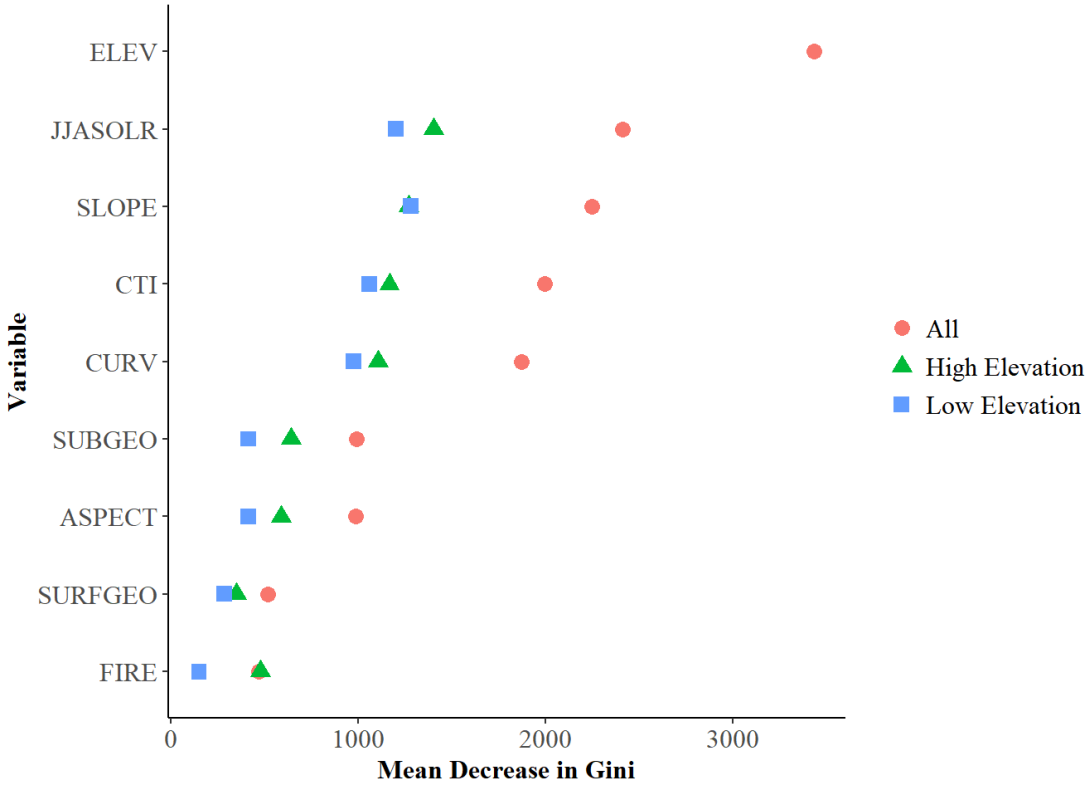

Figure 4.9 - Variable Importance Ranked by MDG.

4.6 Discussion

4.6.1 Accuracy

The random forest model demonstrated the ability to predict historic change in the WCW, based on proxies of climatic, topographic, geologic, and disturbance variables. However, the large sample of areas without land cover change over the 92-year observation period introduced uncertainty in accuracy assessment. The high level of sensitivity for the *no change* class (0.998) compared to the other change classes (0.394-0.568) indicated that the accuracy predictions were potentially a function of the large sample improving the probability of a correct classification. Sensitivity of change class identification increases when the potential for confusion with *no change* class is removed (0.778-0.943), suggesting that future attempts to model ATE change with this method might benefit from using a training dataset with a large sample of ATE variability.

Accuracy of the *high elevation* model was lower than accuracy of the *low elevation* model, which was potentially a result in the discrepancy in the size of the training dataset (high elevation n = 38,014, low elevation n = 51,426). Canopy cover change in *low elevation* data was generally more homogenous, and experienced less change over the 92-year observation period. Thus, with less variability in change classes, the model provided more accurate classification at lower elevations. The low kappa value of the *low elevation* area (0.30) compared to the *high elevation* area (0.49) supports this reasoning.

The reported accuracies are only valid for the area of overlap between the training data and the prediction area, and do not reflect the accuracy of the spatial extension of the

model outside of the training area. The best estimate of spatial extension accuracy come from the out-of-bag estimate of error, which showed overall accuracy to be 75.8%.

4.6.2 Elevation, Air Temperature, and Precipitation

Given that ATE is recognized as being a function of lower temperatures at high elevation, it is unsurprising that elevation ranked as the most important variable by MDG. This finding supports the work in chapter three, which showed that the degree of both mortality and succession in the ATE was positively correlated to elevation; stated differently, changes in mortality and succession were more exaggerated at higher elevations.

One of the objectives of this research was to disentangle the relative importance of temperature and precipitation on tree establishment following fire disturbance, in an effort to explain observed patterns of mortality on north- and south-facing aspects. Unfortunately, the method that was used to generate proxy values for the effect of lapse rates on temperature and precipitation (Randin et al. 2009) did not adequately distinguish between the effect of elevation on temperature and precipitation. The method used IDW to interpolate the residual values at each meteorological station across the study area, but did not provide sufficient resolution to outweigh the impact of elevation in each calculation. The impact of the interpolated residual surfaces was small enough that summer temperature and precipitation values were correlated to elevation at 1.0, as they were both primarily functions of elevation.

The results call into question whether the method of Macias-Fauria and Johnson (2013) accurately distinguished between climatic and geologic factors in determining

upslope treeline advance. As in the present study, Macias-Fauria and Johnson (2013) were not able to separate elevation, air temperature, and precipitation using the method of Randin et al. (2009). This is not insignificant, as the general finding of their research was that upslope treeline advance will be limited by a lack of adequate geologic and geomorphic conditions at high elevations.

The inability to distinguish between the effects of lapse rate on temperature and precipitation underscores the need for improved understanding of local, meso-scale variations climate, and their relationship to elevation. An elevational transect of meteorological stations began collecting data in WCW as of the summer of 2014 and was completed in 2017 with precipitation a high and low elevations. The observations from these stations could inform improved modeling of air temperature and precipitation in the future.

Until modeled variables have the resolution required for this analysis, an understanding of the relative importance of air temperature versus precipitation on ATE dynamics can be gained through experimentation. Kueppers et al. (2017) used experimental heating and watering across an elevation transect to study the effect of changing air temperature and precipitation regimes on tree establishment in the ATE. Heating limited the establishment of Engelmann spruce at elevations above treeline, but this effect was mitigated with watering. This finding suggests that precipitation or moisture provided through accumulated snow could be essential for upslope treeline advance to results from increases in atmospheric temperature.

4.6.3 Solar Radiation, PET, and Aspect

Solar radiation also had high variable importance, as ranked by MDG. Previous models have demonstrated that solar radiation can explain variability of ATE at multiple spatial scales (Case & Duncan 2014), and that this effect was independent of the influence of insolation on soil moisture availability. Unfortunately, insolation and moisture availability could not be directly compared in the present model, as the Oudin et al. (2005) equation to calculate PET used solar radiation as a parameter, causing a high degree of correlation. Given the a prior expectation that these variables would be highly correlated, it is surprising they were used in Macias-Fauria and Johnson (2013).

In chapter three, a strong aspect effect was observed, where the majority of mortality seen over the observation period occurred on south-facing, fire-exposed slopes. One of the expectations of this model would be that aspect would have a high MDG ranking, but paradoxically, aspect ranked low. It is worth considering that this result may be a function of the way in which random forest handles continuous versus categorical variables. Strobl et al. (2006) showed that the classification and regression tree algorithm (Breiman et al. 1984) used in random forest is biased such that continuous variables rank higher in importance than categorical variables. Additionally, categorical variables with a greater number of classes are biased towards higher variable importance rank. Indeed, when looking at variable importance rank in the present study, they are perfectly sorted, first by continuous variable, then in order of the number of classes in the categorical variables. Macias-Fauria and Johnson (2013) treated aspect as a categorical variable, also finding that it ranked low in variable importance; aspect was treated as a categorical variable in the present chapter, in order to maintain comparison between the studies.

4.6.4 Slope, CTI, and Curvature

The topographic variables of slope, CTI, and curvature were midway in rankings of importance. Slope has been shown to affect ATE through mechanical disturbance, with many treelines in Montana regulated by rockslide and avalanche (Butler & Walsh 1994; Walsh & Butler 1997; Walsh et al. 1994). WCW has numerous chutes where ATE appears to be suppressed, potentially by avalanche, but the episodic nature of these events may not have been captured in the two observations, separated by 92 years. Previous research indicated that the high mortality class had significantly higher slope than other change classes (chapter three), suggesting that mortality may have been the result of avalanche. It is conceivable that in specific circumstances, the effect of slope might outweigh that of elevation and aspect, but if this were broadly the case then slope would have had higher predictive value in the model.

CTI has been used in ATE research as a proxy for cool air-pooling (CAP) (Case & Duncan 2014), where radiative transfer and advection reduce air temperatures at ground surface. CAP is known to occur in the Rocky Mountains (Holden et al. 2011), which implies several possibilities: 1) CAP is occurring, and affecting ATE position, but CTI is not acting as a proxy for CAP, 2) CAP is occurring, and is correlated to CTI, but the effect is not dominant over other temperature mediators like elevation and insolation, 3) CAP is not occurring in the WCW. The results suggest that options 2 and 3 are the most plausible, but future ATE research in WCW should incorporate either high resolution, topographically distributed temperature measurements or modeling methods other than CTI to account for the potential effect of air-pooling.

The response of the curvature variable had middling rank, indicating that local convexity and concavity had a marginal effect on ATE dynamics. One issue with this finding is potentially the resolution. The curvature operates on a 3 x 3 moving window, which means that curvature was based on a 60 x 60 m observation space. This resolution is ideal for distinguishing gullies from ridgelines, but may be inadequate to identify smaller features associated with microsite formation and pedogenesis. Curvature was identified as the primary variable driving divergence from the climatic treeline maximum in the random forest model of Case and Buckley (2015).

4.6.5 Surficial and Bedrock Geology

Surficial and bedrock geology both rank low in variable importance, but this finding must be considered with the understanding that they are both categorical variables, and are subject to bias in the random forest model. Bedrock geology ranked higher in importance than surficial geology, but this is likely a function of bedrock geology containing more categories. These variables were included in the model in order to account for the finding of Macias-Fauria and Johnson (2013), that upslope ATE advance under climate warming projections would be limited by geologic constraints such as bedrock. If these geologic constraints did limit ATE advance in the WCW, then these variables would have had higher ranks. This finding does not preclude future geologic limitations to ATE advance in the WCW.

4.6.6 Fire

The ranked importance of fire exposure in the present research diverged the most from expectation. In the preceding research (chapter three), an asymmetric response to fire exposure was observed, with fire causing higher mortality on south-facing slopes than on north-facing slopes. Given that finding, the fire-exposure variable was expected to rank high, however the results showed that fire-exposure was the least important variable. It must be taken into account that as a categorical variable with only two classes, fire-exposure may have been subject to the same model bias described for the other categorical variables.

An intriguing finding came from the elevation partition analysis. The largest difference in MDG between *high elevation* and *low elevation* datasets was seen in the fire-exposure variable. Fire-exposure provided a higher explanatory power for land cover change in *high elevation* areas than *low elevation areas*. One interpretation of this finding is that fire may interact with other topo-climatic variables at ATE elevations in a way that it does not at lower elevations. For example, a stand-clearing fire in the 1930s which occurred at low elevation would have ample resources (soil moisture, insolation, adequate growing season temperature) to replace the stand before the 2006 observation, thus recording *no change*. At ATE elevation, where these resources are limited, soil moisture and growing season temperatures which may have been adequate for a mature tree stand pre-fire may have posed limits to tree establishment post-fire. This effect would result in the observed increase in the ability for fire to predict land cover change at *high elevations* versus *low elevations*.

Evidence of this threshold effect of fire can be seen in a recent study of post-fire tree establishment in the ATE (Stine & Butler 2015). This study reported significant soil erosion by wind and water following the removal of vegetation and duff layers by fire. While effective soil depth did not significantly vary between burned and unburned sites, seedling establishment was significantly higher in burned areas with deeper soil and more rock shelter. This finding was curious, as previous studies had shown these variables did not affect seedling establishment in unburned areas (Malanson et al. 2002). Thus, variables related to topography and climate that do not appear to affect tree establishment in normal ATE conditions can become critically important to tree establishment following disturbance by fire. Future research should investigate patterns of post-fire tree establishment using a method that controls for the effect of aspect on climatic variables.

4.7 Conclusion

A random forest model of WCW was trained to classify historic changes in forest cover, based on a set of climatic, topographic, geologic, and disturbance variables. Elevation had the highest explanatory power in determining forest cover change, but air temperature and precipitation may also be considered to have high explanatory power in the model but given high correlation among variables. Insolation also ranked highly. While several multi-scale models suggest that at a landscape scale, topography can outweigh the importance of temperature in ATE position (Case & Duncan 2014; Weiss et al. 2015), the topographic factors of slope, CTI, and curvature rank lower in importance than climatic variables. Lowest variable importance was seen in the categorical variables surficial geology, bedrock geology, and fire-exposure; these findings were unexpected, as

previous studies had suggested strong effects from geologic variables (Macias-Fauria & Johnson 2013) and fire-exposure. Interpretation of variable importance ranking was made difficult by an apparent bias towards continuous variables. Future implementations of this method will better understand variable importance by applying random forests which use conditional interference trees for variable selection, avoiding bias (Strobl et al. 2006).

Partitioning the data into areas at and above ATE and below had little effect on the rank of variable importance. However, a discrepancy in the MDG of fire-exposure between elevation ranges provided an indication of the potential for 'threshold effects', where climatic and topographic stressors which are not limiting to tree establishment in the pre-fire ATE become limiting post-fire. These threshold effects may explain the correlation between fire-exposure, aspect, and mortality/succession at ATE described in chapter three. Future research should focus on an understanding of how climatic variables which correlate to aspect (i.e. insolation, wind exposure, PET, soil moisture, soil temperature) alter patterns of post-fire tree establishment. While the modeling techniques used were generally inadequate to distinguish between factors at the resolution required to observe these micro-site formation effects, *in situ* measurements of hydroclimate at a range of elevations and aspects in WCW will provide this ability. Additionally, recent wildfires in southern Alberta, such as the Lost Creek Fire of 2003 and the Kenow Fire of 2017, could be useful for observing 'threshold effects' of post-fire tree establishment in the ATE in a variety of aspects and growth stages.

Given the increased frequency of ATE fire (Cansler et al. 2016), and the paucity of research investigating fire at high elevation (Rogeau & Armstrong 2017; Stine &

Butler 2015), the potentially limiting effect of fire on upslope treeline advance should remain an area of research focus.

Chapter 5 - Conclusion

5.1 Chapter Summaries

This research successfully applied a novel method for assessing canopy cover change in the ATE, increasing the spatial extent, spatial resolution, and temporal window of observation. The data were used to assess the role of climatic, topographic, and disturbance modulating factors on change in the ATE.

In chapter two it was demonstrated that the Stockdale method (Stockdale et al. 2015), which extracted land cover from oblique photography at a resolution of 100 m, could be adapted to determine qualitative classification of canopy cover at a resolution of 20 m (McCaffrey & Hopkinson 2017). This method facilitated the quantitative measurement of ATE area, offering considerable improvement over previous methods of spatializing ATE data from oblique photographs (Roush et al. 2007). Initial accuracy estimates for the method were encouraging: photograph interpreters agreed on qualitative canopy class in 88.4% of cases, canopy classes agreed in 78.4% of areas that were observed in multiple photographs, and canopy classes were up to 64.7% accurate compared to discretized fractional cover from airborne lidar.

Chapter three used the method described in chapter two to record changes in canopy cover between 1914-2006. High levels of mortality were seen in anthropogenically disturbed areas compared to undisturbed areas. In areas without anthropogenic disturbance, *full cover* canopy was dominant, but declined between 1914 and 2006. The degree of both mortality and succession increased with elevation, meaning change was more intense in the ATE region. An aspect effect was observed, in which N- and NE-facing aspects had greater proportions of succession, and S- and SW-facing

aspects had higher-than-expected proportions of mortality. This finding is consistent with other reported aspect effects (Bader & Ruijten 2008; Dang et al. 2015; Elliott & Cowell 2015; Germino et al. 2002; Greenwood et al. 2014). Factoring by fire suggested that the aspect effect interacted with fire exposure; 58% of all mortality occurred on SW-, SE-, and E-facing, fire-exposed slopes, and 66% of all succession occurred on NW-, N-, NE-, and E-facing aspects. The highest level of mortality and succession was seen in SW-facing, fire-exposed slopes, which is notable because SW is the primary wind direction in the WCW.

Chapter four used random forest to create a predictive model of historic change in unobserved areas of WCW, using climate and topographic proxies outlined in Macias-Fauria and Johnson (2013). The proxies were generally insufficient in providing useful estimates of climatic variable importance. However, the predictive model demonstrated that century-scale estimates of change values can be generated from a small subset of oblique photographs.

5.2 Future Research

Each of the three research chapters presented in the thesis provided both limitations and opportunities for further investigation. These topics are examined in the following three sections, corresponding to the three research chapters.

5.2.1 Automated Monoplotting and Multi-Scale Analysis of ATE Dynamics

Chapter two described use of the Stockdale method (Stockdale et al. 2015) to assess historic change in the ATE, with oblique repeat photography and high-resolution

DEMs. A notable limitation of this method was that manual classification of the seven photo pairs took hundreds of research hours to complete. Some progress has been made towards automated classification of oblique imagery from the MLP (Jean et al. 2015), but advances in computer vision and image segmentation are required before the processing of large repeat photograph databases becomes feasible and efficient. These advancements may be several years away, but periodically revisiting this task with state-of-the-art technology could one day provide a bounty of data on ATE dynamics across western Canada.

Chapter two also reviewed a model for evaluating positional error in orthogonally transformed, monoplotted images. This method used a general linear model of error vector length (v), which described positional error as a function of distance to the camera (D) and angle of viewing incidence (A). Unfortunately, given that the present study was restricted to single watershed, the only comparison for the model was the initial work of Stockdale et al. (2015). The models shared generally similar values for D, however chapter two found a positive correlation between v and A, while Stockdale et al. (2015) found a negative correlation between v and A. A larger sample of monoplotted images will be required to determine exactly how the topography of a given watershed affects positional error in the monoplotting method. This information may prove valuable to future efforts to automate monoplotting and classification of the MLP database.

Automation of the MLP repeat photography database would introduce the possibility of a multi-scale historical analysis of ATE dynamics. The analyses in chapters two, three, and four were performed at a landscape scale (~100 km^2), but repeat photography and lidar data on which these studies were based provide the ability to scale

down to a microsite resolution (< 10 m^2), or scale up to a regional/continental resolution (> 1,000 km^2). For example, the seven landscape scale photograph pairs of WCW were selected from a larger set of 40, many of which covered spatial areas much smaller than the landscape scale in the target photographs. Figure 5.1 shows two such image pairs in which changes can be seen at a hill slope resolution. The monoplotting technique used 1 m lidar data that was aggregated to 20 m as a minimum resolution for the landscape scale, but it may be possible to grid land cover change a scale of 5 m or less using the WSL-MT. The MLP provides 6,000 of these repeat photographs, at various spatial scales, over latitudes of the Canadian Rockies roughly between 49° 0’ N and 54° 1’ N. Standardizing and automating observations of land cover change in this incredible historical resource could prove immensely beneficial to our understanding of interactions between climate, topography, disturbance, and high elevation vegetation, building on recent multi-scale approaches to ATE research (Case & Duncan 2014; Weiss et al. 2015).

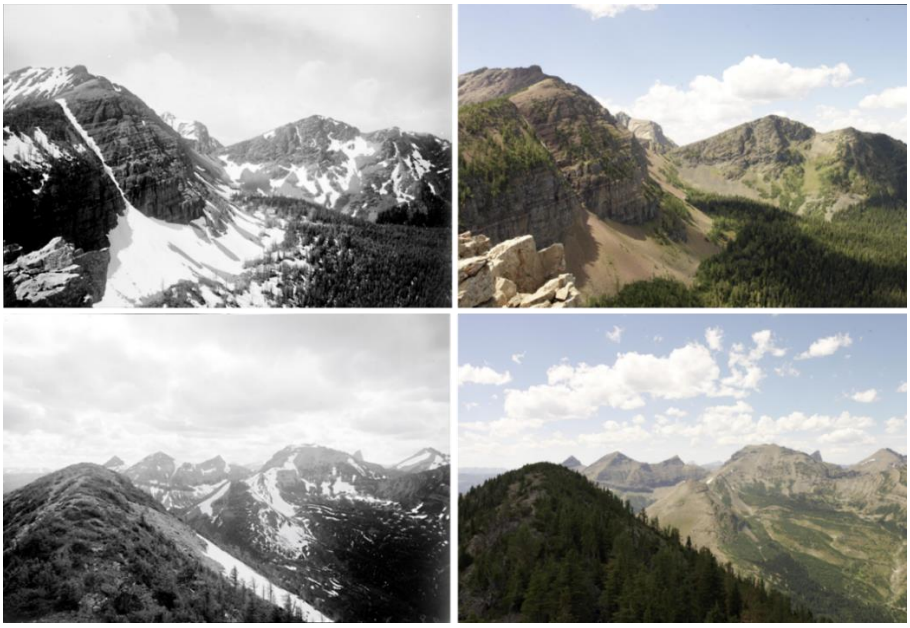

Figure 5.1 - Examples of microsite and hillslope scale images from the MLP.

5.2.2 Investigation of the Fire-Exposure/Aspect Effect

The research presented in chapter three demonstrated an aspect effect, where fire-exposure appeared to selectively increase mortality on south-facing aspects in the WCW. The first step in identifying a causal mechanism driving this correlation is to understand if the aspect effect is limited to the present area of study, or if it is more wide-spread in subalpine forest systems. There is a limited body of research showing aspect effects on fire return intervals (FRIs) (Rogeau & Armstrong 2017) and post-fire establishment (Stueve et al. 2009) in subalpine forests. While informative, these studies are insufficient to deem aspect selective post-fire establishment to be a widespread phenomenon. Future research on this topic should first seek to establish the frequency and spatial distribution of aspect selective post-fire establishment.

If systematic historical analysis suggest that the aspect effect is indeed widespread, then a number of questions can be posed to help identify processes underlying the observations; e.g., is the phenomenon associated with a particular climate, range of latitudes, or continentality? Does the aspect effect preferentially occur when the post-fire period is one of climatic extremes, as the 1930s were in WCW? Is there a threshold in elevation or climate at which the aspect effect is no longer observed?

In addition to historical analysis, direct observation of post-fire establishment from contemporary fires may also provide useful data. At least two large, high-elevation fires have occurred in the 21st-Century, in areas of southern Alberta which are nearby WCW. The Lost Creek fire occurred in 2003, affecting an area of more than 210 km^2 roughly 30 km North of the WCW site. If topographic patterns in post-fire establishment occurred following the Lost Creek fire, they should now be apparent in fire-exposed

areas. Several of the sub-watersheds in the area were instrumented with hydrometeorological stations following the Lost Creek fire (Silins et al. 2009). These data could be useful in determining how temperature, precipitation, insolation, erosion, runoff and other hydroclimatic parameters affect post-fire establishment in subalpine areas. The Kenow fire occurred in 2017, covering an area of more than 350 km^2, roughly 30 km Southeast of the WCW site. The Kenow fire presents an opportunity to monitor the climatic and hydrologic conditions of the region, beginning with the first post-fire winter, and observe the potential affect of these variables on subalpine post-fire establishment in subsequent growing seasons. In addition to standard forest mensuration, remote sensing technologies such as lidar could play an active role in post-fire monitoring, both in high-resolution mapping of subalpine snow depth and long-term observation of the spatial distribution of post-fire tree establishment and growth.

5.2.3 Random Forest to Predict Canopy Cover Change in Hydrologic Models

Land cover is a common parameter in hydrologic models, impacting various hydrologic processes such as infiltration, evapotranspiration, and canopy interception. When parameterizing land cover, several models specifically address canopy cover (e.g. SWAT (Neitsch et al. 2011) and HEC-HMS (Scharffenberg & Fleming 2006)), making the historical assessment of canopy cover change described in chapters two and three a potentially valuable dataset for mountain hydrology research.

One of the limitations of the canopy cover change analysis is that change classification was only possible in areas that were observed in the oblique repeat photography, or roughly 37% of WCW. This restriction poses a problem for hydrologic

modeling, as most tools require that input parameters are known across a catchment area. Chapter four showed that random forest prediction could be utilized to extend change classifications from observed areas to full catchments.

The canopy cover reconstruction method may be particularly useful when running hydrologic models of event-based disturbances, such as wildfires. Wildfire has significant impact on hydrologic processes in forested mountain areas, including increases to snow accumulation and insolation (Burles & Boon 2011) and runoff erosion (Gould et al. 2016). The ability to provide estimates of land cover before and after historic wildfires could uniquely contribute to the understanding of hydrologic responses to wildfire (Mahat et al. 2015). Indeed, the knowledge gaps in the interactions between wildfire, hydrological processes, and post-fire re-establishment of subalpine vegetation are of sufficient scope that they could be addressed in a future thesis.

REFERENCES

Abdel-Aziz, Y., & Karara, H. (1971). *Direct linear transformation from comparator coordinates into object-space coordinates in close-range photogrammetry.* Paper presented at the Proceedings ASP/VI Symp. On Close-Range Photogrammetry.

Agee, J. K. (1996). *Fire ecology of Pacific Northwest forests*: Island press.

Alberta Environment and Parks. (2012). *Alberta Vegetation Inventory*. Edmonton, Alberta, Canada.

Alftine, K. J., Malanson, G. P., & Fagre, D. B. (2003). Feedback-driven response to multidecadal climatic variability at an alpine treeline. *Physical Geography, 24*(6), 520-535.

Allen, T. R., & Walsh, S. J. (1996). Spatial and compositional pattern of alpine treeline, Glacier National Park, Montana. *Photogrammetric Engineering and Remote Sensing, 62*(11), 1261-1268.

Aschenwald, J., Leichter, K., Tasser, E., & Tappeiner, U. (2001). Spatio-temporal landscape analysis in mountainous terrain by means of small format photography: a methodological approach. *IEEE Transactions on Geoscience and Remote Sensing, 39*(4), 885-893.

Aumann, G., & Eder, K. (1996). An integrated system of digital monoplotting and DTM modelling for forestry applications. *International Archives of Photogrammetry and Remote Sensing, 31*(B7), 221-225.

Bader, M. Y., Rietkerk, M., & Bregt, A. K. (2008). A simple spatial model exploring positive feedbacks at tropical alpine treelines. *Arctic, Antarctic, and Alpine Research, 40*(2), 269-278.

Bader, M. Y., & Ruijten, J. J. A. (2008). A topography-based model of forest cover at the alpine tree line in the tropical Andes. *Journal of Biogeography, 35*(4), 711-723.

Beaudoin, A. (1986). Using Picea/Pinus ratios from the Wilcox Pass core, Jasper National Park, Alberta, to investigate Holocene timberline fluctuations. *Géographie physique et Quaternaire, 40*(2), 145-152.

Bekker, M. F. (2005). Positive Feedback between Tree Establishment and Patterns of Subalpine Forest. *Arctic, Antarctic, and Alpine Research, 37*(1), 97-107.

Beven, K. J., & Kirkby, M. J. (1979). A physically based, variable contributing area model of basin hydrology / Un modèle à base physique de zone d'appel variable de l'hydrologie du bassin versant. *Hydrological Sciences Bulletin, 24*(1), 43-69.

Bozzini, C., Conedera, M., & Krebs, P. (2012). A New Monoplotting Tool to Extract Georeferenced Vector Data and Orthorectified Raster Data from Oblique Non-Metric Photographs. *International Journal of Heritage in the Digital Era, 1*(3), 499-518.

Breiman, L. (2001). Random forests. *Machine learning, 45*(1), 5-32.

Breiman, L., Friedman, J., Stone, C. J., & Olshen, R. A. (1984). *Classification and regression trees*: CRC press.

Broll, G., & Holtmeier, F.-K. (2010). Wind as an Ecological Agent at Treelines in North America, the Alps, and the European Subarctic. *Physical Geography, 31*(3), 203-233.

Burles, K., & Boon, S. (2011). Snowmelt energy balance in a burned forest plot, Crowsnest Pass, Alberta, Canada. *Hydrological Processes, 25*(19), 3012-3029.

Butler, D. R., & DeChano, L. M. (2001). Environmental Change in Glacier National Park, Montana: An Assessment Through Repeat Photography from Fire Outlooks *Physical Geography, 22*(5), 291-304.

Butler, D. R., Malanson, G. P., & Cairns, D. M. (1994). Stability of Alpine Treeline in Northern Montana, USA. *Phytocoenologia, 22*(4), 485-500.

Butler, D. R., Malanson, G. P., Walsh, S. J., & Fagre, D. B. (2007). Influences of geomorphology and geology on alpine treeline in the American West—More important than climatic influences? *Physical Geography, 28*(5), 434-450.

Butler, D. R., Malanson, G. P., Walsh, S. J., & Fagre, D. B. (2009). *The Changing Alpine Treeline: The Example of Glacier National Park, MT, USA* (Vol. 12): Elsevier.

Butler, D. R., & Walsh, S. J. (1994). Site characteristics of debris flows and their relationship to alpine treeline. *Physical Geography, 15*(2), 181-199.

Cairns, D. M. (2001). Patterns of Winter Desiccation in Krummholz Forms of Abies Lasiocarpa at Treeline Sites in Glacier National Park, Montana, USA. *Geografiska Annaler: Series A, Physical Geography, 83*(3), 157-168.

Cansler, C. A., McKenzie, D., & Halpern, C. B. (2016). Area burned in alpine treeline ecotones reflects region-wide trends. *International Journal of Wildland Fire, 25*(12), 1209.

Case, B. S., & Buckley, H. L. (2015). Local-scale topoclimate effects on treeline elevations: a country-wide investigation of New Zealand's southern beech treelines. *PeerJ, 3*, e1334.

Case, B. S., & Duncan, R. P. (2014). A novel framework for disentangling the scale-dependent influences of abiotic factors on alpine treeline position. *Ecography, 37*(9), 838-851.

Cohen, J. (1968). Weighted kappa: Nominal scale agreement provision for scaled disagreement or partial credit. *Psychological bulletin, 70*(4), 213.

Colombaroli, D., Henne, P. D., Kaltenrieder, P., Gobet, E., & Tinner, W. (2010). Species responses to fire, climate and human impact at tree line in the Alps as evidenced by palaeo-environmental records and a dynamic simulation model. *Journal of Ecology, 98*(6), 1346-1357.

Conedera, M., Bozzini, C., Scapozza, C., Rè, L., Ryter, U., & Krebs, P. (2013). Anwendungspotenzial des WSL-Monoplotting-Tools im Naturgefahrenmanagement. *Schweizerische Zeitschrift fur Forstwesen, 164*(7), 173-180.

Coops, N. C., Morsdorf, F., Schaepman, M. E., & Zimmermann, N. E. (2013). Characterization of an alpine tree line using airborne LiDAR data and physiological modeling. *Global Change Biology*, *19*(12), 3808-3821.

Corripio, J. G. (2004). Snow surface albedo estimation using terrestrial photography. *International Journal of Remote Sensing, 25*(24), 5705-5729.

Cullen, R. M., & Marshall, S. J. (2011). Mesoscale Temperature Patterns in the Rocky Mountains and Foothills Region of Southern Alberta. *Atmosphere-Ocean, 49*(3), 189-205.

Cutler, D. R., Edwards, T. C., Beard, K. H., Cutler, A., Hess, K. T., Gibson, J., & Lawler, J. J. (2007). Random forests for classification in ecology. *Ecology, 88*(11), 2783-2792.

Danby, R. K. (2011). Monitoring Forest-Tundra Ecotones at Multiple Scales. *Geography Compass, 5*(9), 623-640.

Danby, R. K., & Hik, D. S. (2007). Evidence of Recent Treeline Dynamics in Southwest Yukon from Aerial Photographs. *Arctic, 60*(4).

Dang, H., Zhang, Y., Zhang, Y., Zhang, K., & Zhang, Q. (2015). Variability and rapid response of subalpine fir (Abies fargesii) to climate warming at upper altitudinal limits in north-central China. *Trees, 29*(3), 785-795.

Doytsher, Y., & Hall, J. K. (1997). Interpolation of DTM using bi-directional third-degree parabolic equations, with FORTRAN subroutines. *Computers & Geosciences, 23*(9), 1013-1020.

Efford, J. T., Clarkson, B. D., & Bylsma, R. J. (2014). Persistent effects of a tephra eruption (AD 1655) on treeline composition and structure, Mt Taranaki, New Zealand. *New Zealand Journal of Botany, 52*(2), 245-261.

Elliott, G. P. (2012). The Role of Thresholds and Fine-Scale Processes in Driving Upper Treeline Dynamics in the Bighorn Mountains, Wyoming. *Physical Geography, 33*(2), 129-145.

Elliott, G. P., & Cowell, C. M. (2015). Slope Aspect Mediates Fine-Scale Tree Establishment Patterns at Upper Treeline during Wet and Dry Periods of the 20th Century. *Arctic, Antarctic, and Alpine Research, 47*(4), 681-692.

Ellison, L. (1954). Subalpine vegetation of the Wasatch plateau, Utah. *Ecological Monographs, 24*(2), 89-184.

Esri. (2014). ArcGIS 10.3 for Desktop: Environmental Systems Research Institute Redlands, CA USA.

Fagre, D. B., Walsh, S. J., Malanson, G. P., & Butler, D. R. (2007). Influences of Geomorphology and Geology on Alpine Treeline in the American West—More Important than Climatic Influences? *Physical Geography, 28*(5), 434-450.

Fenton, M., Waters, E., Pawley, S., Atkinson, N., Utting, D., & Mckay, K. (2013). Surficial geology of Alberta. *Alberta Geological Survey, AER/AGS Map, 601*.

Fluehler, M., Niederoest, J., & Akca, D. (2005). *Development of an educational software system for the digital monoplotting*: ETH, Eidgenössische Technische Hochschule Zürich, Institute of Geodesy and Photogrammetry.

Geological Survey of Canada, & Price, R. A. (1961). *Fernie map-area, east half, Alberta and British Columbia 82 GE 1/2 (Report and Map 35-1961)*.

Germino, M. J., Smith, W. K., & Resor, A. C. (2002). Conifer seedling distribution and survival in an alpine-treeline ecotone. *Plant Ecology, 162*(2), 157-168.

Glass, D. (1990). Lexicon of Canadian Stratigraphy, Volume 4, Western Canada, including Eastern British Columbia, Alberta, Saskatchewan and Southern Manitoba. *Canadian Society of Petroleum Geologists, 8*, p109-118.

Gould, G. K., Liu, M., Barber, M. E., Cherkauer, K. A., Robichaud, P. R., & Adam, J. C. (2016). The effects of climate change and extreme wildfire events on runoff erosion over a mountain watershed. *Journal of Hydrology, 536*, 74-91.

Grace, J., Berninger, F., & Nagy, L. (2002). Impacts of climate change on the tree line. *Annals of Botany, 90*(4), 537-544.

Grafius, D. R., & Malanson, G. P. (2015). Biomass distributions in dwarf tree, krummholz, and tundra vegetation in the alpine treeline ecotone. *Physical Geography, 36*(4), 337-352.

Greenwood, S., Chen, J. C., Chen, C. T., & Jump, A. S. (2014). Strong topographic sheltering effects lead to spatially complex treeline advance and increased forest density in a subtropical mountain region. *Global Change Biology, 20*(12), 3756-3766.

Gruell, G. E. (1983). *Fire and vegetative trends in the Northern Rockies: interpretations from 1871-1982 photographs*. Lakewood, CO: United States Forest Service.

Hagedorn, F., Shiyatov, S. G., Mazepa, V. S., Devi, N. M., Grigor'ev, A. A., Bartysh, A. A., Fomin, V. V., Kapralov, D. S., Terent'ev, M., Bugman, H., Rigling, A., & Moiseev, P. A. (2014). Treeline advances along the Urals mountain range - driven by improved winter conditions? *Global Change Biology, 20*(11), 3530-3543.

Harrison, A. (1974). Reoccupying unmarked camera stations for geological observations. *Geology, 2*(9), 469-471.

Harsch, M. A., & Bader, M. Y. (2011). Treeline form–a potential key to understanding treeline dynamics. *Global Ecology and Biogeography, 20*(4), 582-596.

Harsch, M. A., Hulme, P. E., McGlone, M. S., & Duncan, R. P. (2009). Are treelines advancing? A global meta-analysis of treeline response to climate warming. *Ecology Letters, 12*(10), 1040-1049.

Hart, R. H., & Laycock, W. A. (1996). Repeat photography on range and forest lands in the western United States. *Journal of Range Management*, 60-67.

Hattersley-Smith, G. (1966). The symposium on glacier mapping. *Canadian Journal of Earth Sciences, 3*(6), 737-741.

Heiri, C., Bugmann, H., Tinner, W., Heiri, O., & Lischke, H. (2006). A model-based reconstruction of Holocene treeline dynamics in the Central Swiss Alps. *Journal of Ecology, 94*(1), 206-216.

Hermes, K. (1955). *Die Lage der oberen Waldgrenze in den Gebirgen der Erde und ihr Abstand zur Schneegrenze*. Kölner geographische Arbeiten, (5).

Holden, Z. A., Abatzoglou, J. T., Luce, C. H., & Baggett, L. S. (2011). Empirical downscaling of daily minimum air temperature at very fine resolutions in complex terrain. *Agricultural and Forest Meteorology, 151*(8), 1066-1073.

Holtmeier, F.-K. (2009). *Mountain timberlines: ecology, patchiness, and dynamics* (Vol. 36): Springer Science & Business Media.

Holtmeier, F.-K., & Broll, G. (2017). Treelines—Approaches at Different Scales. *Sustainability, 9*(5), 808.

Holtmeier, F. K., & Broll, G. (2005). Sensitivity and response of northern hemisphere altitudinal and polar treelines to environmental change at landscape and local scales. *Global Ecology and Biogeography, 14*(5), 395-410.

Holtmeier, F. K., & Broll, G. (2012). Landform Influences on Treeline Patchiness and Dynamics in a Changing Climate. *Physical Geography, 33*(5), 403-437.

Hopkinson, C., & Chasmer, L. (2009). Testing LiDAR models of fractional cover across multiple forest ecozones. *Remote Sensing of Environment, 113*(1), 275-288.

IBM. (2016). SPSS Statistics for Windows. Armonk, NY: IBM Corp.

Isenburg, M. (2013). LAStools-efficient tools for LiDAR processing. Version 161114.

Jean, F., Albu, A. B., Capson, D., Higgs, E., Fisher, J. T., & Starzomski, B. M. (2015). The Mountain Habitats Segmentation and Change Detection Dataset. 603-609.

Jensen, M. E., & Haise, H. R. (1963). Estimating evapotranspiration from solar radiation. *Proceedings of the American Society of Civil Engineers, Journal of the Irrigation and Drainage Division, 89*, 15-41.

Kienzle, S. (2004). The effect of DEM raster resolution on first order, second order and compound terrain derivatives. *Transactions in GIS, 8*(1), 83-111.

Klasner, F. L., & Fagre, D. B. (2002). A Half Century of Change in Alpine Treeline Patterns at Glacier National Park, Montana, U.S.A. *Arctic, Antarctic, and Alpine Research, 34*(1), 49-56.

Kolecka, N., Kozak, J., Kaim, D., Dobosz, M., Ginzler, C., & Psomas, A. (2015). Mapping Secondary Forest Succession on Abandoned Agricultural Land with LiDAR Point Clouds and Terrestrial Photography. *Remote Sensing, 7*(7), 8300-8322.

Körner, C. (1998). A re-assessment of high elevation treeline positions and their explanation. *Oecologia, 115*(4), 445-459.

Körner, C. (2003a). *Alpine Plant Life: Functional Plant Ecology of High Mountian Ecosystems*: Springer Science & Business Media.

Körner, C. (2003b). Carbon limitation in trees. *Journal of Ecology, 91*(1), 4-17.

Körner, C. (2012). *Alpine treelines: functional ecology of the global high elevation tree limits*: Springer Science & Business Media.

Körner, C., & Paulsen, J. (2004). A world-wide study of high altitude treeline temperatures. *Journal of Biogeography, 31*(5), 713-732.

Kueppers, L. M., Conlisk, E., Castanha, C., Moyes, A. B., Germino, M. J., de Valpine, P., Torn, M. S., & Mitton, J. B. (2017). Warming and provenance limit tree recruitment across and beyond the elevation range of subalpine forest. *Glob Chang Biol, 23*(6), 2383-2395.

Kullman, L. (1986). Recent tree-limit history of Picea abies in the southern Swedish Scandes. *Canadian Journal of Forest Research, 16*(4), 761-771.

Kullman, L. (2014). Treeline (Pinus sylvestris) landscape evolution in the Swedish Scandes – a 40-year demographic effort viewed in a broader temporal context. *Norsk Geografisk Tidsskrift - Norwegian Journal of Geography, 68*(3), 155-167.

Kullman, L., & Öberg, L. (2009). Post-Little Ice Age tree line rise and climate warming in the Swedish Scandes: a landscape ecological perspective. *Journal of Ecology, 97*(3), 415-429.

Leonelli, G., Masseroli, A., & Pelfini, M. (2016). The influence of topographic variables on treeline trees under different environmental conditions. *Physical Geography, 37*(1), 56-72.

Liang, E., Dawadi, B., Pederson, N., & Eckstein, D. (2014). Is the growth of birch at the upper timberline in the Himalayas limited by moisture or by temperature? *Ecology, 95*(9), 2453-2465.

Liang, E., Wang, Y., Piao, S., Lu, X., Camarero, J. J., Zhu, H., Zhu, L., Ellison, A. M., Ciais, P., & Peñuelas, J. (2016). Species interactions slow warming-induced upward shifts of treelines on the Tibetan Plateau. *Proceedings of the National Academy of Sciences, 113*(16), 4380-4385.

Liaw, A., & Wiener, M. (2002). Classification and regression by randomForest. *R news, 2*(3), 18-22.

Lloyd, A. H., & Graumlich, L. J. (1997). Holocene dynamics of treeline forests in the Sierra Nevada. *Ecology, 78*(4), 1199-1210.

Luckman, B. H., & Kavanagh, T. A. (1998). Documenting the effects of recent climate change at treeline in the Canadian Rockies *The impacts of climate variability on forests* (pp. 121-144): Springer.

Luckman, B. H., & Wilson, R. J. S. (2005). Summer temperatures in the Canadian Rockies during the last millennium: a revised record. *Climate Dynamics, 24*(2-3), 131-144.

Lumley, T., Diehr, P., Emerson, S., & Chen, L. (2002). The importance of the normality assumption in large public health data sets. *Annual review of public health, 23*(1), 151-169.

MacDonald, G. M. (2003). *Biogeography: space, time and life*.

Macias-Fauria, M., & Johnson, E. A. (2013). Warming-induced upslope advance of subalpine forest is severely limited by geomorphic processes. *Proceedings of the National Academy of Sciences, 110*(20), 8117-8122.

MacLaren, I., Higgs, E., & Zezulka-Mailloux, G. (2005). *Mapper of Mountains: MP Bridgland in the Canadian Rockies, 1902-1930*: University of Alberta.

Mahat, V., Anderson, A., & Silins, U. (2015). Modelling of wildfire impacts on catchment hydrology applied to two case studies. *Hydrological Processes, 29*(17), 3687-3698.

Maher, E. L., & Germino, M. J. (2006). Microsite differentiation among conifer species during seedling establishment at alpine treeline. *Ecoscience, 13*(3), 334-341.

Malanson, G. P., Brown, D. G., Butler, D. R., Cairns, D. M., Fagre, D. B., & Walsh, S. J. (2009). Ecotone dynamics: invasibility of alpine tundra by tree species from the subalpine forest. *Developments in Earth Surface Processes, 12*, 35-61.

Malanson, G. P., Butler, D. R., Cairns, D. M., Welsh, T. E., & Resler, L. M. (2002). Variability in an edaphic indicator in alpine tundra. *Catena, 49*(3), 203-215.

Malanson, G. P., Resler, L. M., Bader, M. Y., Holtmeier, F.-K., Butler, D. R., Weiss, D. J., Daniels, L. D., & Fagre, D. B. (2011). Mountain treelines: a roadmap for research orientation. *Arctic, Antarctic, and Alpine Research, 43*(2), 167-177.

Mamet, S. D., & Kershaw, G. P. (2012). Subarctic and alpine tree line dynamics during the last 400years in north-western and central Canada. *Journal of Biogeography, 39*(5), 855-868.

McCaffrey, D. R., & Hopkinson, C. (2017). Assessing Fractional Cover in the Alpine Treeline Ecotone Using the WSL Monoplotting Tool and Airborne Lidar. *Canadian Journal of Remote Sensing, 43*(5), 504-512.

McGuinness, J. L., & Bordne, E. F. (1972). *A comparison of lysimeter-derived potential evapotranspiration with computed values*: US Dept. of Agriculture.

Mitishita, E., Machado, A., Habib, A., & Gonçalves, G. (2004). *3D monocular restitution applied to small format digital airphoto and laser scanner data.* Paper presented at the Proceedings of Commission III, ISPRS Congress, Istanbul.

Moiseev, P. A., & Shiyatov, S. G. (2003). Vegetation Dynamics at the Tree-Line Ecotone in the Ural Highlands, Russia *Alpine Biodiversity in Europe* (Ecological Studies ed., Vol. 167, pp. 423-435). Berlin, Germany: Springer Science and Business Media.

Moyes, A. B., Germino, M. J., & Kueppers, L. M. (2015). Moisture rivals temperature in limiting photosynthesis by trees establishing beyond their cold-edge range limit under ambient and warmed conditions. *New Phytologist, 207*(4), 1005-1014.

Murphy, P. J. (2006). Alberta forest service: Protection and management of Alberta's forests. *Canadian Research Index*.

Mustaphi, C. J. C., Pisaric, M. F. J., & Williams, J. (2013). Varying influence of climate and aspect as controls of montane forest fire regimes during the late Holocene, south-eastern British Columbia, Canada. *Journal of Biogeography, 40*(10), 1983-1996.

Neitsch, S. L., Arnold, J. G., Kiniry, J. R., & Williams, J. R. (2011). *Soil and water assessment tool theoretical documentation version 2009*. Retrieved from

Neuner, G. (2007). *Trees at their upper limit: treelife limitation at the alpine timberline* (Vol. 5): Springer Science & Business Media.

Neuner, G. (2014). Frost resistance in alpine woody plants. *Front Plant Sci, 5*.

Nowak, D. J., & Greenfield, E. J. (2012). Tree and impervious cover change in U.S. cities. *Urban Forestry & Urban Greening, 11*(1), 21-30.

Oudin, L., Hervieu, F., Michel, C., Perrin, C., Andréassian, V., Anctil, F., & Loumagne, C. (2005). Which potential evapotranspiration input for a lumped rainfall–runoff model? *Journal of Hydrology, 303*(1-4), 290-306.

Paulsen, J., & Körner, C. (2014). A climate-based model to predict potential treeline position around the globe. *Alpine Botany, 124*(1), 1-12.

Pepin, N., Bradley, R. S., Diaz, H. F., Baraer, M., Caceres, E. B., Forsythe, N., Fowler, H., Greenwood, G., Hashmi, M. Z., Liu, X. D., Miller, J. R., Ning, L., Ohmura, A., Palazzi, E., Rangwala, I., Schöner, W., Severskiy, I., Shahgedanova, M., Wang, M. B., Williamson, S. N., & Yang, D. Q. (2015). Elevation-dependent warming in mountain regions of the world. *Nature Climate Change, 5*(5), 424-430.

R Core Team. (2017). A language and environment for statistical computing R Foundation for Statistical Computing Department of Agronomy, Faculty of Agriculture of the University of the Free State. *Vienna, Austria. www. R-project. org*.

Randin, C. F., Engler, R., Normand, S., Zappa, M., Zimmermann, N. E., Pearman, P. B., Vittoz, P., Thuiller, W., & Guisan, A. (2009). Climate change and plant distribution: local models predict high-elevation persistence. *Global Change Biology, 15*(6), 1557-1569.

Resler, L. M. (2006). Geomorphic controls of spatial pattern and process at alpine treeline. *The Professional Geographer, 58*(2), 124-138.

Rogeau, M.-P., & Armstrong, G. W. (2017). Quantifying the effect of elevation and aspect on fire return intervals in the Canadian Rocky Mountains. *Forest Ecology and Management, 384*, 248-261.

Rogeau, M.-P., Flannigan, M. D., Hawkes, B. C., Parisien, M.-A., & Arthur, R. (2016). Spatial and temporal variations of fire regimes in the Canadian Rocky Mountains and Foothills of southern Alberta. *International Journal of Wildland Fire, 25*(11), 1117-1130.

Rogers, G. F., Malde, H. E., & Turner, R. M. (1984). *Bibliography of repeat photography for evaluating landscape change*.

Roush, W., Munroe, J. S., & Fagre, D. B. (2007). Development of a spatial analysis metho using ground-based repeat photography to detect changes in the alpine treeline ecotone, Glacier National Park, Montana, USA. *Arctic, Antarctic, and Alpine Research, 39*(2), 297-308.

Sakulich, J. (2016). Reconstruction and spatial analysis of alpine treeline in the Elk Mountains, Colorado, USA. *Physical Geography, 36*(6), 471-488.

Scapozza, C., Lambiel, C., Bozzini, C., Mari, S., & Conedera, M. (2014). Assessing the rock glacier kinematics on three different timescales: a case study from the southern Swiss Alps. *Earth Surface Processes and Landforms, 39*(15), 2056-2069.

Scharffenberg, W. A., & Fleming, M. J. (2006). *Hydrologic modeling system HEC-HMS: user's manual*: US Army Corps of Engineers, Hydrologic Engineering Center.

Schwörer, C., Gavin, D. G., Walker, I. R., & Hu, F. S. (2017). Holocene tree line changes in the Canadian Cordillera are controlled by climate and topography. *Journal of Biogeography, 44*(5), 1148-1159.

Schwörer, C., Henne, P. D., & Tinner, W. (2014). A model-data comparison of Holocene timberline changes in the Swiss Alps reveals past and future drivers of mountain forest dynamics. *Global Change Biology, 20*(5), 1512-1526.

Schwörer, C., Kaltenrieder, P., Glur, L., Berlinger, M., Elbert, J., Frei, S., Gilli, A., Hafner, A., Anselmetti, F. S., Grosjean, M., & Tinner, W. (2013). Holocene climate, fire and vegetation dynamics at the treeline in the Northwestern Swiss Alps. *Vegetation History and Archaeobotany, 23*(5), 479-496.

Silins, U., Stone, M., Emelko, M. B., & Bladon, K. D. (2009). Sediment production following severe wildfire and post-fire salvage logging in the Rocky Mountain headwaters of the Oldman River Basin, Alberta. *Catena, 79*(3), 189-197.

Speed, J. D. M., Martinsen, V., Mysterud, A., Mulder, J., Holand, Ø., & Austrheim, G. (2014). Long-Term Increase in Aboveground Carbon Stocks Following Exclusion of Grazers and Forest Establishment in an Alpine Ecosystem. *Ecosystems, 17*(7), 1138-1150.

Stine, M. B., & Butler, D. R. (2015). Effects of fire on geomorphic factors and seedling site conditions within the alpine treeline ecotone, Glacier National Park, MT. *Catena, 132*, 37-44.

Stockdale, C. A., Bozzini, C., Macdonald, S. E., & Higgs, E. (2015). Extracting ecological information from oblique angle terrestrial landscape photographs: Performance evaluation of the WSL Monoplotting Tool. *Applied Geography, 63*, 315-325.

Strausz, D. A., & Doel, R. (2001). An application of photogrammetric techniques to the measurement of historic photographs. *Geography Master of Science Thesis, Oregon State University*.

Strickler, G. S. (1961). Vegetation and soil condition changes on a subalpine grassland in eastern Oregon.

Strickler, G. S., & Hall, W. B. (1980). The Standley allotment: a history of range recovery. *The Standley allotment: a history of range recovery.*(PNW-278).

Strobl, C., Boulesteix, A.-L., Zeileis, A., & Hothorn, T. (2006). Bias in Random Forest Variable Importance Measures: Illustrations, Sources and a Solution.

Stueve, K. M., Cerney, D. L., Rochefort, R. M., & Kurth, L. L. (2009). Post-fire tree establishment patterns at the alpine treeline ecotone: Mount Rainier National Park, Washington, USA. *Journal of Vegetation Science, 20*(1), 107-120.

Thompson, M. M. (1966). Manual of photogrammetry. *Geoscience Abstracts*.

Tinner, W., & Theurillat, J.-P. (2003). Uppermost limit, extent, and fluctuations of the timberline and treeline ecocline in the Swiss Central Alps during the past 11,500 years. *Arctic, Antarctic, and Alpine Research, 35*(2), 158-169.

Tranquillini, W. (1979). *Physiological ecology of the alpine timberline. Tree existence at high altitudes with special reference to the European Alps.* Berlin, Germany: Springer-Verlag.

Trant, A. J., Starzomski, B. M., & Higgs, E. (2015). A publically available database for studying ecological change in mountain ecosystems. *Frontiers in Ecology and the Environment, 13*(4), 187-187.

Ucar, Z., Bettinger, P., Merry, K., Siry, J., Bowker, J. M., & Akbulut, R. (2016). A comparison of two sampling approaches for assessing the urban forest canopy cover from aerial photography. *Urban Forestry & Urban Greening, 16*, 221-230.

Vale, T. R. (1987). Vegetation change and park purposes in the high elevations of Yosemite National Park, California. *Annals of the Association of American Geographers, 77*(1), 1-18.

Vankat, J. L., & Major, J. (1978). Vegetation changes in sequoia national park, California. *Journal of Biogeography*, 377-402.

von Humboldt, A. (1886). *Cosmos: A sketch of a physical description of the universe, vol. 5*: George bell and sons.

Walsh, S. J., & Butler, D. R. (1997). Morphometric and multispectral image analysis of debris flows for natural hazard assessment. *Geocarto International, 12*(1), 59-70.

Walsh, S. J., Butler, D. R., Allen, T. R., & Malanson, G. P. (1994). Influence of Snow Patterns and Snow Avalanches on the Alpine Treeline Ecotone. *Journal of Vegetation Science, 5*(5), 657-672.

Walsh, S. J., Butler, D. R., Malanson, G. P., Crews-Meyer, K. A., Messina, J. P., & Xiao, N. (2003). Mapping, modeling, and visualization of the influences of geomorphic processes on the alpine treeline ecotone, Glacier National Park, MT, USA. *Geomorphology, 53*(1), 129-145.

Wei, T., & Simko, V. (2016). corrplot: Visualization of a Correlation Matrix. R package version 0.77. *CRAN, Vienna, Austria*.

Weiss, D. J., Malanson, G. P., & Walsh, S. J. (2015). Multiscale Relationships Between Alpine Treeline Elevation and Hypothesized Environmental Controls in the Western United States. *Annals of the Association of American Geographers, 105*(3), 437-453.

Werth, P. A., Potter, B. E., Clements, C. B., Finney, M., Goodrick, S. L., Alexander, M. E., Cruz, M. G., Forthofer, J. A., & McAllister, S. S. (2011). Synthesis of knowledge of extreme fire behavior: volume I for fire managers.

Wildfire Management Branch - Alberta Agriculture and Forestry. (2017). *Fire History Polygons C5 FMU*.

Williams, C. K., Engelhardt, A., Cooper, T., Mayer, Z., Ziem, A., Scrucca, L., Tang, Y., Candan, C., Hunt, T., & Kuhn, M. M. (2017). Package 'caret'.

Wulf, A. (2015). *The invention of nature: Alexander von Humboldt's new world*: Knopf.

Yadava, A. K., Sharma, Y. K., Dubey, B., Singh, J., Singh, V., Bhutiyani, M. R., Yadav, R. R., & Misra, K. G. (2017). Altitudinal treeline dynamics of Himalayan pine in western Himalaya, India. *Quaternary International, 444*, 44-52.

Yao, Y., & Zhang, B. (2015). The mass elevation effect of the Tibetan Plateau and its implications for Alpine treelines. *International Journal of Climatology, 35*(8), 1833-1846.

Zevenbergen, L. W., & Thorne, C. R. (1987). Quantitative analysis of land surface topography. *Earth Surface Processes and Landforms, 12*(1), 47-56.

Zhao, F., Zhang, B.-p., Zhang, S., Qi, W.-w., He, W.-h., Wang, J., & Yao, Y.-h. (2015). Contribution of mass elevation effect to the altitudinal distribution of global treelines. *Journal of Mountain Science, 12*(2), 289-297.

APPENDIX A - SCRIPTS

Chapter two describes the use of an *observation-parameter routine*, which calculates the distance to camera (*D*) and angle of viewing incidence (*A*) for every DEM grid cell in a watershed, which enables the calculation of *Error Vector Length* (*v*) through the application of a general linear model. The python script for this analysis is maintained here:

https://github.com/dramccaffrey/msc_scripts/tree/master/EVL_model

Chapter four describes the use of a random forest model, to predict canopy cover change using proxies of climatic, topographic, and disturbance variables. The R script for this model execution is maintained here:

https://github.com/dramccaffrey/msc_scripts/tree/master/RF_model